NPS-68-86-009

NAVAL POSTGRADUATE SCHOOL

Monterey, California

THESIS

REAL-TIME AIRBORNE OCEAN SAMPLING AND APPLICATIONS TO NAVAL OPERATIONS

John J. Rendine

December 1986

Thesis Co-Advisors: Christopher N.K. Mooers
Gordon W. Groves

Prepared for:
Office of Naval Research
Environmental Sciences Directorate (Code 1122)
Arlington, VA 22217

NAVAL POSTGRADUATE SCHOOL
Monterey, California 93943

Rear Admiral R.C. Austin
Superintendent

D. A. Schrady
Provost

This thesis was prepared in conjunction with the research project "Ocean Prediction Through Observation, Modeling and Analysis" (OPTOMA), sponsored by the Physical Oceanography Program of the Office of Naval Research under Program Element 61153N.

RITY CLASSIFICATION OF THIS PAGE

REPORT DOCUMENTATION PAGE

EPORT SECURITY CLASSIFICATION CLASSIFIED	1b. RESTRICTIVE MARKINGS
ECURITY CLASSIFICATION AUTHORITY	3 DISTRIBUTION / AVAILABILITY OF REPORT Approved for public release; distribution is unlimited.
ECLASSIFICATION / DOWNGRADING SCHEDULE	
RFORMING ORGANIZATION REPORT NUMBER(S) -68-86-009	5 MONITORING ORGANIZATION REPORT NUMBER(S)
AME OF PERFORMING ORGANIZATION: val Postgraduate School 6b OFFICE SYMBOL (If applicable): 68	7a NAME OF MONITORING ORGANIZATION Naval Postgraduate School
DDRESS (City, State, and ZIP Code) terey, California 93943-5000	7b. ADDRESS (City, State, and ZIP Code) Monterey, California 93943-5000
AME OF FUNDING / SPONSORING RGANIZATION: fice of Naval Research 8b OFFICE SYMBOL (If applicable): 1122	9 PROCUREMENT INSTRUMENT IDENTIFICATION NUMBER
DDRESS (City, State, and ZIP Code) ironmental Sciences Directorate ington, Virginia 22217	10 SOURCE OF FUNDING NUMBERS PROGRAM ELEMENT NO: 61153N PROJECT NO: RR031036 TASK NO: WORK UNIT ACCESSION NO:
TLE (Include Security Classification) L-TIME AIRBORNE OCEAN SAMPLING AND APPLICATIONS TO NAVAL OPERATIONS	
RSONAL AUTHOR(S) dine, John J.	
YPE OF REPORT ter's Thesis	13b TIME COVERED FROM _____ TO _____
14 DATE OF REPORT (Year, Month, Day) 1986 December	15 PAGE COUNT 101
PPLEMENTARY NOTATION pared in conjunction with the research project "Ocean Prediction Through ervation, Modeling and Analysis"(OPTOMA).	
COSATI CODES ELD / GROUP / SUB-GROUP	18 SUBJECT TERMS (Continue on reverse if necessary and identify by block number) Airborne Expendable Bathythermograph (AXBT), objective analysis, synoptic mapping

STRACT (Continue on reverse if necessary and identify by block number)

The Airborne Digital Data Acquisition System (ADDAS) was developed by joint Naval Postgraduate School/Harvard University research project, led the Ocean Prediction Through Observation, Modeling, and Analysis TOMA) Program, for the real-time synoptic mapping of oceanic features.

Given the capabilities of such a system, an aerial sampling strategy developed based on the spatial scales of oceanic variables and the craft and ADDAS limitations. This strategy was applied to "simulated" T survey flights on "synthetic" fields. The simulated AXBT observations e objectively analyzed and compared to the synthetic field. By varying simulated AXBT spacing and the objective analysis parameters, an timum" AXBT spacing to adequately represent the synthetic structure of domain was deduced.

To further develop such a system for both airborne and shipboard use,

TRIBUTION / AVAILABILITY OF ABSTRACT NCLASSIFIED/UNLIMITED ☐ SAME AS RPT ☐ DTIC USERS	21 ABSTRACT SECURITY CLASSIFICATION UNCLASSIFIED
AME OF RESPONSIBLE INDIVIDUAL istopher N.K. Mooers	22b TELEPHONE (Include Area Code) (408) 646-2673 22c OFFICE SYMBOL 68Mr

RM 1473, 84 MAR 83 APR edition may be used until exhausted
All other editions are obsolete

SECURITY CLASSIFICATION OF THIS PAGE

9. (continued)
a proposed Ship/Aircraft Data Acquisition, Display, and Analysis System (SADADAS) was presented. The following synoptic mappings produced could provide a possible tactical decision aid for antisubmarine warfare (ASW) operations: 1) Sea surface temperature; 2) Temperature/Sound speed at selected depths; 3) Maps of mixed layer depth; 4) Subsurface ducts/sound channels; and 5) Vertical sections of temperature/soundspeed.

Approved for public release; distribution is unlimited.

Real-Time Airborne Ocean Sampling and Applications to Naval Operations

by

John J. Rendine
Lieutenant, United States Navy
B.S., United States Naval Academy, 1979

Submitted in partial fulfillment of the
requirements for the degree of

MASTER OF SCIENCE IN METEOROLOGY AND OCEANOGRAPHY

from the

NAVAL POSTGRADUATE SCHOOL
December 1986

ABSTRACT

The Airborne Digital Data Acquisition System (ADDAS) was developed by the joint Naval Postgraduate School/Harvard Unversity research project, called the Ocean Prediction Through Observation, Modeling, and Analysis (OPTOMA) Program, for the real-time synoptic mapping of oceanic features.

Given the capabilities of such a system, an aerial sampling strategy was developed based on the spatial scales of oceanic variables and the aircraft and ADDAS limitations. The strategy was applied to "simulated" AXBT survey flights on "synthetic" fields. The simulated AXBT observations were objectively analyzed and compared to the synthetic field. By varying the simulated AXBT spacing and the objective analysis parameters, an "optimum" AXBT spacing to adequately represent the synthetic structure of the domain was deduced.

To further develop such a system for both airborne and shipboard use, a proposed Ship/Aircraft Data Acquisition, Display, and Analysis System (SADADAS) was presented. The following synoptic mappings produced could provide a possible tactical decision aid for antisubmarine warfare (ASW) operations: 1) Sea surface temperature; 2) Temperature/Sound speed at selected depths; 3) Maps of mixed layer depth; 4) Subsurface ducts/sound channels; and 5) Vertical sections of temperature/sound speed.

TABLE OF CONTENTS

I. INTRODUCTION 11
A. OBJECTIVES 11
B. BACKGROUND 11
C. MOTIVATION 12

II. THE AIRBORNE DIGITAL DATA ACQUISITION SYSTEM (ADDAS) 13
A. ADDAS DEVELOPMENT 13
B. THE PRESENT ADDAS 13
C. ADDAS LIMITATIONS 14
1. Intrinsic Limitations 14
2. Extrinsic Limitations 14
D. SIMILAR SYSTEMS IN USE TODAY 15

III. OCEANOGRAPHIC APPLICATION OF THE ADDAS IN THE OPTOMA PROGRAM 17
A. AXBT SURVEY FLIGHT PLANNING 17
B. AXBT SURVEY FLIGHT EXECUTION 19
1. OPTOMA18P 20
2. OPTOMA20P 27

IV. DEVELOPMENT OF AN AIRBORNE OCEAN SAMPLING STRATEGY 46
A. SAMPLING CONSIDERATIONS 46
1. External Considerations 47
2. Internal Considerations 48
B. GENERAL APPLICATION 49
C. THE OBJECTIVE ANALYSIS TECHNIQUE 49
1. Theory 49
2. ADDAS Software Application 52
3. Possible Problem Areas 57

D. THE OPTOMA PROGRAM SAMPLING STRATEGY 58

V. SIMULATED APPLICATION OF THE SAMPLING STRATEGY 60

A. DEVELOPING THE SYNTHETIC FIELDS 60

B. THE SYNTHETIC FIELDS 62

C. PROCEDURE 62

1. Synthetic Field Generation 62

2. Simulated AXBT Surveys 65

3. Application of Objective Analysis 66

4. Comparisons 66

D. SUMMARY OF RESULTS 67

1. SYNFLD1 67

2. SYNFLD2 75

3. Overall 85

VI. SUMMARY, RECOMMENDATIONS, CONCLUSIONS 89

A. SUMMARY 89

B. RECOMMENDATIONS 89

1. A Proposed Ship-Aircraft Data Acquisition, Display, and Analysis System (SADADAS) 89

C. CONCLUSIONS 92

APPENDIX A: ADDAS HARDWARE COMPONENTS 94

LIST OF REFERENCES 95

INITIAL DISTRIBUTION LIST 97

LIST OF TABLES

1. AXBT EXPENDITURE SUMMARY OPTOMA18P 22
2. AXBT EXPENDITURE SUMMARY OPTOMA20P 34
3. SYNTHETIC FIELD SPECIFIC PARAMETERS 65
4. AUTOCOVARIANCE AND CORRELATION FUNCTION CALCULATIONS, SYNFLD1 67
5. OBJECTIVE ANALYSES SUMMARY, SYNFLD1 75
6. COMPARISON COMPUTATIONS, SYNFLD1 82
7. CALCULATIONS, SYNFLD2 86

LIST OF FIGURES

3.1	OPTOMA Program survey region subdomains. Isobaths are in meters	18
3.2	Flight Plan, OPTOMA18P	21
3.3a	Shallow AXBT Drop Locations, OPTOMA18P. Origin 38°N, 126°W. Tick marks = 25 km	23
3.3b	Depth of the 8-C Isotherm (m), as in Figure 3.3a	24
3.3c	Sea Surface Temperature (°C), as in Figure 3.3a	25
3.3d	Sound Speed at 150 m (m/s), as in Figure 3.3a	26
3.4a	Recovered AXBT Drop Locations, OPTOMA18P	28
3.4b	Depth of the 8° C Isotherm (m), OPTOMA18P. Contour Interval 10 m	29
3.4c	Sea Surface Temperature (°C), OPTOMA18P. Contour Interval, 0.25-C	30
3.4d	Sound Speed at 150 m (m/s), OPTOMA18P. Contour Interval, 0.5 m/s	31
3.5	Flight Plan, OPTOMA20P	32
3.6a	Representative Temperature Profiles, OPTOMA20P	35
3.6b	As in Figure 3.6a	36
3.7a	Shallow AXBT Drop Locations, OPTOMA20P. Origin 38°N, 125°W. Tick marks = 25 km	37
3.7b	Depth of the 8-C Isotherm (m), as in Figure 3.7a	38
3.7c	Sea Surface Temperature (°C), as in Figure 3.7a	39
3.7d	Mixed Layer Depth (m), as in Figure 3.7a	40
3.8a	Recovered AXBT Drop Locations, OPTOMA20P	41
3.8b	Depth of the 8°C Isotherm (m), OPTOMA20P. Contour interval, 5 m	43
3.8c	Sea Surface Temperature (°C), OPTOMA20P. Contour interval, 0.1-C	44
3.8d	Mixed Layer Depth (m), OPTOMA20P. Contour interval, 2 m	45
4.1	Optimum Sampling Strategy Flow Diagram	50
4.2	Flow Diagram of Objective Analysis Inputs	53
5.1	Synthetic field, SYNFLD1 and sample subdomain (dashed line), representing SST in °C. Contour interval 0.5°C	63

5.2 Synthetic field, SYNFLD2 and sample subdomain (dashed line), representing MLD in meters. Contour interval 2.5 m 64

5.3 SYNFLD1, Progression 1, Sample S1-42. (a) Observation positions. (b) Autocorrelations (solid) and fitted function (dashed). 95 % confidence limits (shaded) 68

5.4 SYNFLD1, Progression 1, Sample S1-42X. (a) Observation positions. (b) Autocorrelations (solid) and fitted function (dashed). 95 % confidence limits (shaded) 69

5.5 SYNFLD1, Progression 1, Sample S1-56X. (a) Observation positions. (b) Autocorrelations (solid) and fitted function (dashed). 95 % confidence limits (shaded) 70

5.6 SYNFLD1, Progression 2, Sample S1-42N. (a) Observation positions. (b) Autocorrelations (solid) and fitted function (dashed). 95 % confidence limits (shaded) 71

5.7 SYNFLD1, Progression 2, Sample S1-42XN. (a) Observation positions. (b) Autocorrelations (solid) and fitted function (dashed). 95 % confidence limits (shaded) 72

5.8 SYNFLD1, Progression 2, Sample S1-56XN. (a) Observation positions. (b) Autocorrelations (solid) and fitted function (dashed). 95 % confidence limits (shaded) 73

5.9 SYNFLD1, Progression 1, Sample S1-42. (a) Objective analysis. Contour interval 0.5°C. (b) RMS interpolation error (%) 76

5.10 SYNFLD1, Progression 1, Sample S1-42X. (a) Objective analysis. Contour interval 0.5-C. (b) RMS interpolation error (%) 77

5.11 SYNFLD1, Progression 1, Sample S1-56X. (a) Objective analysis. Contour interval 0.5-C. (b) RMS interpolation error (%) 78

5.12 SYNFLD1, Progression 2, Sample S1-42N. (a) Objective analysis. Contour interval 0.5-C. (b) RMS interpolation error (%) 79

5.13 SYNFLD1, Progression 2, Sample S1-42XN. (a) Objective analysis. Contour interval 0.5-C. (b) RMS interpolation error (%) 80

5.14 SYNFLD1, Progression 2, Sample S1-56XN. (a) Objective analysis. Contour interval 0.5-C. (b) RMS interpolation error (%) 81

5.15 SYNFLD2. Sample observations (open symbols) and objective analysis interpolation points (dots) 83

5.16 Correlation functions as used with SYNFLD2 84

5.17 SYNFLD2, Run A2 (a) Objective analysis (m). (b) RMS interpolation error (%) 87

5.18 SYNFLD2, Run B2 (a) Objective analysis (m). (b) RMS interpolation error (%) 88

ACKNOWLEDGEMENTS

I would especially like to thank my co-advisors, Professor Chris Mooers and Dr. Gordon Groves, for their support, motivation, and guidance throughout the past year. Special thanks go to Dr. Michele Rienecker for her patience and direction in the computer programming aspects, especially in the area of objective analysis, as well as for most of the computer programs used. Additionally, I would like to thank Ms. Marie Colton for her knowledge of, and work with the Airborne Digital Data Acquisition System (ADDAS) on the OPTOMA18 survey flight, which provided the background for this work. Also, Mr. Paul Wittmann deserves special recognition for the behind-the-scenes logistics for the both the OPTOMA18 and OPTOMA20 survey flights, as well as the editing and storage of the flight data which is a major part of this thesis.

I. INTRODUCTION

The development of an Ocean Descriptive/Predictive System (ODPS) for the study and forecasting of oceanic synoptic mesoscale features and the study of the California Current System are the goals of the Ocean Prediction Through Observation, Modeling, and Analysis (OPTOMA) Program, a cooperative effort between the Naval Postgraduate School (NPS) and Harvard University. The Airborne Digital Data Acquisition System (ADDAS) was developed at NPS in response to the need for a real-time, large-scale synoptic mapping of the mesoscale features for both the initialization of dynamic model forecasts and the verification of the dynamic models used.

A. OBJECTIVES

To develop a system such as the ADDAS for use in operational antisubmarine warfare (ASW) is the primary objective of this thesis. With the capabilities of such a system: 1) What optimal aerial sampling strategy should be utilized to acquire oceanic data for naval planning and operations? 2) What further enhancements could be developed for a system like the ADDAS, and how could such a system be applied to shipboard operations as well? 3) What operationally applicable synoptic fields can be developed from the data, and how could such fields be applied in planning and execution of Naval operations, specifically in ASW?

B. BACKGROUND

With the availability of expendable aircraft deployable instruments such as airborne expendable bathythermographs (AXBTs), sound speed profilers (AXSVPs), current profilers (AXCPs), and soon-to-be-available air-launched conductivity, temperature, depth profilers (AXCTDs), the aircraft is the platform of choice for near real-time data acquisition. The P-3 Orion ASW patrol aircraft supports a system such as the ADDAS exceptionally well. It has the payload capacity and avionics for air launched sensors as well as substantial on-station endurance and all-weather capability. It can cover a sizable oceanic region in a matter of hours as compared to days for a research vessel. The ADDAS has been deployed on six OPTOMA P-3 missions to date and is a proven (research) operational system. It has been invaluable as a primary

means of data acquisition for the OPTOMA Program. Additionally, carrier-based ASW aircraft such as the S-3 Viking, and rotary-wing ASW aircraft including the SH-2 Sea Sprite, SH-3 Sea King, and the SH-60 Seahawk, can provide additional airborne sensor deployment platforms.

C. MOTIVATION

The capability for near real-time mapping of oceanic variables has a direct application to ASW operations. As submarines become quieter, the warfare commander will have an even more difficult task of localizing and tracking them. An increased knowledge of the submariners' environment will be required. An AXBT survey flight can provide a "nowcast" of the region for use in tactical briefings, and such planning should be a key factor in ASW operations. With maps from such AXBT surveys, the effects of the ocean structure on standard tactics can be addressed and appropriate modifications to tactical doctrine can be suggested. Additionally, subsequent survey flights could be completed to identify the temporal and spatial changes over the course of the exercise or operation and to refresh the original survey.

Traditionally, ASW tactics and training are based on a "generic" ocean structure, and usually only one or two AXBT's are deployed in an exercise which tends to reenforce this concept. One may argue that a single AXBT could be representative of the ocean thermal structure in some region. However, if an AXBT was deployed in the middle of an eddy or in an area of strong temperature gradients, as are observed in the Gulf Stream, it may not be representative of that region. In the research field, the ADDAS has proved itself as a powerful tool. It is time for this capability to be developed for operational use in the fleet.

The current version of the ADDAS and similar systems in use today are presented, followed by the oceanographic application of the ADDAS in the OPTOMA Program. Next, an optimal aerial sampling strategy is developed and applied to "synthetic" oceanic domains and compared through use of the objective analysis technique. A proposed Ship/Aircraft Data Acquisition, Display, and Analysis System (SADADAS) concludes, with application to both land-based and shipboard aircraft operations.

II. THE AIRBORNE DIGITAL DATA ACQUISITION SYSTEM (ADDAS)

A. ADDAS DEVELOPMENT

The OPTOMA Program's Airborne Thermal Structure Mapping Project at NPS culminated with the development of the ADDAS and its successful research use. In the early survey flights of this project, AXBT analog traces were recorded onboard the P-3 aircraft by the AQA-7 lofargram system recorder. The traces were hand digitized using gridded templates based on the standard Navy frequency-to-temperature and fall-rate-to-depth equations. This produced traces of coarse resolution and resulted in a substantial time-lag for the generation of "real-time" synoptic maps.

At the Scripps Institute of Oceanography, Mr. Meredith H. Sessions had developed a system for the recording and real-time digital conversion of an AXBT analog signal, which had been used successfully in the North Pacific Experiment (NORPAX) (Sessions, 1980). The Scripps system was made available to the OPTOMA Program and was used for the post-flight digitization of analog tape recordings of the AXBT signals acquired by the OPTOMA11P flight on 18 July 1984. Inspired by the relative ease of data acquisition and the improved resolution of AXBT profiles provided by the Scripps system, as well as the recent development of an AXBT digitizing circuit for the Sippican MK9 digitizing unit, a prototype ADDAS became feasible and was developed at NPS (Colton and Mooers, 1985). First deployed on the OPTOMA13P flight on 27 October 1984, the ADDAS has proven invaluable in acquiring real-time data for synoptic mappings and model initialization.

B. THE PRESENT ADDAS

The ADDAS is a self-contained, semi-portable data acquisition, processing, and analysis system. It utilizes off-the-shelf hardware and modified shipboard XBT and CTD data acquisition and analysis software developed by the OPTOMA Program at NPS. The heart of the system is a HP9816 MC68000 16-bit microprocessor with a HP9121 dual 3.5 inch microfloppy disk drive. Aircraft 28 VDC power is inverted to 115 VAC, 60 Hz power by an internal static inverter. AXBT drop positions can be entered either manually by the operator through the computer keyboard (latitude and longitude, as determined by the Tactical Coordinator/Navigator from aircraft inertial navigation) or automatically by the ADDAS's optional LORAN C unit. The AXBT

audio signal is received through the ARR-72 aircraft sonobuoy receiver, digitized in real-time by a Sippican MK9 front-end processor, and the trace is displayed on the computer monitor. Once the AXBT has completed its fall, the digitized profile is stored on a data diskette. Currently, the ADDAS is capable of digitizing only one AXBT at a time. To simulate a multi-channel capability, one channel of a stereo hi-fi video cassette recorder (VCR) is used to record the simultaneous audio signal from a second AXBT (of different VHF carrier channel) for post-flight digitization and analysis. The audio signal of the digitized AXBT is also recorded on the other VCR channel as a backup. An oscilloscope provides a visual display of the AXBT audio signal to help detect failures both in the aircraft sonobuoy receiving system and in the AXBTs. Once the survey is complete, maps of objectively analyzed variables are produced on the monitor and hard-copy output is generated by a HP7470A two-pen plotter, either on the return flight or on the ground. A list of ADDAS hardware components and their current retail cost is included in Appendix A.

C. ADDAS LIMITATIONS

Limitations to the system can be classed into two categories, intrinsic and extrinsic. These limitations affect ADDAS operation and ultimately the density of AXBT coverage in a survey.

1. Intrinsic Limitations

These limitations are specifically inherent in the system design and operation. They are:

- Not multi-channel capable (presently). Two AXBT's of different channels cannot be digitized simultaneously. An additional MK9 or the development of a multi-channel MK9 would be required. In addition, an advanced microprocessor with a multi-tasking capability is required. These are very feasible with today's technology.
- No hardware redundancy. Although the system has proven exceptionally reliable, if one component should fail the real-time capability will be lost.
- Inverter operation. The inverter is rated at 5.6 amps. With only the microprocessor, disk drives, MK9, and VCR in the circuit, the inverter operates at 6.3 amps continuous. This has not been a problem to date since the VCR is only used during data acquisition and it is disconnected when the plotter is being used. An inverter with a higher current rating may be required.

2. Extrinsic Limitations

These limitations affect the overall capability of the system to perform its given mission and are related to the sampling platform and the sensors employed. They are:

- Aircraft weight and balance. Aircraft are constrained by a maximum gross weight for take off. It is a function of the environmental conditions at the

departure point. For navy aircraft, these limitations are specified in the respective NATOPS (Naval Air Training and Operations Procedures Standardization) Manual for each aircraft type and govern safety of flight. In order to carry enough fuel to complete the mission, and have the required reserve fuel at landing, there may need to be a reduction in the number of AXBT's or other sensors to be deployed in order to remain within NATOPS limitations.

- Aircraft airspeed and altitude. These factors affect aircraft fuel consumption. Aircraft engines operate more efficiently at high altitude yet the ADDAS requires a lower altitude for effective operation. A compromise is made. Normally, transit to and return from the survey region will is accomplished at high altitude (> 10,000 ft MSL) and at an optimum speed (~310 kts indicated airspeed). Once on-station, the aircraft will be operated at loiter airspeed (180 to 210 kts) and altitude will normally be between 500 and 1000 ft AGL (above ground level). This will cover as large an area as possible, and provide for optimum ADDAS performance. Aircraft altitude affects the time it takes for the AXBT to impact the water after deployment from the aircraft and the line-of-sight radio transmission range. At higher altitudes, the transmission range is increased and interference from other sensors on the same RF channel may affect the AXBT transmission. Airspeed and altitude must be considered in fuel planning (weight and balance) for the mission. Additionally, safety of flight requirements as specified by NATOPS and squadron SOP (standard operating procedures) may require higher altitudes for certain evolutions such as pilot changes.

- AXBT fall duration through the water; for shallow (300 m) and deep (760 m) AXBT's, 200 and 500 seconds, respectively (Sessions, *et al.*, 1976, Bane and Sessions, 1984).

- Number of AXBT channels. Only three channels, 12, 14, and 16 (corresponding to 170.5, 172.0, and 173.5 Mhz, respectively.) are currently manufactured (Gent, 1982). Two or more AXBT's of the same channel must not be deployed within the line-of-sight RF transmission range. The conflicting signals can trigger the MK9 and result in the loss of a profile. It is basically a function of aircraft altitude and speed.

- External radio interference on AXBT carrier channels. Once the MK9 is initialized and awaiting the AXBT signal, spurious radio transmissions on the receiving channel can pre-trigger the MK9 and the digitized profile may be lost.

D. SIMILAR SYSTEMS IN USE TODAY

In addition to the Scripps system, the Naval Ocean Research and Development Activity (NORDA) also has a similar system, the Airborne Data Acquisition and Processing System (ADAPS) (Miles, 1984). ADAPS is currently used by NAVOCEANO for work in acoustics. These systems were designed for specific missions and are multi-channel capable. The organizations have the advantage of a technical staff and maintenance support, and as a result these systems are one-of-a-kind in design and operation. The NPS ADDAS, in comparison, utilizes totally off-the-shelf hardware. It also has the added capability of being employed in shipboard XBT surveys as well with a modified software package and different digitizing circuit board for the MK9. However, the ADDAS is limited in that it is only single-channel capable at the present. With further advances in expendable sensors, off-the-shelf digitizing units, and computer systems capable of multi-tasking, systems

such as the ADDAS, ADAPS, and the Scripps system can become available to the Naval Oceanographer and research community to more fully describe the oceanic environment.

III. OCEANOGRAPHIC APPLICATION OF THE ADDAS IN THE OPTOMA PROGRAM

Near-real-time synoptic mappings of the mesoscale eddy field are a key facet in the observational network of an ODPS. These mappings, using data acquired through the OPTOMA Program's AXBT survey flights, provide nowcasts of the mesoscale variablity in the OPTOMA domains which are used for shipboard survey planning, dynamic model initialization, model forecast verification, and assessment of the interannual variability in the domains.

The NOCAL (Northern California) and CENCAL (Central California) subdomains are the major survey regions for the OPTOMA program (Figure 3.1). Each subdomain is an open ocean region in the California Current System (CCS) about 150-km square with water depths of the order of 4 km. The NOCAL subdomain, 150-km downstream from the Mendocino Escarpment and about 150-km offshore, is the primary survey subdomain. Its bottom topography is characterized by a gently sloping seafloor and no seamounts, although seamounts, the Mendocino Escarpment, and the continental margin are nearby. NOCAL is the simplest domain that can be found off California for a region this size (Mooers, 1986). AXBT survey flights generally expand the subdomains to about 260-km square in order to acquire sufficient data to initialize the boundary conditions for model runs.

A. AXBT SURVEY FLIGHT PLANNING

As with any oceanographic survey, planning is essential for the successful completion of the mission. Formal tasking for research flights is requested through the chain of command from the research sponsor. AXBT survey flights are then scheduled on a not-to-interfere basis and are contingent upon the operational tasking of the patrol wing. Once flight time has been authorized, coordination with the Patrol Wing Schedules Officer, preferably two to three months in advance of the date of the proposed survey flight, should begin. Flexibility is the key, and periodic contact should be maintained at least bi-monthly as changes in operational commitments (within both parties) may require the rescheduling of the flight. One month prior to the flight, a draft flight plan is prepared, and required mission personnel, supplies, equipment, and transportation are identified. Within two weeks of the flight, the Schedules Officer

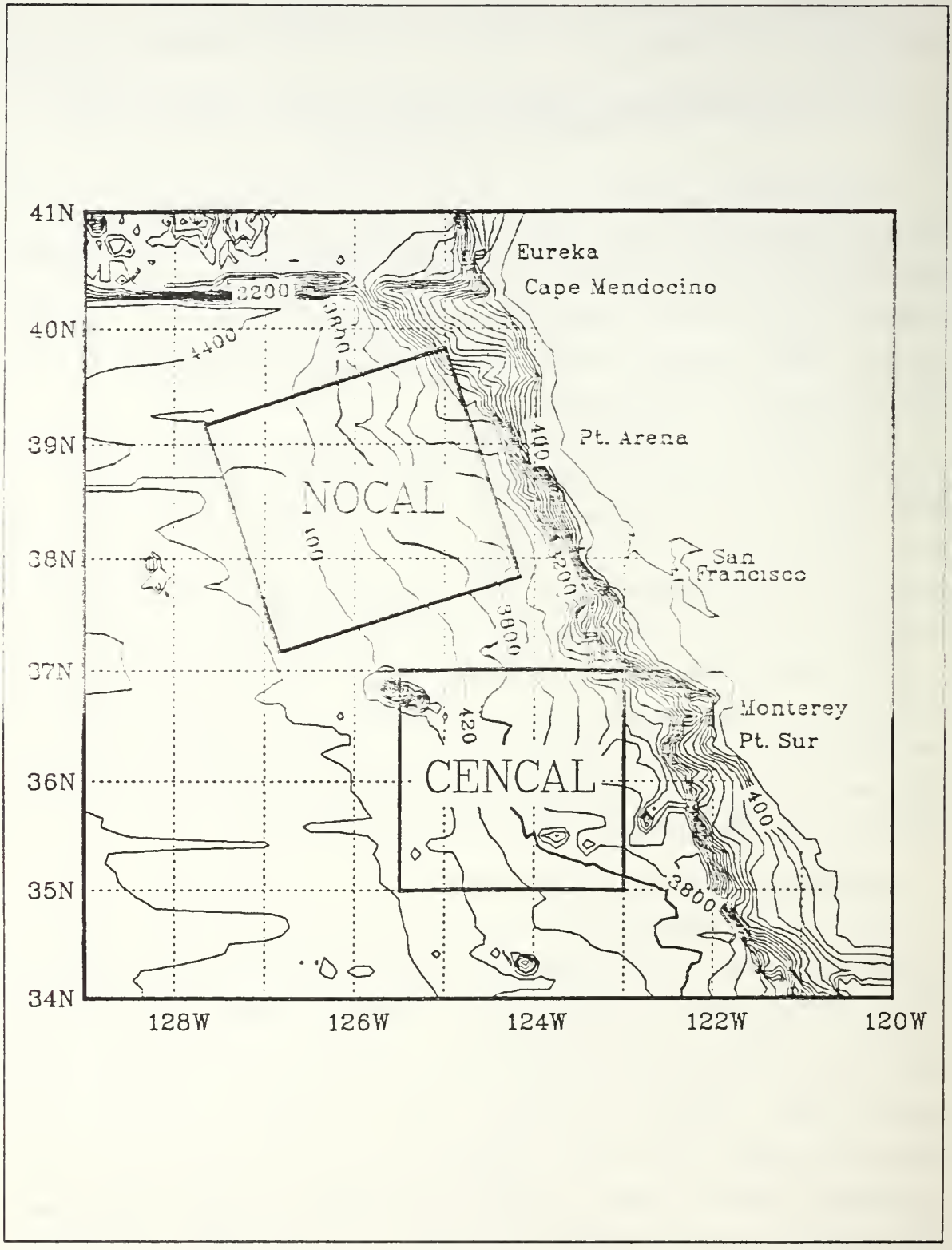

Figure 3.1 OPTOMA Program survey region subdomains. Isobaths are in meters.

should know which squadron will be tasked to provide the services. Coordination is now primarily with the squadron.

The proposed flight plan should be discussed with the squadron Operations Officer and Schedules Officer. Changes for safety-of-flight, number of AXBT's to be deployed, and the planned flight itinerary should be included in the revised flight plan. Additionally, squadron personnel should be requested for unloading and preparing the AXBT's for the flight and loading them onto the aircraft.

B. AXBT SURVEY FLIGHT EXECUTION

OPTOMA survey flights have generally deployed between 70 and 96 AXBT's per mission. Once on station in the survey subdomain, AXBT's are normally launched at 15 nautical mile (NM) intervals, alternating shallow and deep AXBT's. The SSQ-36A AXBT is manufactured in two factory-set depths, 305 m (currently the Navy standard AXBT) and 760 m (primarily used for research). The shallow AXBT's are digitized in real-time and stored by the ADDAS, while the deep AXBT's are recorded on tape for post-flight digitizing. A flight log is maintained with specific information about each drop: time, latitude, longitude, remarks. All shallow AXBT's are of one channel, while all the deep AXBT's are of a different channel. This limits the radio interference between AXBT drops since only two channels, 14 and 16, can be used in the OPTOMA survey regions. (Channel 12 is not used as it is the California Forest Service emergency broadcast channel.)

With the survey completed, the stored AXBT profiles are read and the desired output variables; e.g., sea surface temperature (SST), mixed layer depth (MLD), depth of the 8°C isotherm (D8C), sound speed at a chosen depth (CSZ), or dynamic height relative to a specific depth (DHZ), are selected. These variables are then entered into a statistical objective analysis routine based on an application by Carter and Robinson (1981). A discussion of the objective analysis technique as it is applied in the ADDAS software is presented in Chapter IV. This technique uses a two-dimensional correlation function based on the statistics of the data set. The five most correlated values within a 55 km radius of an interpolation point are then used to compute a value at the interpolation point. Contoured maps of the selected fields are then generated and printed on the plotter. These plots are available prior to landing so that an immediate debrief can be accomplished. Upon return to NPS, the recorded deep AXBT's are digitized and added to the data set. The objectively analyzed fields are then generated on the IBM 3033 mainframe using both the shallow and deep AXBT's.

The most recent AXBT survey flights were OPTOMA18P consisting of two consecutive flights on 31 October and 2 November 1985, and OPTOMA20P on 16 March 1986. Summaries of each mission and the data acquired are presented below.

1. **OPTOMA18P**

Aircraft and flight crews were provided by Patrol Squadron Forty-Six, assigned to Commander, Patrol Wing Ten, for the 31 October flight and Patrol Squadron Ninety-One, assigned to Commander, Reserve Patrol Wing Pacific Fleet, for the 2 November flight. Both are based at NAS Moffett Field. The flight tracks were executed as planned (Figure 3.2). A total of 180 AXBT's were deployed on the two flights. Spacing was at 15 NM intervals, alternating deep (Ch. 16) and shallow (Ch. 14) AXBT's. On-station ground speed averaged 200 kts for each flight and the altitude varied between 500 and 800 ft AGL, depending on the low-level visibility. The logged positions were obtained from the aircraft inertial navigation system with an accuracy of 2 NM (~4 km).

a. Mission Critique

Two different models of the P-3 aircraft were utilized on the flights: a P-3C on 31 October, and a P-3B on 2 November. The following differences are noted between the two models for ADDAS installation:

- The 28VDC power connections in the P-3C were made to terminal board 426 (TB426) located just aft of sensor station 2 (SS2) bulkhead. The terminals used were C10 (+28VDC power SS2) and C11 (ground). In the P-3B, power connections were made to TB431 located above SS2. Terminal A24 provided +28VDC power while the ground was a stud located on the far right side of the terminal board. The sonobuoy pin connections were the same for both models of aircraft. (Please see Colton and Mooers, 1985, for a complete description of ADDAS installation.)
- The P-3C model does not have a LORAN system incorporated into its avionics package. Thus, no LORAN antenna was available to be connected to the ADDAS LORAN unit, so all AXBT positions were obtained from the inertial navigation system and checked against the OMEGA radio navigation unit.
- The physical internal layout of the P-3C is different from the P-3B. There is much less room for the ADDAS and operator in the P-3C at sensor station 2 due to the bulkhead separating stations. The ADDAS operator had to work literally "shoulder to shoulder" with the sensor station 1 operator.

The 31 October flight with Patrol Squadron Forty-Six went very well. Since the ADDAS LORAN was not used, the positions of each AXBT drop were taken from the inertial navigation and entered manually into the AXBT program.

The 2 November flight proceeded very smoothly due to the experience gained by Patrol Squadron Ninety-One from previous OPTOMA flights. ADDAS installation was completed in a record time of forty minutes. AXBT positions were

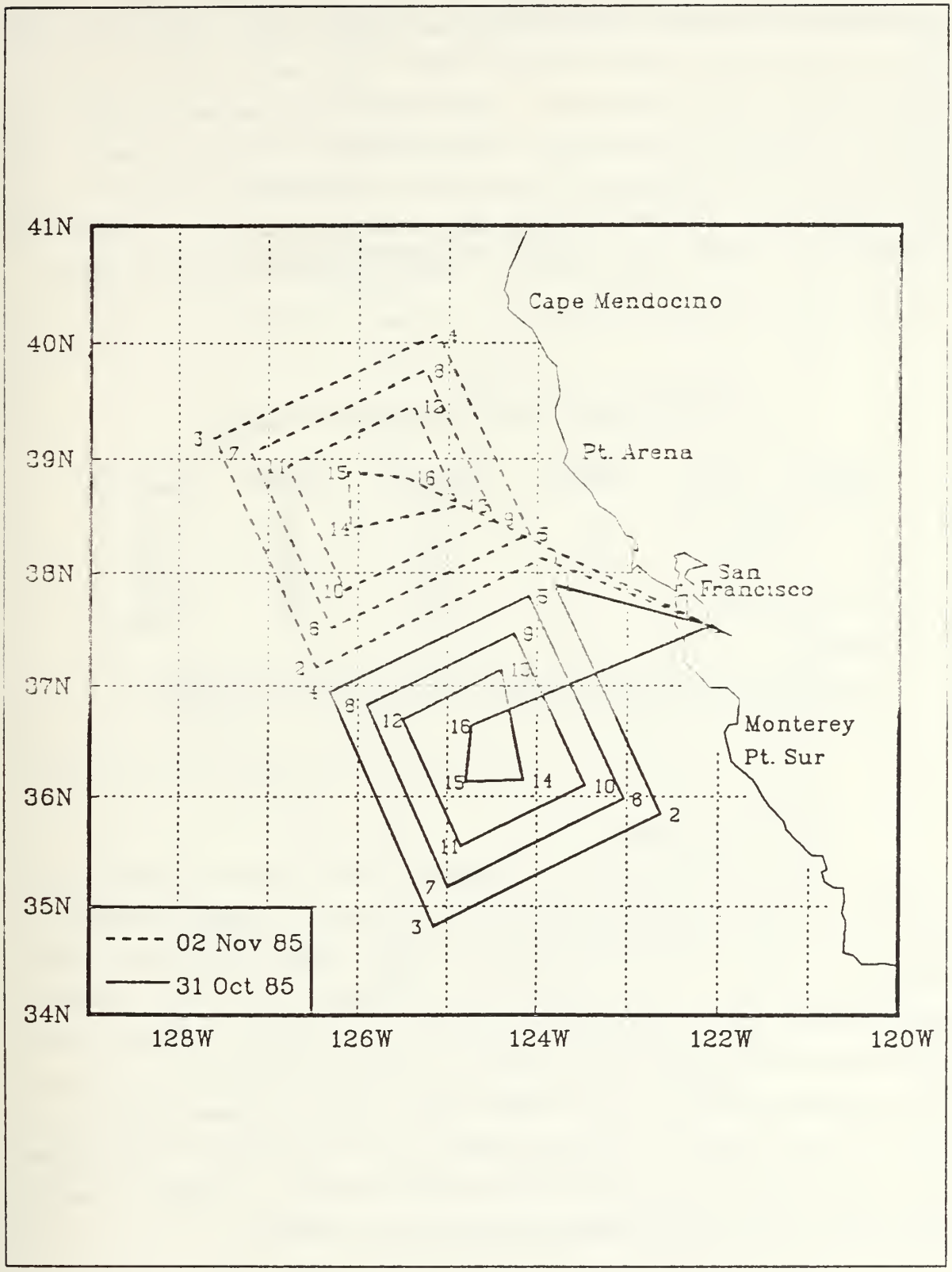

Figure 3.2 Flight Plan, OPTOMA18P.

obtained as on 31 October due to problems encountered on previous flights with RF interference from aircraft radios affecting the LORAN signal. The only notable difficulty on this flight was that a low-level (500 ft) stratus deck required an on station altitude of 800 ft AGL for flight safety. This increased the transmission range of the AXBT's. On the first southbound leg, a tailwind increased aircraft groundspeed to 235 kts and resulted in pre-triggering of the MK9 due to overlapping AXBT signals on the same channel. On subsequent downwind legs, airspeed was adjusted to maintain 200 kts groundspeed. Table 1 lists a summary of AXBT expenditures for the two flights.

TABLE 1

AXBT EXPENDITURE SUMMARY OPTOMA18P

Flight	Area	Channel	Deployed	Failed [1]	Recovered
31 Oct	CENCAL	16	45	6	39
		14	44	4	40
2 Nov	NOCAL	16	46	6	40
		14	45	4	41
Two-day Total:			180	20	160

Notes:

[1] Due to no radio signal transmission and late light-off of the probe.

b. AXBT Survey Results

The uncorrected positions of the shallow AXBT's, from the 31 October and the 2 November flights, and the analyses of D8C, SST, and CS150 that were generated onboard the aircraft on the return leg from the 2 November flight were examined (Figures 3.3a, 3.3b, 3.3c, 3.3d, respectively). A compiled version of the objective analysis program, using a floating-point accelerator was applied. Only the shallow AXBT data (30 NM spacing) were combined to produce the analyses. The data were used as received and digitized by the ADDAS without editing or filtering performed on profiles in order to provide a real-time analysis on the return flight to NAS Moffett Field. Some quality checks are made by the ADDAS software. A complete summary of the acquired AXBT data is presented by Wittmann *et al.* (1986).

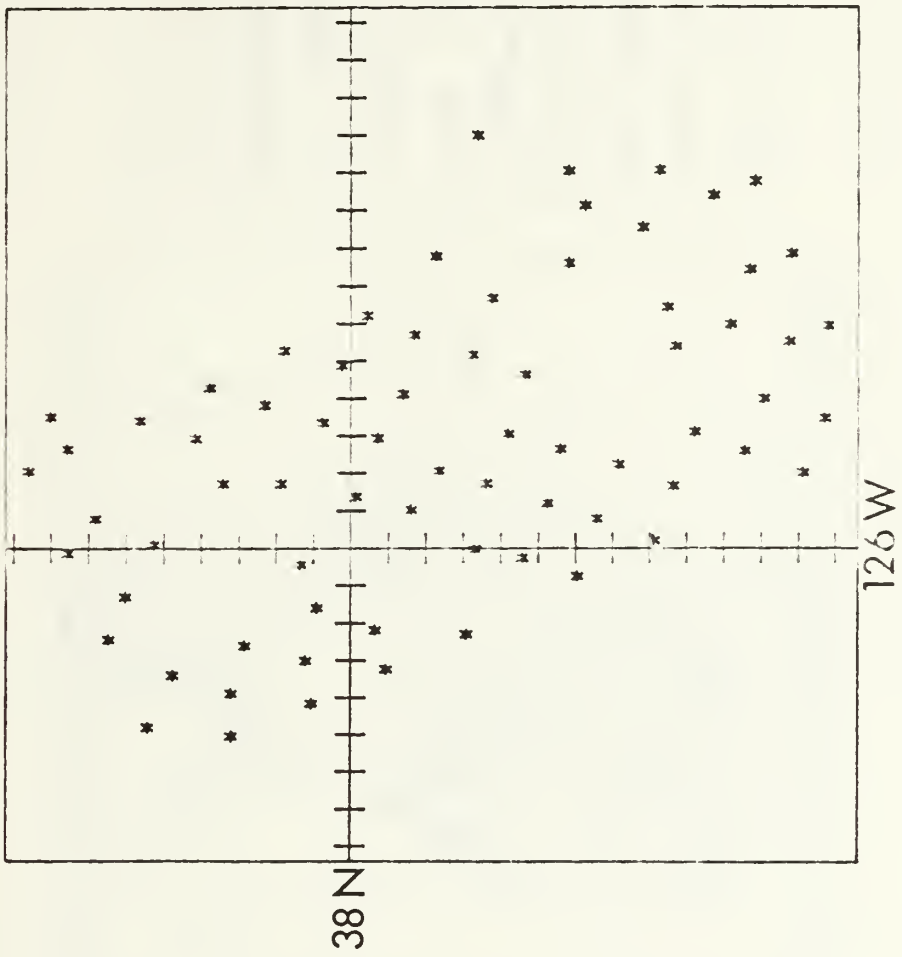

Figure 3.3a Shallow AXBT Drop Locations, OPTOMA18P.
Origin 38°N, 126°W. Tick marks = 25 km.

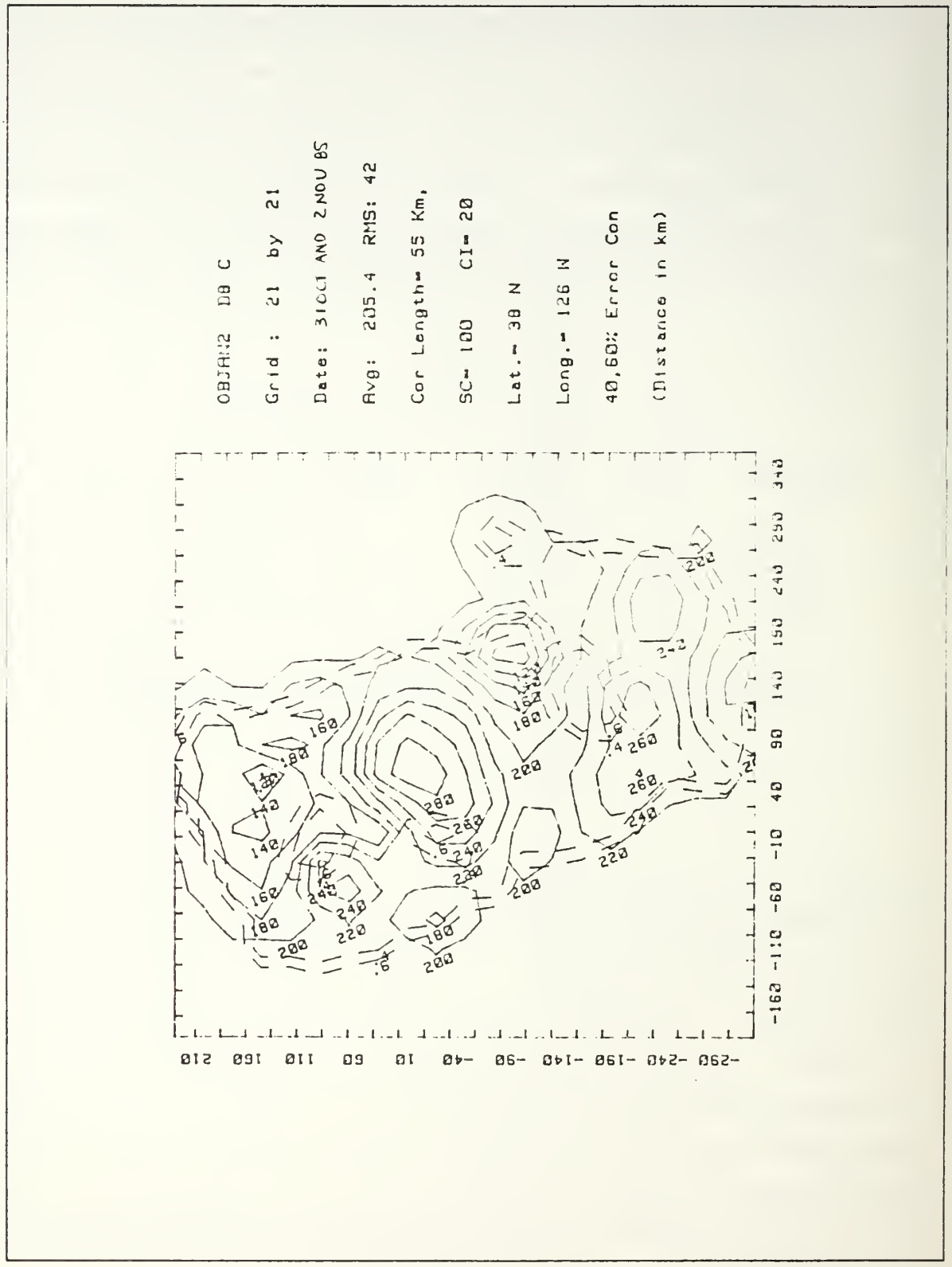

Figure 3.3b Depth of the 8°C Isotherm (m), as in Figure 3.3a.

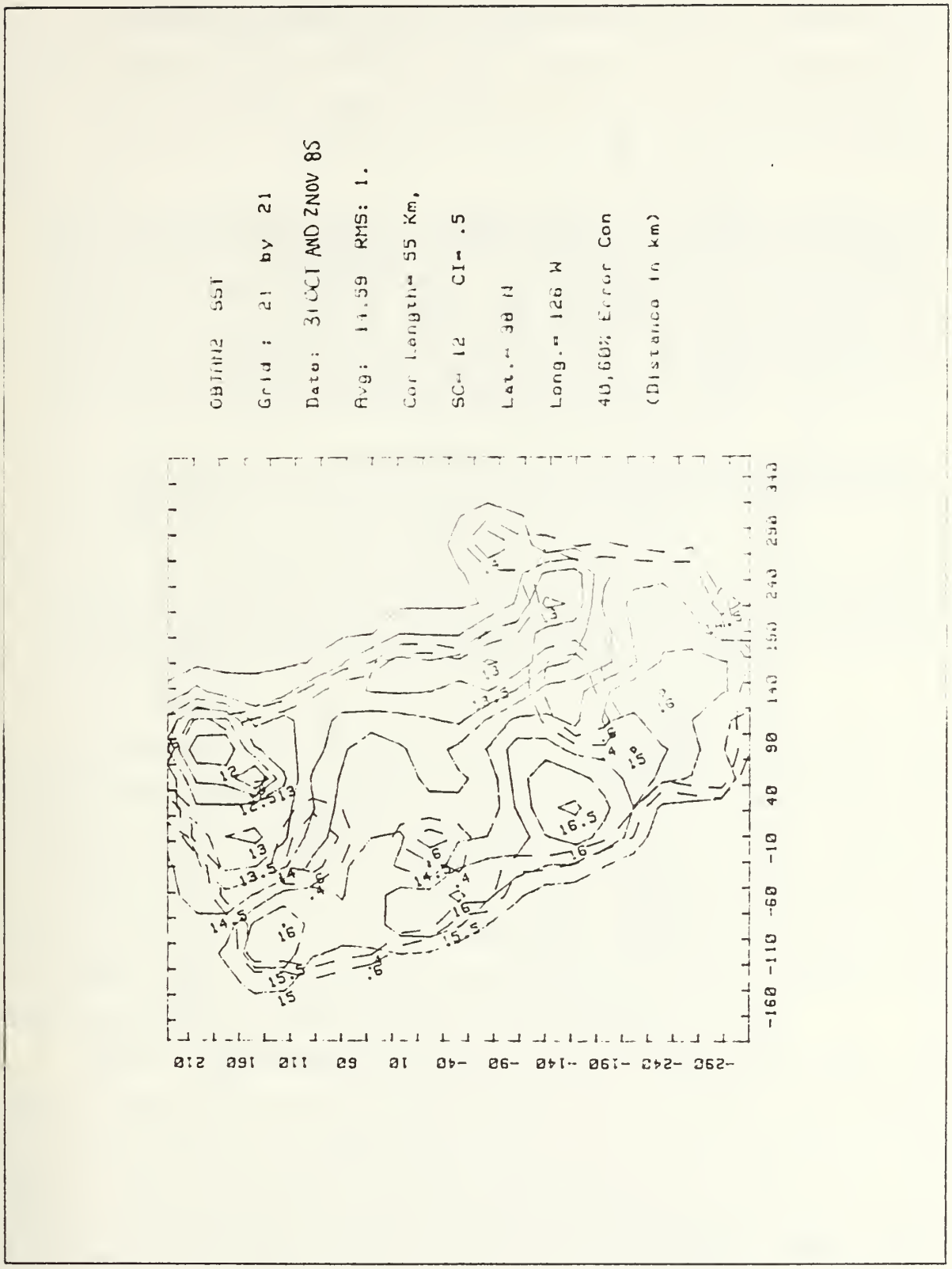

Figure 3.3c Sea Surface Temperature (°C), as in Figure 3.3a.

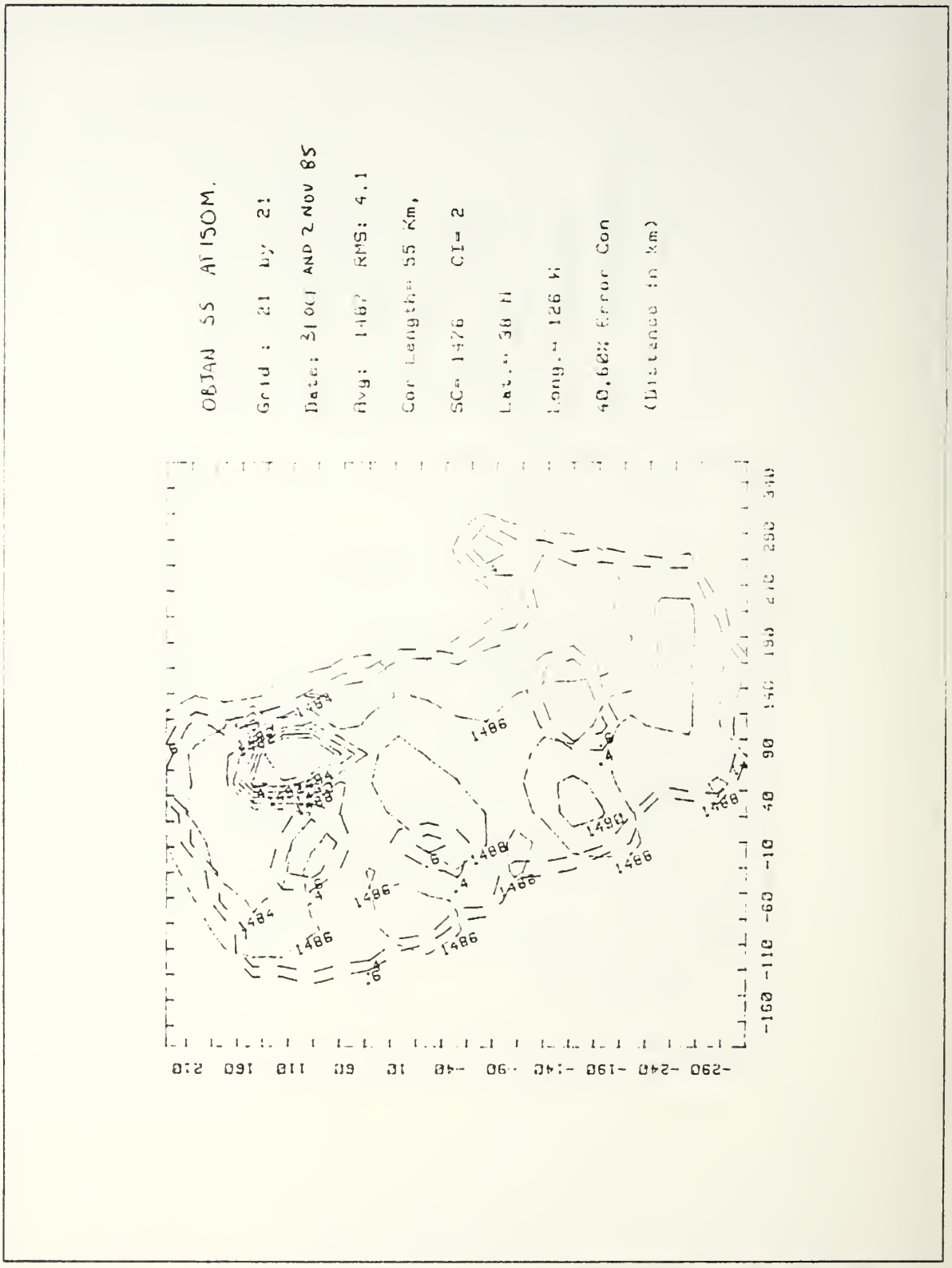

Figure 3.3d Sound Speed at 150 m (m/s), as in Figure 3.3a.

The inflight digitized channel 14 AXBT data were later combined with post-flight digitized channel 16 AXBT at NPS. These data were stored and processed on the IBM 3033 mainframe computer. Profiles were edited to remove spikes, and bad profiles were eliminated. Post-flight, the recovered AXBT locations were examined (Figure 3.4a).

- D8C, meters (Figure 3.4b): This analysis presents a "topographic" map of the depth of the 8°C surface, which is generally accepted as a good indication of the location of the permanent thermocline and pycnocline for this region. From the D8C analyses, the streamfunction for the surface geostrophic flow can be inferred with good accuracy. The major features were two cyclones and two anticyclones (indicated by "C's" and "A's", respectively), alternating along the coast. The cyclone at the far north and the anticyclone at the far south were fairly weak compared to the cyclone close to the coast near Point Reyes (diameter about 100 km, depth variation of over 60 m) and the stronger anticyclone off Point Arena (diameter about 150 km, depth variation of over 60 m). The juxtaposition of these eddies contributed to alternating onshore and offshore flow.

- SST, °C (Figure 3.4c): The main features are two cold core centers (indicated by "X's") near the coast and a generally weak positive offshore temperature gradient. The cold core center in the south of the sampled region was elongated, parallel to the coast, whereas that in the north of the sampled region (near Cape Mendocino) was more circular, slightly elongated offshore.

- CS150, m/s (Figure 3.4d): Sound speed was computed using a constant salinity of 33.5 ppt. The sound speed is fairly constant with only a 6 m/s variability, although there is an obvious correlation between sound speed patterns and the eddy patterns of the depth of the 8 degree isotherm. The strong feature evident in Figure 3.3d just to the south of the northernmost cold center was a problem with the data which was eliminated in the post-flight data processing.

2. OPTOMA20P

A combined flight crew from the Naval Air Reserve Center and Patrol Squadron Ninety-One at NAS Moffett Field performed the mission. The flight plan was executed as shown in Figure 3.5. The ten flight tracks were spaced 15 NM apart. Ten AXBT's were deployed along each track at a 15 NM spacing, with the exception of only eight AXBT's deployed on tracks 1 and 10 (no AXBT's were deployed at the corners of the survey region), for a total of 96 AXBT's. Groundspeed averaged 220 kts and on-station altitude varied between 500 and 2000 ft AGL for safety of flight due to turbulence and scattered convective activity and thunderstorms in the area.

AXBT's were to be deployed alternating channel 16 (deep, 760 m probe) and channel 14 (shallow, 305 m probe). Due to inventory error, all AXBT's for this flight, both channel 14 and 16, were shallow (305 m). This was not realized until the first few channel 16 AXBT's were deployed and their time of fall observed. AXBT's were then launched at approximately four minute intervals, alternating between channel 16 and 14 AXBT's. AXBT positions were obtained from the aircraft inertial navigation system (2 NM accuracy) and entered in the flight data log. The positions were not corrected

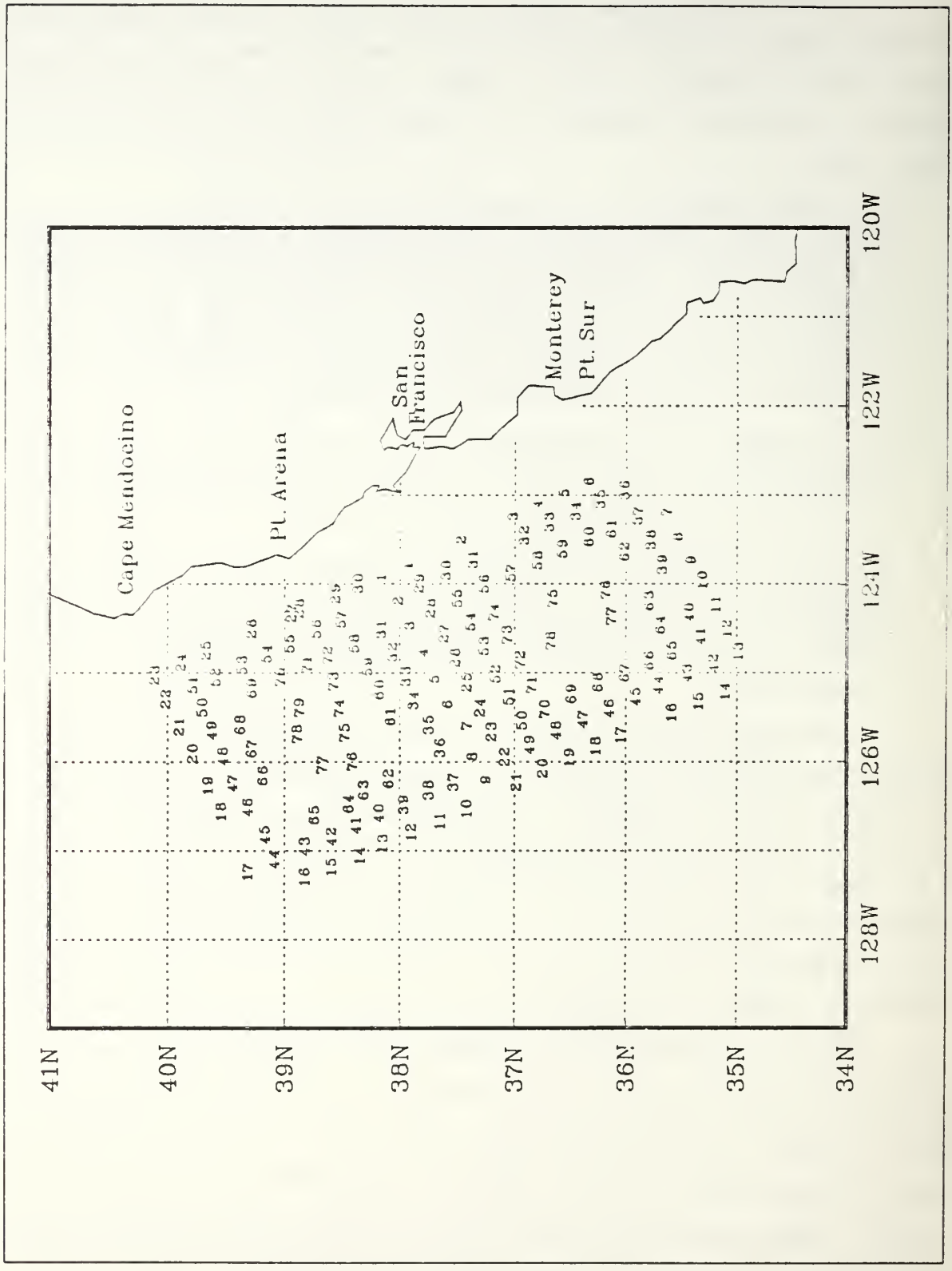

Figure 3.4a Recovered AXBT Drop Locations, OPTOMA18P.

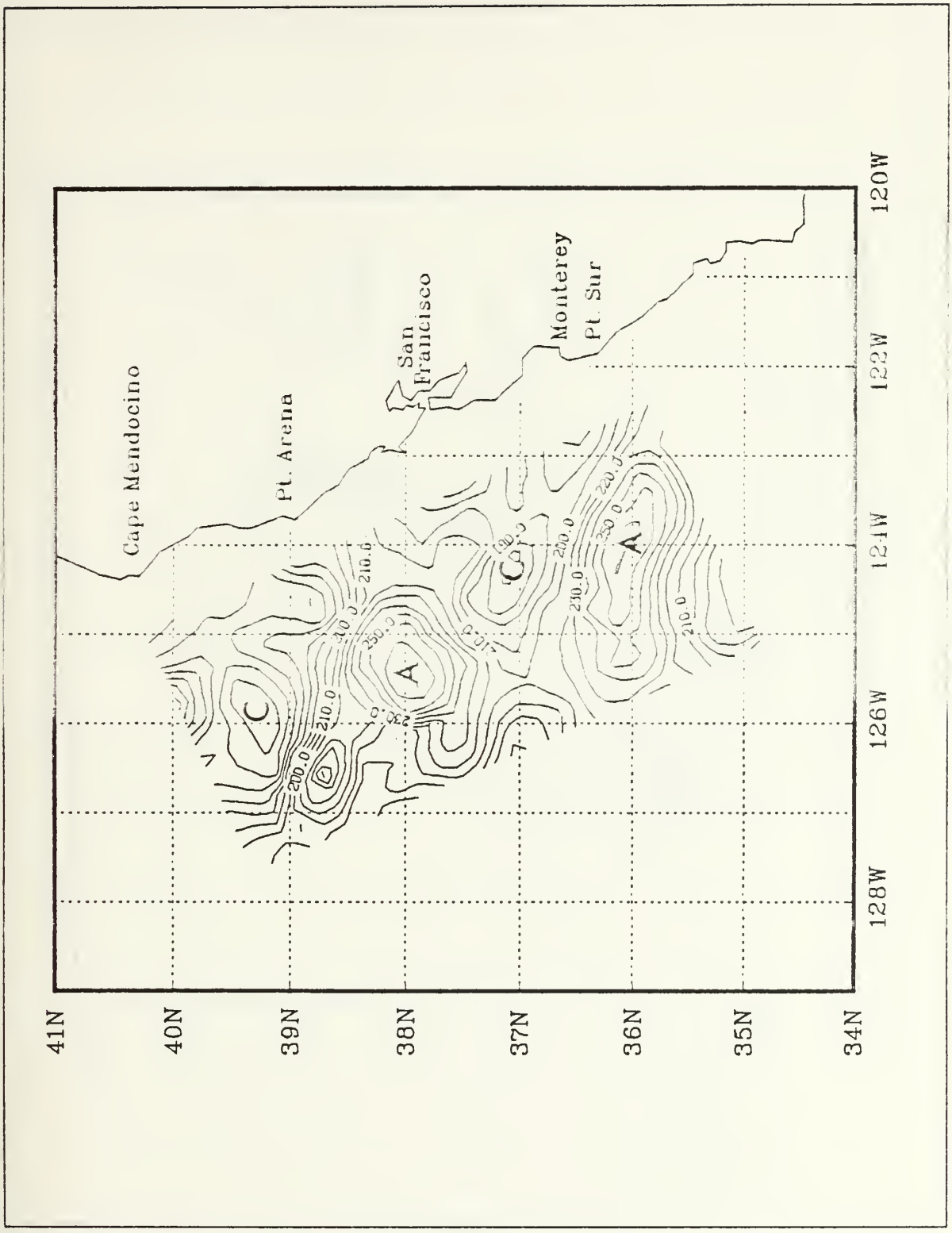

Figure 3.4b Depth of the 8° C Isotherm (m), OPTOMA18P.
Contour Interval 10 m.

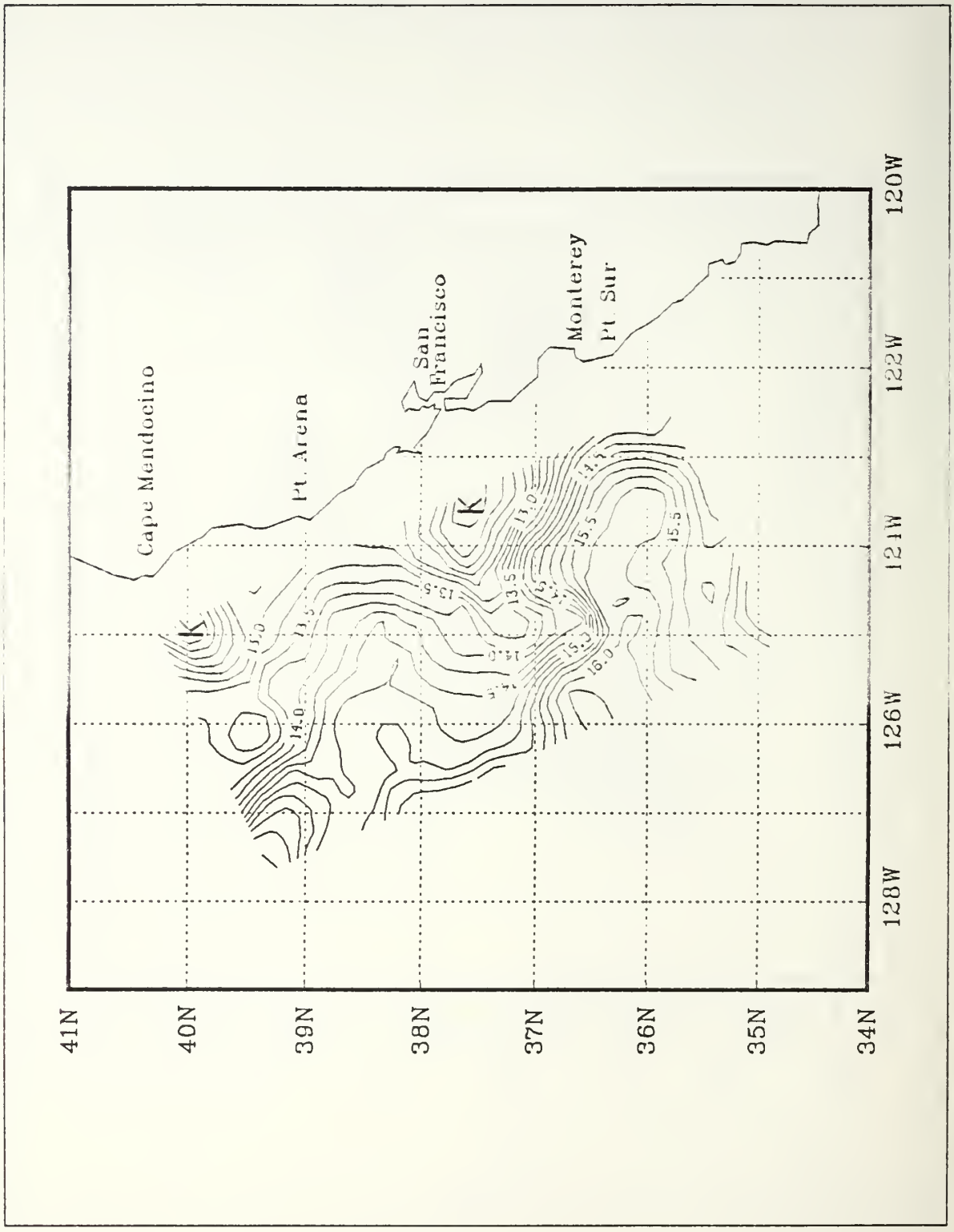

Figure 3.4c Sea Surface Temperature (°C), OPTOMA18P.
Contour Interval, 0.25°C.

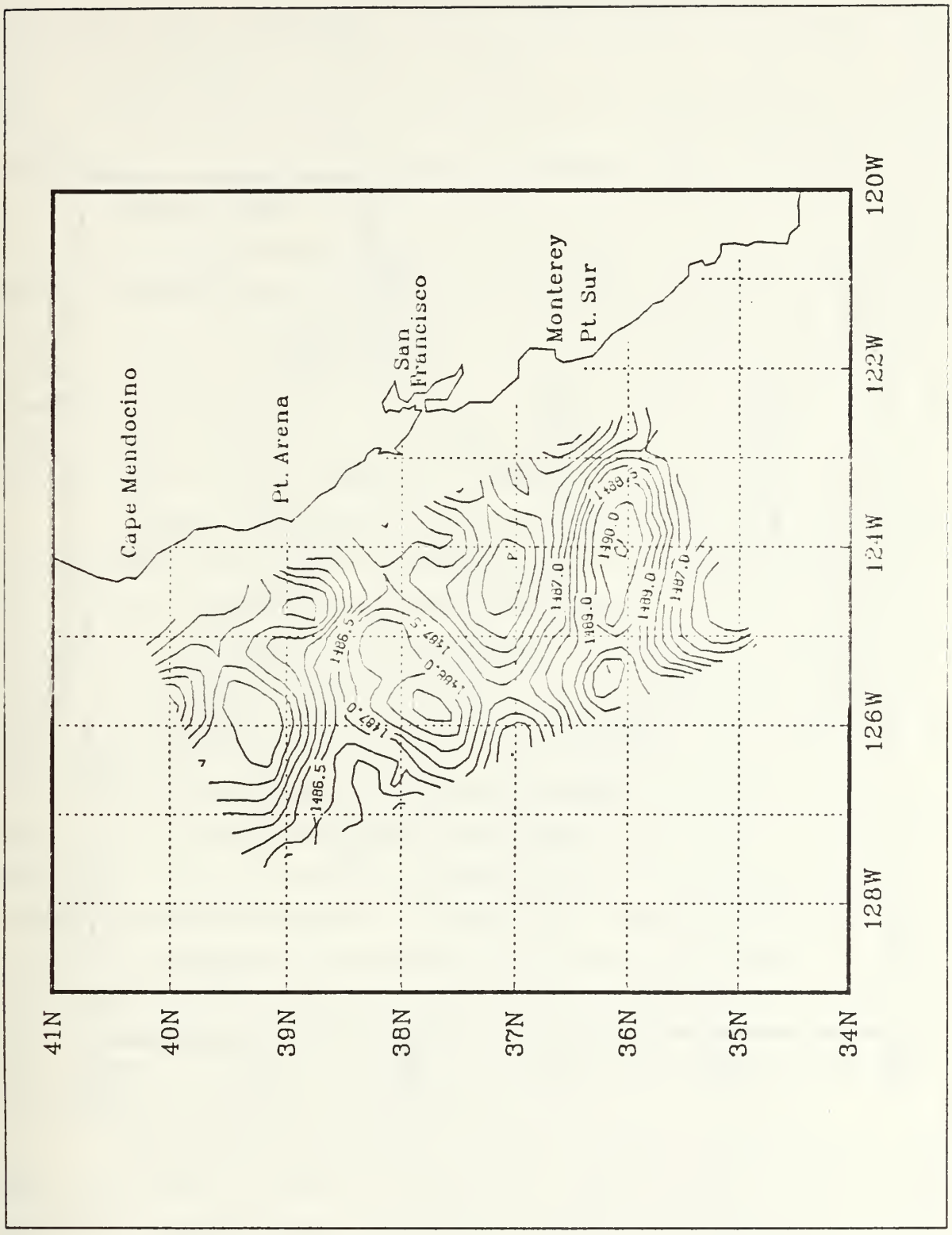

Figure 3.4d Sound Speed at 150 m (m/s), OPTOMA18P.
Contour Interval, 0.5 m/s.

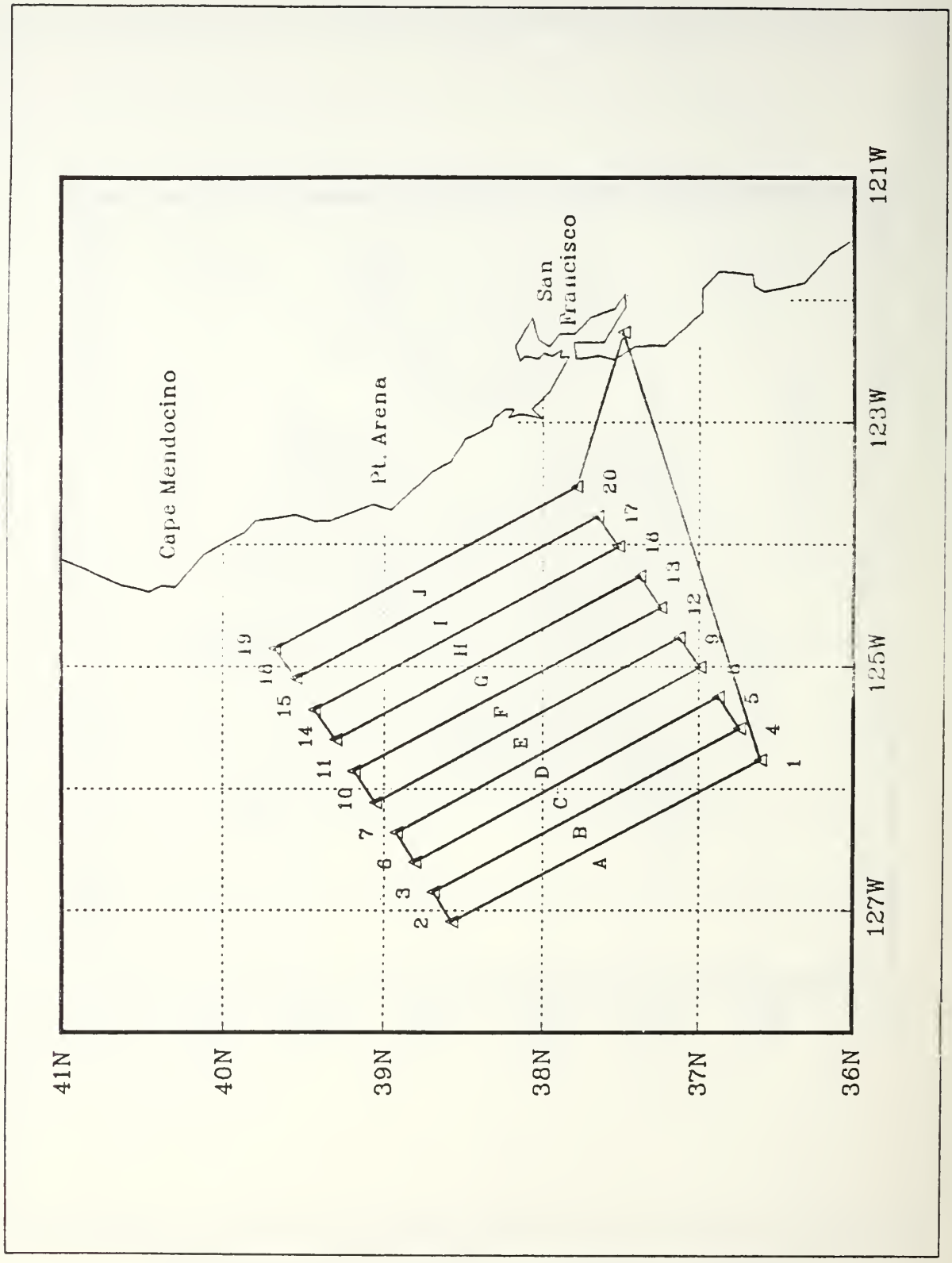

Figure 3.5 Flight Plan, OPTOMA20P.

for navigation error. The channel 14 positions were manually entered in the AXBT acquisition program and the signal was digitized in real time by the ADDAS and stored on diskette. Both channel 14 and 16 AXBT analog audio signals were recorded on magnetic tape using a stereo hi-fi VCR. Channel 16 AXBT's were digitized on return to NPS.

c. Mission Critique

The flight proceeded very well even though the weather was less than optimum. The survey region was dominated by low stratus and cumulus clouds as well as a few towering cumulus. Moderate turbulence was experienced throughout the duration of the flight. Additionally, scattered rain squalls required deviation from the planned flight tracks for safety of flight. Winds at flight level were southeastward at 30 knots, and the sea state was 3. The navigation team did an excellent job and the resulting AXBT drops ended up very nicely spaced and close to planned drop positions.

A malfunctioning channel 16 sonobuoy receiver on the aircraft distorted the AXBT audio carrier signal. The ADDAS oscilloscope provided a visual reference for the Inflight Technician (IFT) to troubleshoot and repair the receiver. Fortunately, only 8 channel 16 AXBT audio signals were lost and could not be digitized by the Sippican Mark 9 unit upon return to NPS. Due to a minor problem with the lofargram recorder, only 6 of the 8 AXBT traces were obtained and these profiles were hand digitized.

The use of a stereo hi-fi video cassette recorder (VCR) in the audio mode proved to be a worthwhile addition to the ADDAS system. With its capability of recording up to six hours of audio on a T-120 VHS cassette, the operators only had to change the tape once as compared to previous flights where the AXBT audio signal was stored on standard audio cassettes with only 45 minutes of recording on each side of the tape. No profiles were lost during tape changes or because a tape ran out. The VCR was mounted in the ADDAS cabinet on a layer of 3/4-inch foam rubber, which helped insulate it from vibration caused by turbulence encountered during the flight. No degradation in the recorded signal was noted.

The internal ADDAS inverter is rated at 5.6 amps. With the inclusion of a VCR in the system, the inverter was running at 6.3 amps continuous. This did not appear to be a problem and the inverter did not overheat or malfunction. To be on the safe side though, once data acquisition was completed, the VCR was disconnected from the circuit when the plotter was to be used.

The Sippican MK9 digitizes the AXBT audio signal ten times each second. MK9 output was sampled for three-tenths of a second, producing three data points. The median value of the three digitized points was stored. This step was included in an attempt to eliminate non-representative spikes in the temperature trace caused by RF or other interference in the signal. This feature appeared to work well, with the exception of long duration breaks in the signal, possibly caused by sea wash-over of the AXBT transmitter. A minimum of post-flight editing was required on the profiles. (A compilation of the AXBT data is presented by Ciandro *et al.*, 1986.) Table 2 lists a summary of AXBT expenditures for this mission.

TABLE 2

AXBT EXPENDITURE SUMMARY OPTOMA20P

Channel	Deployed	Failed[1]	Lost[2]	Deleted[3]	Recovered
14	48	1	0	0	47
16	48	6	2	1	39
Total:	96	7	2	1	86

Notes:

[1] Due to no radio signal transmission and late light-off of the probe.

[2] Profiles lost due to absence of lofargram trace from which to hand digitize.

[3] Bad profiles deleted during post-flight editing.

b. AXBT Survey Results

A representative sample of AXBT traces show the variability of the thermal structure in the survey region (Figures 3.6a and 3.6b). The AXBT drop positions, and the analyzed fields of D8C, SST, and MLD *were produced by the ADDAS on the return leg of the flight* (Figures 3.7a, 3.7b, 3.7c, 3.7d). Only channel 14 AXBT data (30 NM spacing), as received and digitized by the ADDAS, were used. The fields were generated by a compiled version of the objective analysis program using a floating-point accelerator.

Post-flight digitized channel 16 AXBT data were combined with the inflight digitized channel 14 AXBT data (Figure 3.8a). These data were stored and processed

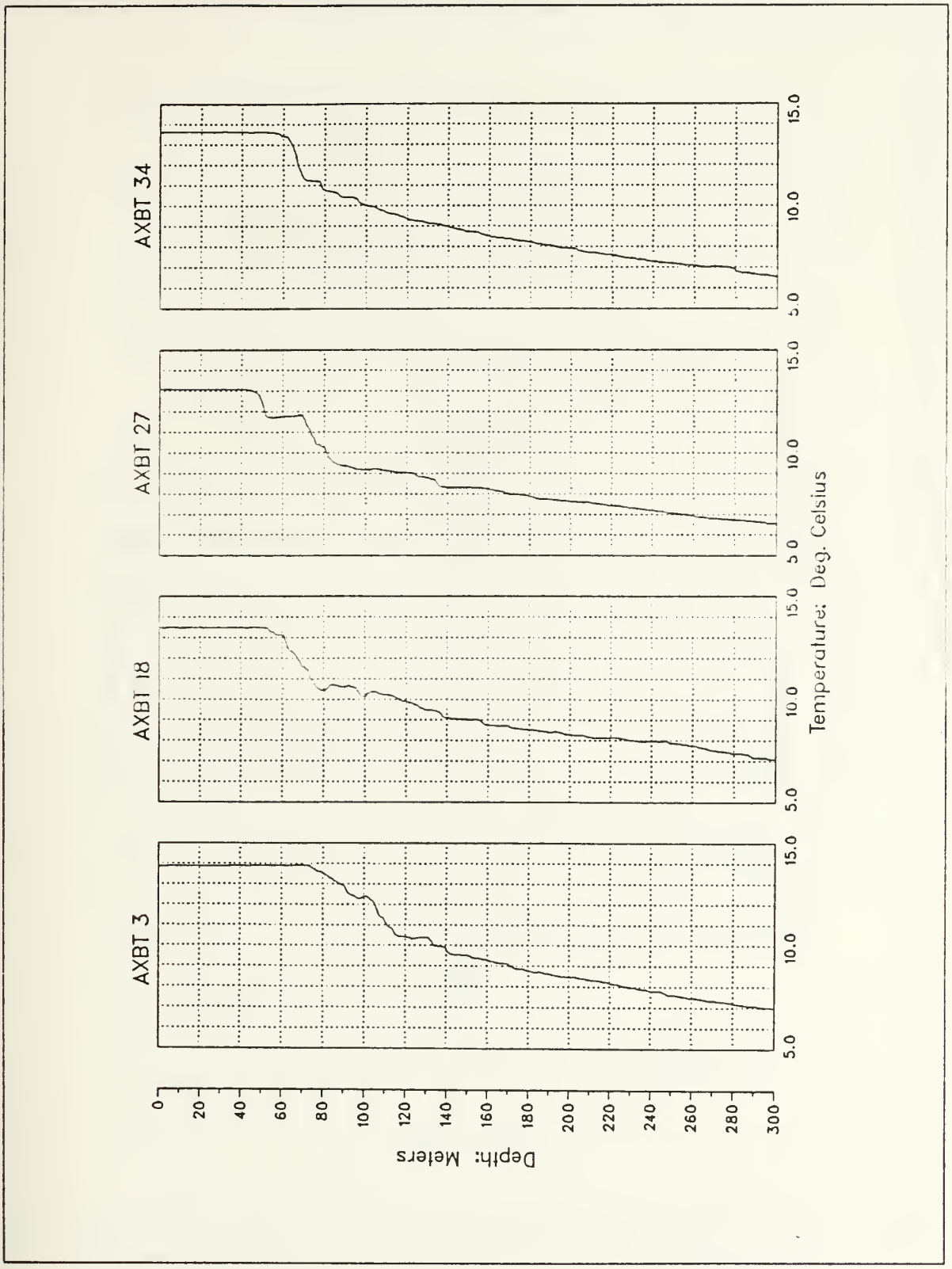

Figure 3.6a Representative Temperature Profiles, OPTOMA20P.

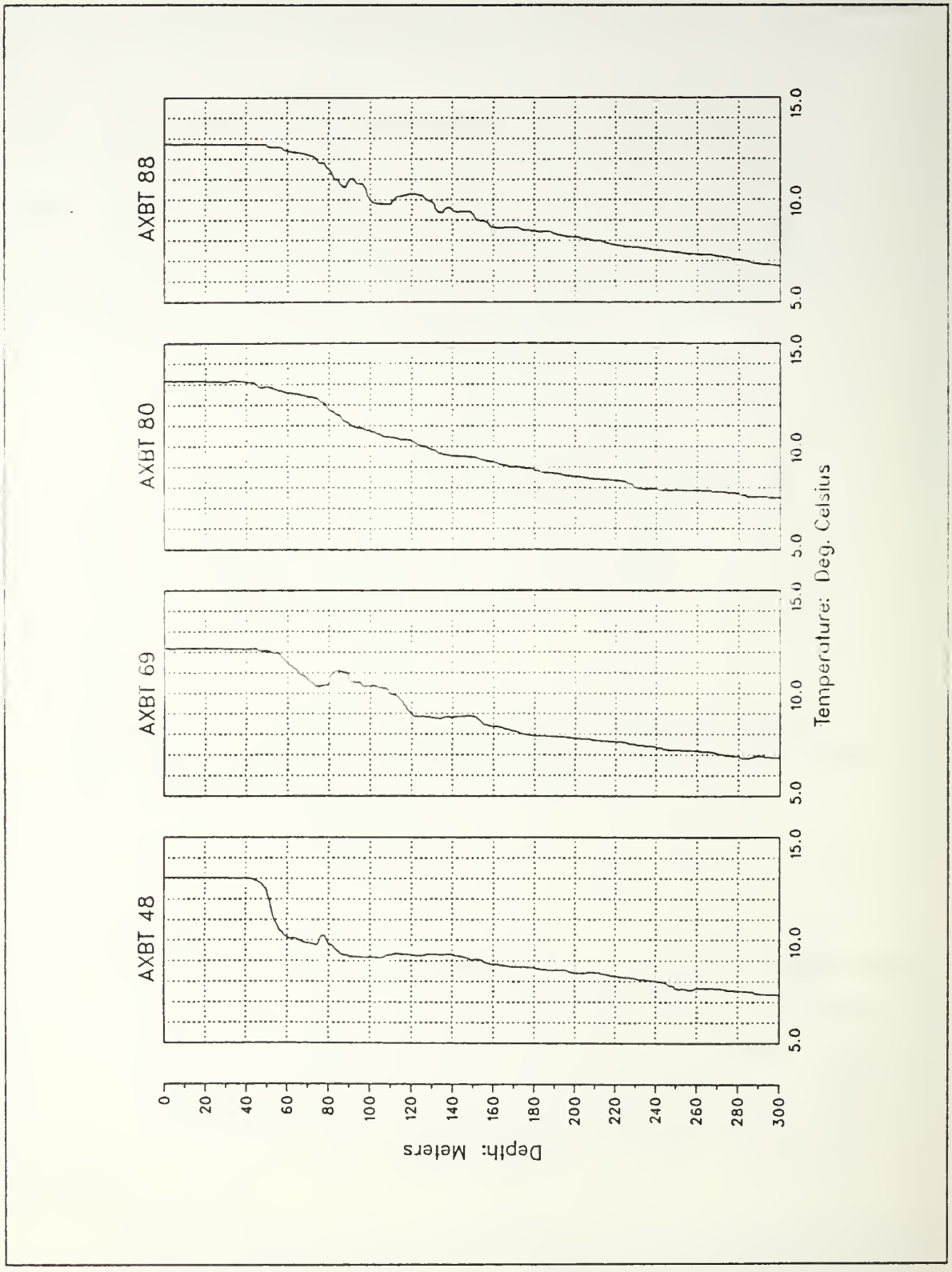

Figure 3.6b As in Figure 3.6a.

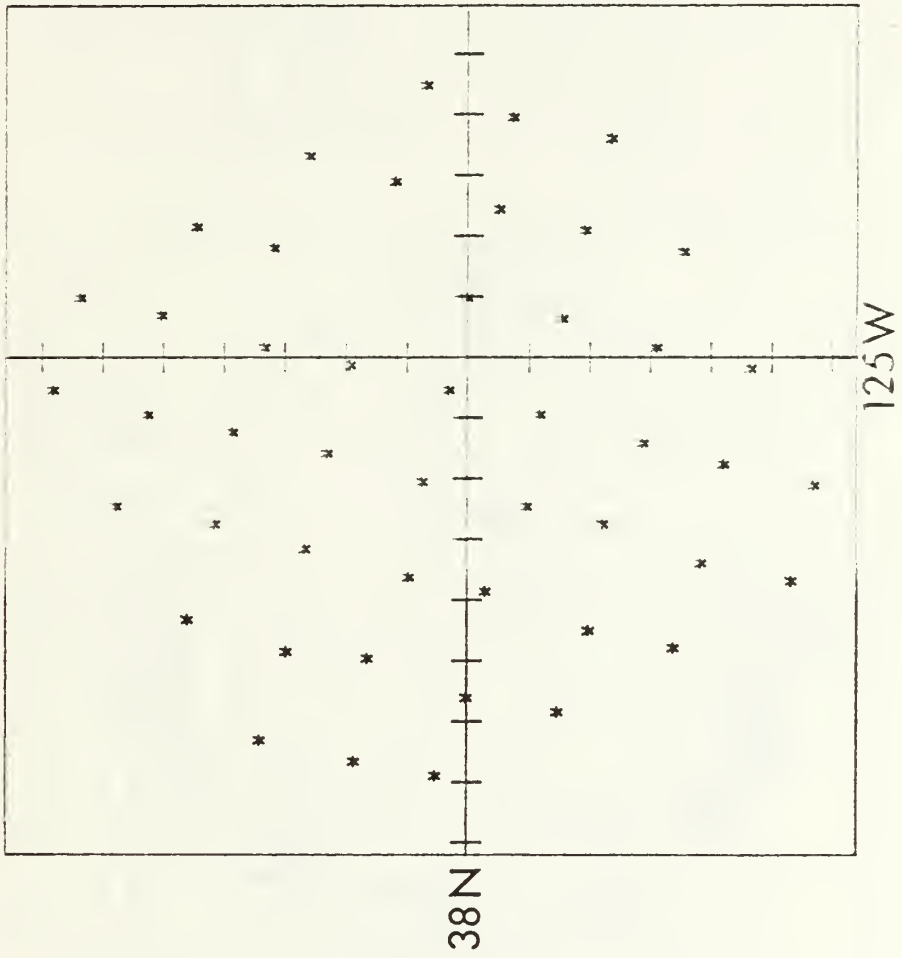

Figure 3.7a. Shallow AXBT Drop Locations, OPTOMA20P.
Origin 38°N, 125°W. Tick marks = 25 km.

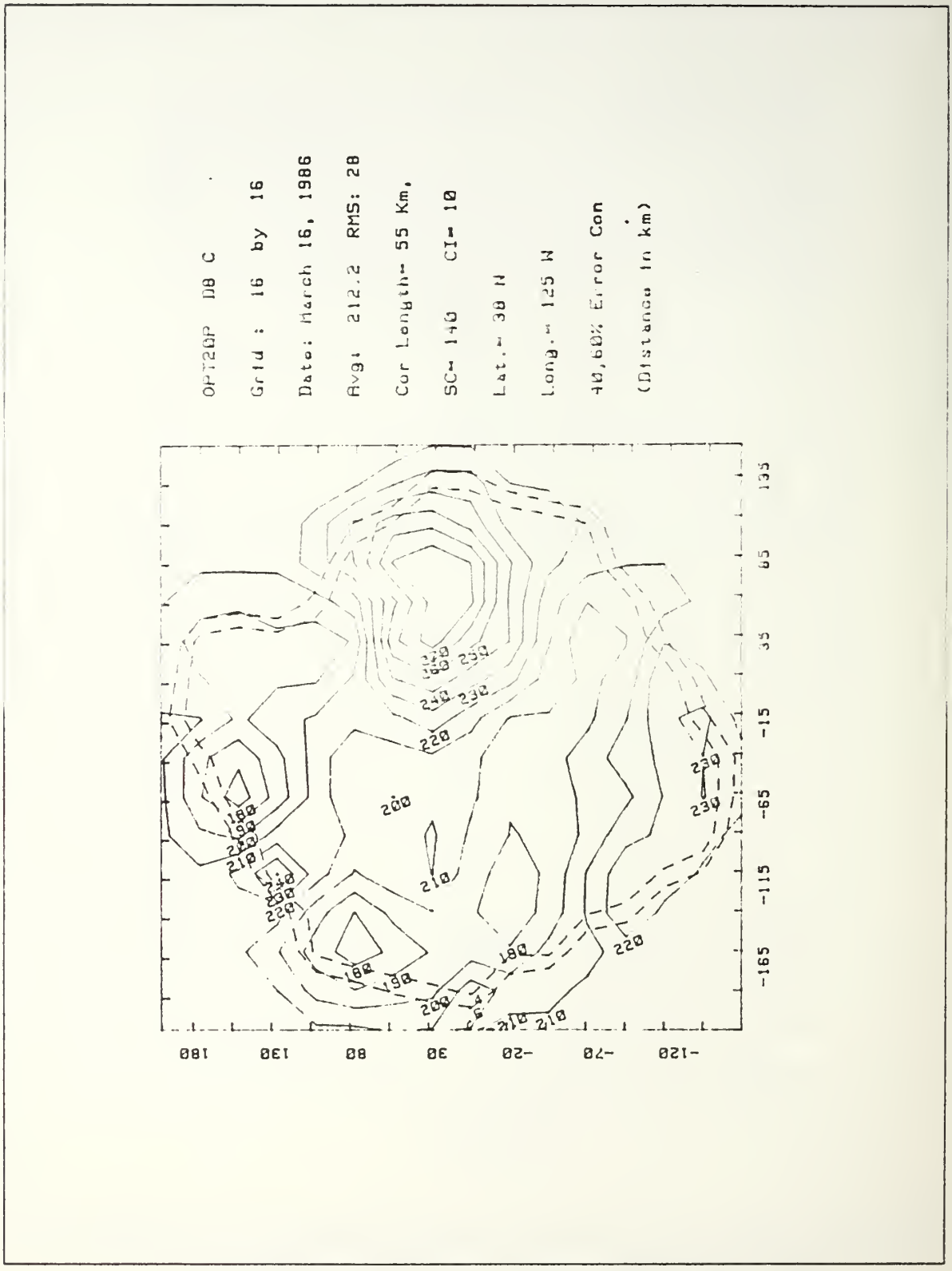

Figure 3.7b Depth of the 8°C Isotherm (m), as in Figure 3.7a.

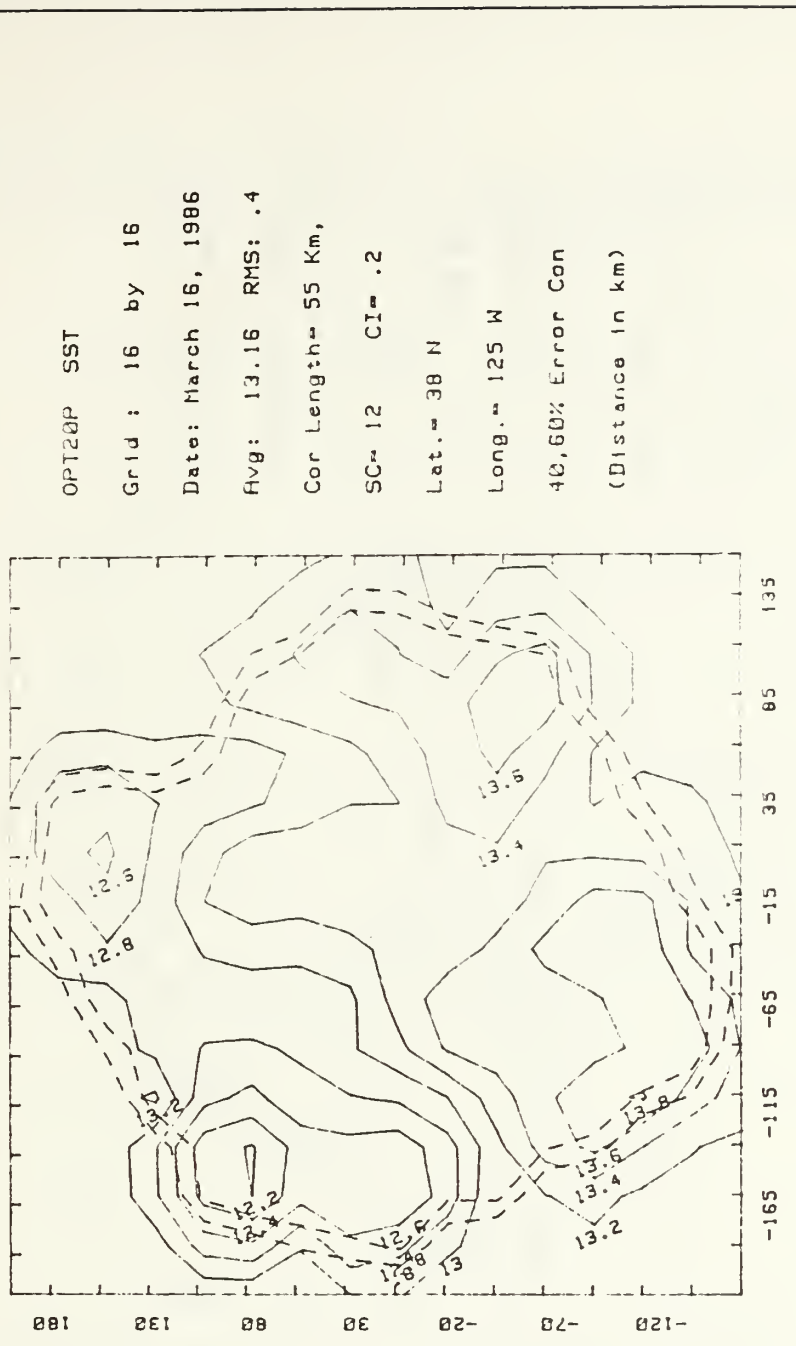

Figure 3.7c Sea Surface Temperature (°C), as in Figure 3.7a.

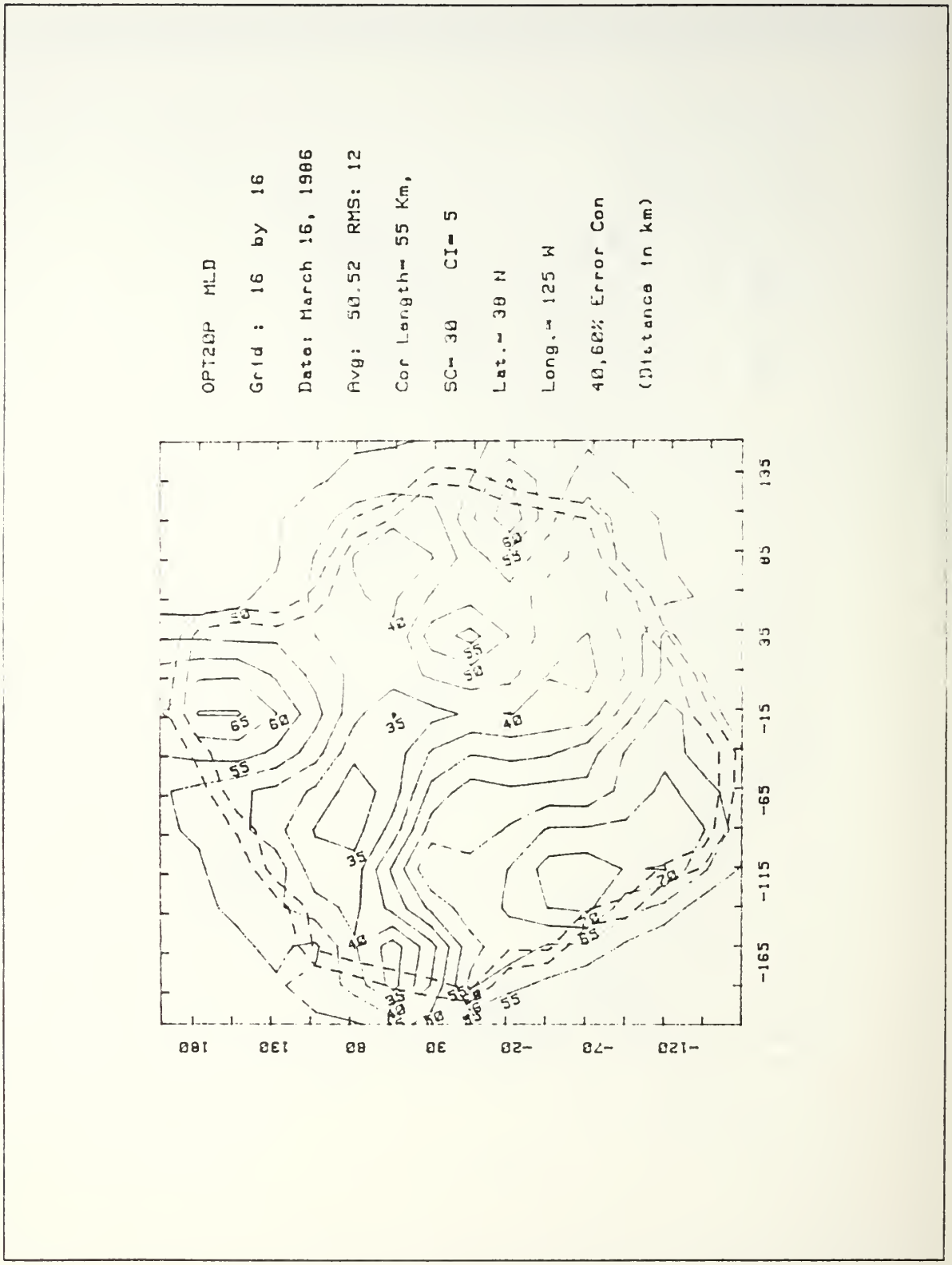

Figure 3.7d Mixed Layer Depth (m), as in Figure 3.7a.

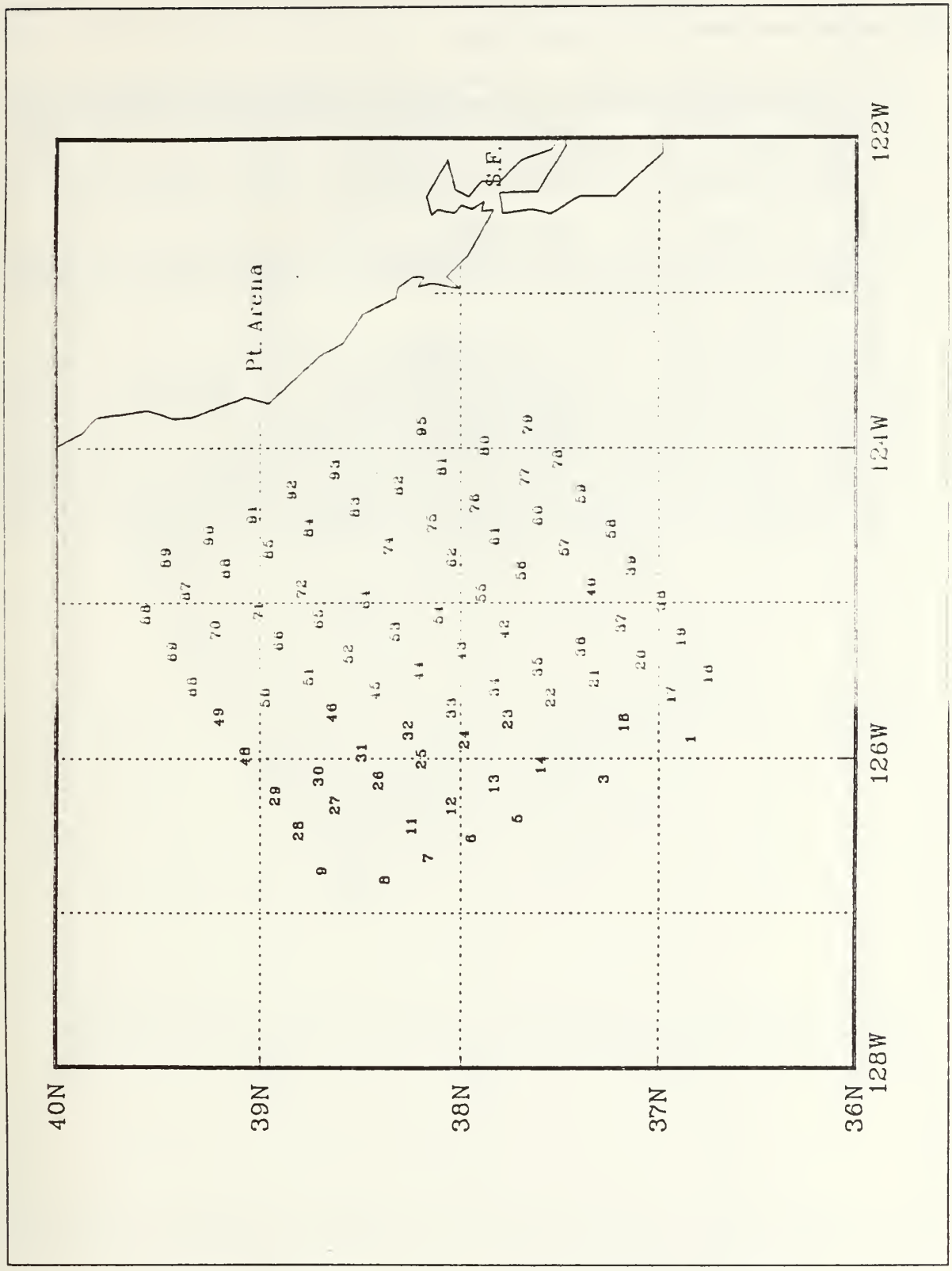

Figure 3.8a Recovered AXBT Drop Locations, OPTOMA20P.

on the IBM 3033 mainframe computer at NPS. Remaining spikes were removed and bad profiles were deleted from the data base.

- D8C, meters (Figure 3.8b): The most notable features are the major cyclonic (counterclockwise, indicated by a "C") center in the northwest with its associated flow zone extending to the south-southeast, as indicated by the shoaler depths, and the very large anticyclonic (clockwise, indicated by an "A") center characterized by the depression in the southeast. Additionally, half of two smaller cyclonic flows are observed in the north as well as a small cyclone near the center of the region. These features indicate an onshore jet off Pt. Arena.
- SST, °C (Figure 3.8c): Major features of interest are the cool zone in the northwest and the warm center (indicated by a "W"), corresponding to the large cyclone in the northwest and the large anticyclone to the southeast, respectively. There is also evidence of a cool center ("K") in the north corresponding to one of the two smaller cyclonic flows.
- MLD, meters (Figure 3.8d): Of interest in this analysis is the wide range of values for MLD, from less than 16 m to more than 68 m. The mean MLD is 50 m. This variability could be the result of the large atmospheric occluded low-pressure system that dominated the region on the previous day. As the system passed, the winds shifted from generally northeastward to southeastward at 20 to 40 knots and the surface layer was apparently in a state of rapid change during the survey period. All AXBT profiles showed a very isothermal surface layer. There was some association of the patterns in MLD with those of D8C; for example, the MLD had prominent minima associated with both the cyclone in the northeast and the anticyclone in the southeast.

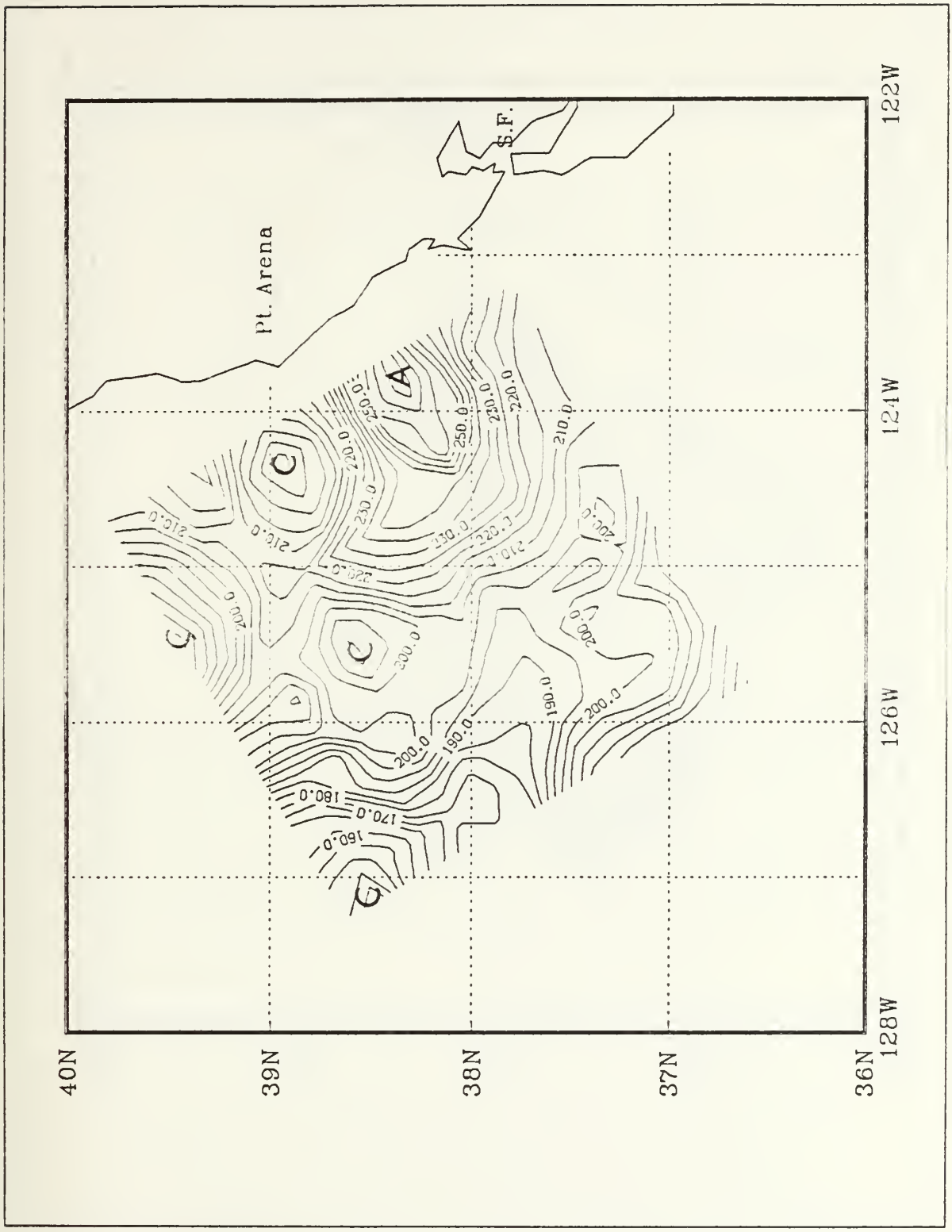

Figure 3.8b Depth of the 8°C Isotherm (m), OPTOMA20P.
Contour interval, 5 m.

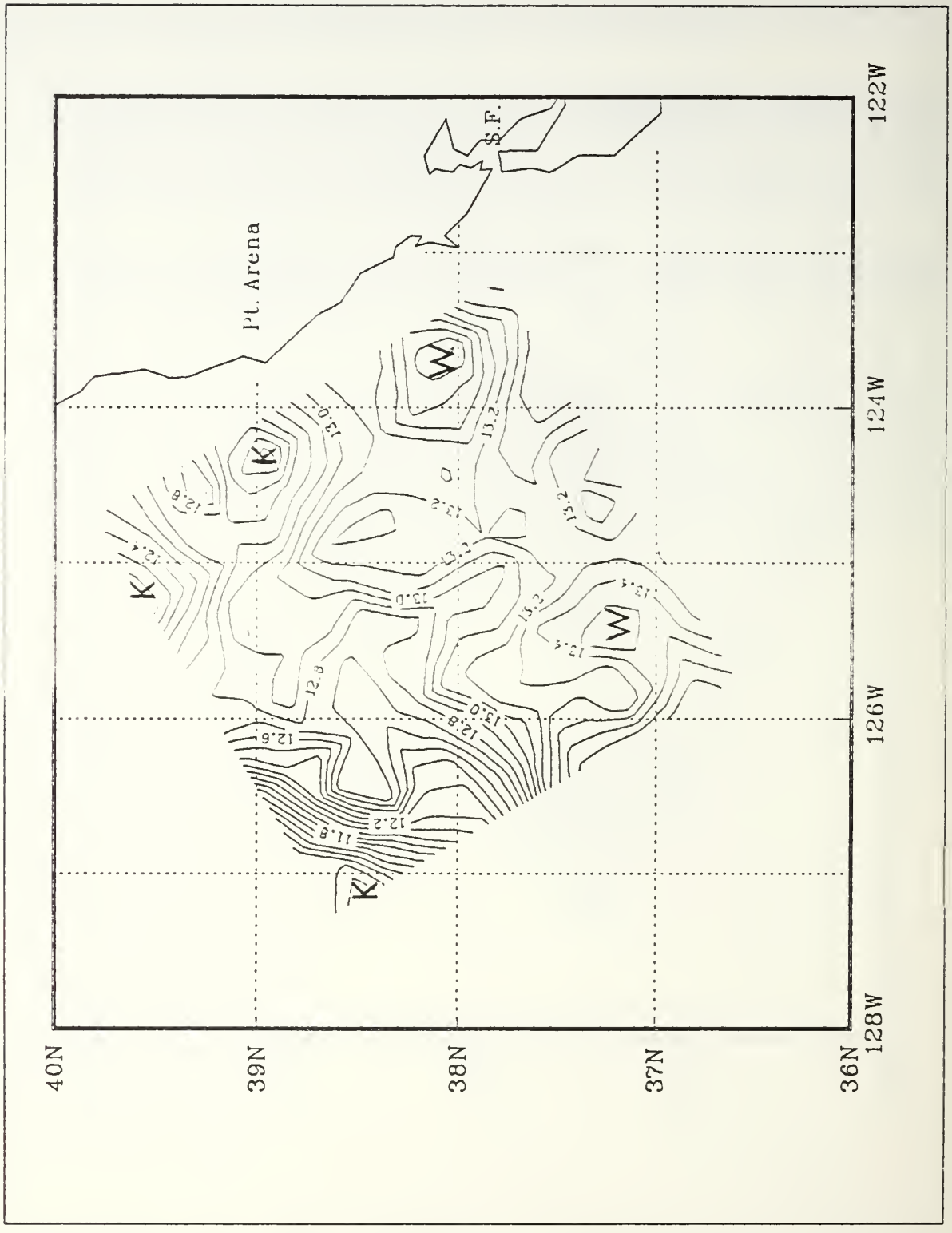

Figure 3.8c Sea Surface Temperature (°C), OPTOMA20P.
Contour interval, 0.1°C.

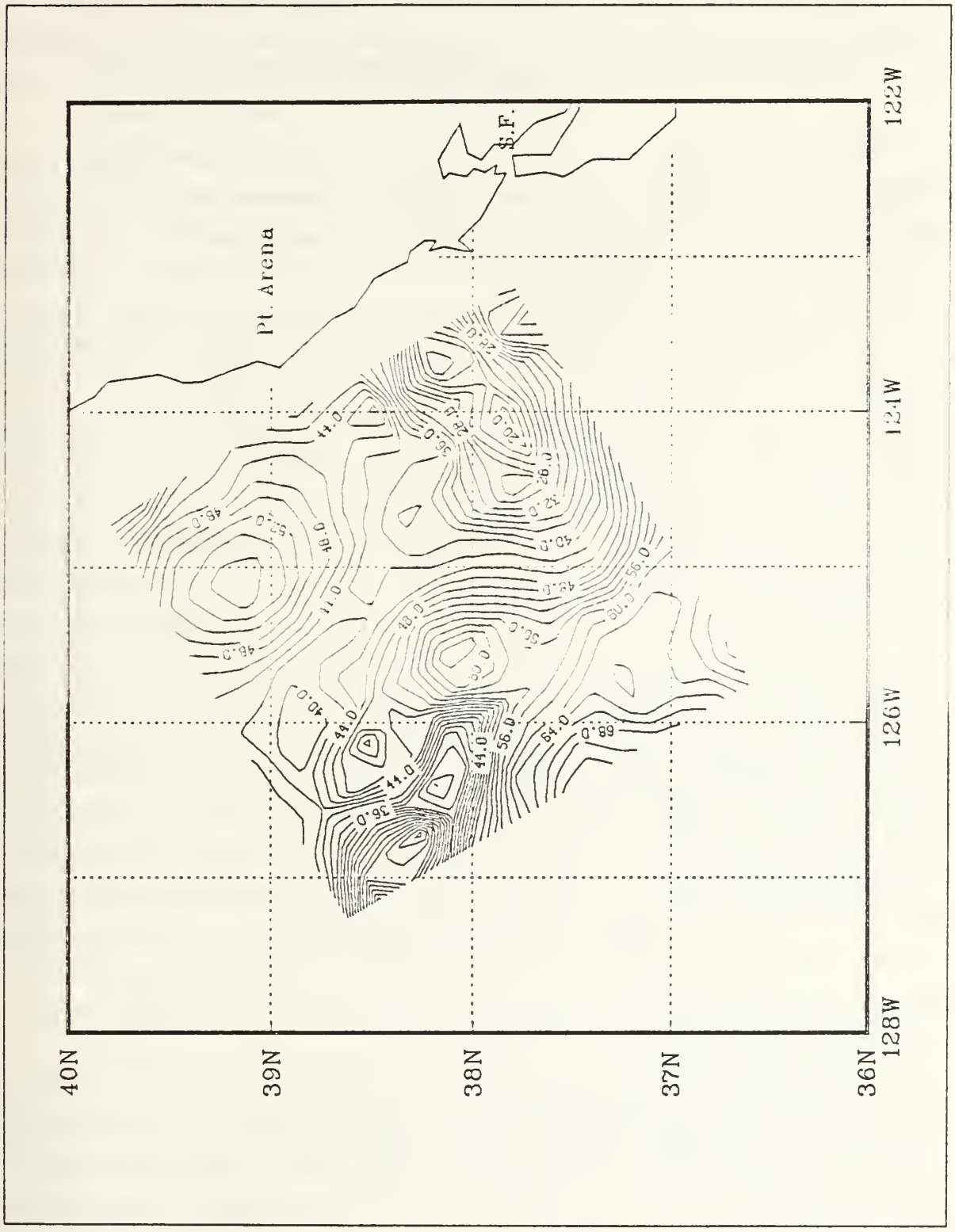

Figure 3.8d Mixed Layer Depth (m), OPTOMA20P.
Contour interval, 2 m.

IV. DEVELOPMENT OF AN AIRBORNE OCEAN SAMPLING STRATEGY

There are two distinct considerations that are related to the successful areal mapping of oceanic variables: 1) The sample density in the survey region; and 2) The application of the objective analysis technique to map these samples.

A. SAMPLING CONSIDERATIONS

Given an ocean region to be synoptically mapped in some variable, and the aircraft asset(s) and air-deployable sensors to measure this variable, what airborne sampling strategy should be employed to acquire a representative sample of the field that will optimize the information returned with the minimum amount of time and effort expended to accurately map this variable?

The ocean is a vast, temporally and spatially varying inhomogeneous domain. Following a similar development by Kelley (1976), this domain can be described by basic probability theory as a sample space, S (S_1, S_2,...S_n), of n observations where $S_i = \{x_i, y_i, t_i\}$, i = 1,...n, is an element of the sample space defined by latitude, longitude, and time. Each element can be further described by an array, $V_{i,j}$ ($V_{i,1}(z)$, $V_{i,2}(z)$,... $V_{i,j}(z)$), j = 1,...,m, of specific oceanic variables (biological, chemical, dynamic, or physical) varying with depth (z). Each $V_{i,j}(z)$ can be defined as a continuous random variable which can have more than one potential value as the chance result of the sampling and that it is assumed to be representative of the oceanic variable being sampled. Due to the inherent capabilities of sampling instruments and systems such as the ADDAS, these oceanic variables are sampled at a specific depth increment and can be represented as discrete random variables. This provides a framework for the development of an "optimum" sampling strategy that can be applied in survey operations.

Deciding which variable to sample is a rather simple task due to the availability of air-deployable sensors. The measurement of ocean temperature is most practical through the use of the SSQ-36 AXBT as it is a proven sensor in the Navy inventory. Synoptic mappings of the temperature field at selected depths can be converted to a sound speed field, using a climatological or representative salinity profile, for use in acoustic forecasting for ASW operations. Soon-to-be-operational AXCTD's and currently available AXSV's could also be used to map the sound speed field .

Having chosen the variable to be sampled, the "external" considerations of the spatial and temporal scales of the variable, and the "internal" considerations relating to aircraft, aircrew, and sensor limitations will be addressed.

1. **External Considerations**

a. Spatial Scales

The ocean contains a multitude of spatial scales ranging from centimeters to thousands of kilometers. In sampling any oceanic variable, prior knowledge of the scales that are "significant" to a specific mission are required. Previous operations in the survey region, satellite imagery, and/or climatology may be available. Additionally, a knowledge of the dynamical properties of the field must also be considered.

The Rossby radius of deformation, R, is a length scale of fundamental importance in both atmospheric and oceanic dynamics for the behavior of rotating density-stratified fluids subject to gravitational restoring forces. For a homogeneous, shallow layer of fluid, it is the distance over which the gravitational tendency to render the free surface flat is balanced by the tendency of the Coriolis acceleration to deform the surface (Pedlosky, 1979; p. 78). It is the pertinent length scale for barotropic phenomena (Emery, *et al.*, 1984). Since the ocean is a continuously stratified fluid, normal mode theory can be applied to a stratified layer and each mode can be represented by a Rossby radius. The barotropic or external Rossby radius (R) was defined above and is a function of only the water depth and latitude. The internal or nth mode baroclinic Rossby radius (Ri) depends on the vertical stratification and is a natural scale in the ocean often associated with fronts and eddies (Gill, 1982; p. 207). For mid-latitude oceans it is the order of 10 to 30 km. The horizontal dimensions of such quasi-geostrophic features should scale as the internal Rossby radius, where the scale is defined as the wavelength over 2π (Emery, *et al.*, 1984).

b. Temporal Scales

Based on the spatial scales of the quasi-geostrophic features, the temporal scales of variability are not a factor in "synoptic" mappings. With phase speeds the order of 2 to 5 km/day, the distance that the features will have propagated over the duration of the survey flight is small compared to the sampling grid cell length. However, temporal scales may have to be considered if the survey domain is too large to be covered in a single flight.

c. Aliasing

The well known problem of aliasing occurring in time series analysis also occurs in spatial sampling. For a one-dimensional sampling, the Nyquist theorem states that some function can be reconstructed from samples taken not more than one-half wavelength apart. This can be applied to a two-dimensional field as well. Identify the highest frequency (shortest wavelength) of significant variability and sample at twice that frequency (one-half of that wavelength). If this is not feasible and a larger sampling distance is chosen, aliasing may be a problem from scales that are smaller than the chosen sampling wavelength and may account for a percentage of the noise in a sample value.

2. Internal Considerations

With the spatial scale of the features determined. and thus the maximum acceptable distance between observations to adequately represent the significant scales. the capabilities of the sampling platform and its sensors must be taken into account. These were presented as extrinsic limitations to the ADDAS in Chapter 2, and are applicable here. They are summarized:

a. Aircraft Limitations

- Weight and balance. Aircraft are constrained by a maximum gross weight for take off as prescribed by the respective NATOPS Manual. There may have to be a trade-off in the number of sensors to be deployed to remain within NATOPS limitations.
- Airspeed and altitude. These directly affect fuel management. Airspeed and altitude will be governed by safety-of-flight and ADDAS/sensor limitations.

Additionally, physiological and safety factors must be considered. All Navy flight operations are governed by the OPNAVINST 3710.7 series (NATOPS General Flight and Operating Instructions). This specifies limits on mission endurance and crew rest policies. It may be further modified by individual squadron standard operating procedure (SOP). These will be the limiting factors in mission duration.

b. Sensor Limitations

- AXBT deployment time from the aircraft, a function of altitude.
- AXBT fall duration through the water, 200 and 500 seconds for deep and shallow AXBT's, respectively.
- Three AXBT channels available. Two AXBT's must not be deployed within line-of-sight transmission range of each other, a function of altitude.

B. GENERAL APPLICATION

The thought process followed in developing an "optimum" sampling strategy is presented in flow diagram form (Figure 4.1). Each step is contingent on the previous step. Maximum observation spacing is generally given as a requirement to gain an adequate representation of the oceanic process. Aircraft maximum gross weight is also a limiting factor. Trade-offs can easily be made between the size of the survey region and the maximum number of AXBT's that can be carried. If the size of the survey region is then too large, two or more consecutive survey flights may be completed as long as the temporal scales of the region are considered. One option, is to sample the larger domain twice. This can be accomplished by sampling in a "checkerboard" pattern, with sample spacing no more than twice the maximum observation spacing, with the first flight deploying AXBT's in the "red" squares, and the second flight deploying in the "black" squares. Another option is to complete two or more surveys at a smaller-than-maximum spacing in adjacent subregions of the sample domain. One drawback to sampling with two or more flights is that the real-time aspect of the synoptic mapping will be lost. This may be acceptable, however, depending on the requirements directing the survey.

C. THE OBJECTIVE ANALYSIS TECHNIQUE

The second area of consideration in developing an optimum sampling strategy is the proper application of the objective analysis technique. This will result in fields that are representative of the data acquired, and available in near-real-time with systems such as the ADDAS.

Based on the Gauss-Markov theorem from statistical estimation and applied to atmospheric data by Gandin (1965), objective analysis was developed by Bretherton, *et al.*, (1976), with application to oceanic data. A more generalized implementation, as adduced by Carter and Robinson, (1981), is applied in the OPTOMA Program.

1. Theory

The basic assumption in objective analysis is that the field from which the observations were acquired has zero mean and a known covariance function. Following Bretherton, *et al*, (1976), and incorporating both a space and time variability, $\theta_{\mathbf{p}}$ is the value of a scalar variable $\theta(x, y, t)$, at a general position $\mathbf{p} = (x, y, t)$, from measurements φ_i at N observations $\mathbf{p}_i$ $(i = 1, \ldots, N)$. Each measurement, φ_i, is presumed to consist of some true value, θ_i, and some random noise, ε_i:

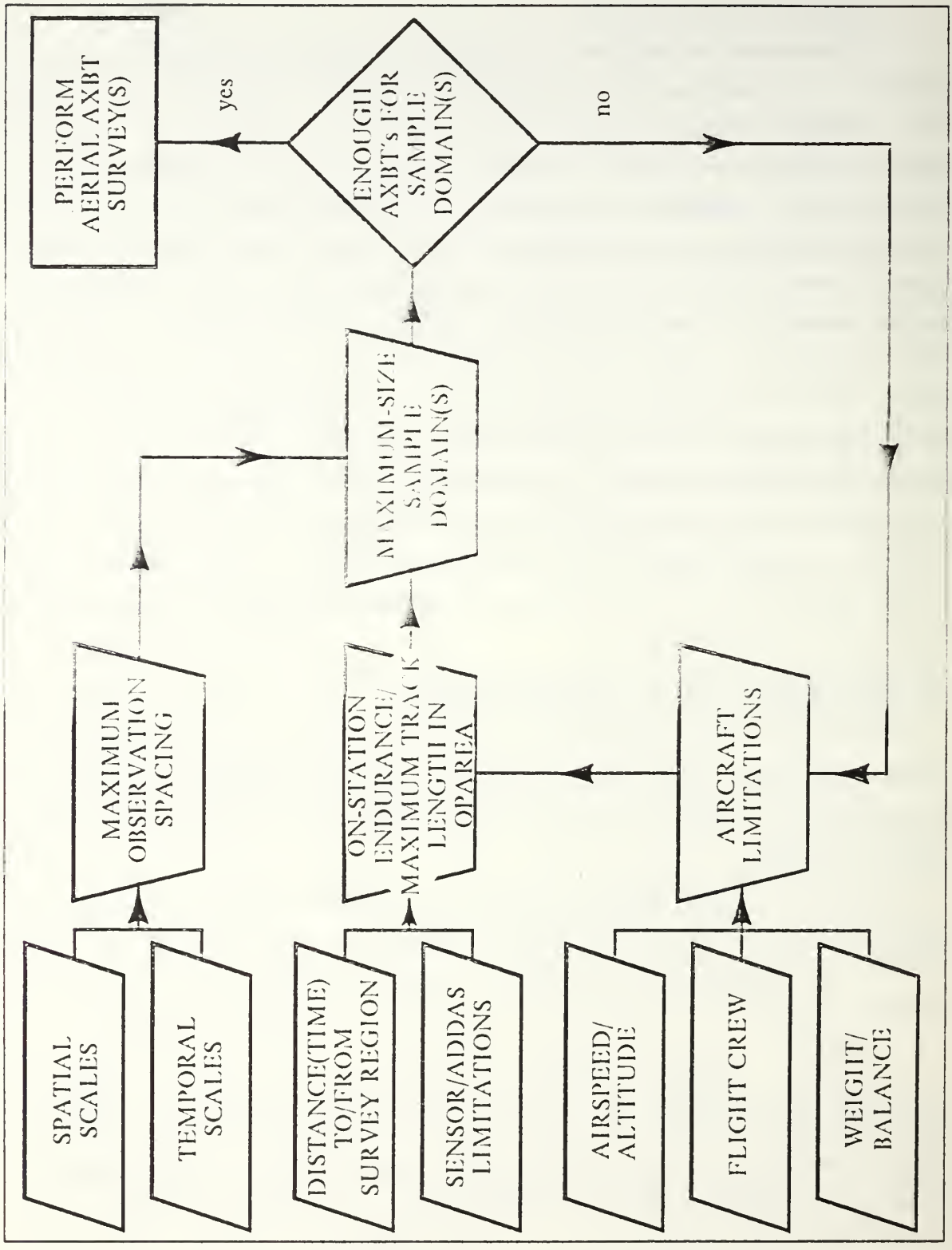

Figure 4.1 Optimum Sampling Strategy Flow Diagram.

$$\varphi_i = \theta(p_i) + \varepsilon_i, \quad (i = 1,...,N),$$

where the errors, ε_i, are uncorrelated with each other and with the true value, θ_i, but have a known variance, E:

$$\overline{\varepsilon_i \theta_j} \equiv 0, \quad \overline{\varepsilon_i \varepsilon_j} = E\delta_{ij}, \quad \text{for } (i, j = 1,...,N),$$

and the overbar indicates an expected value (or average over a large number of realizations). The errors may be sampling error or instrumental error. Systematic or calibration errors are not permitted.

The least squares optimum linear estimator of θ_i is

$$\hat{\theta}_p = \sum_{i=1}^{N} C_{pi} \left(\sum_{j=1}^{N} A_{ij}^{-1} \theta_{ij} \right),$$

where

$$A_{ij} = \overline{\varphi_i \varphi_j} = F(p_i - p_j) + E\delta_{ij},$$

is the covariance matrix between all pairs of the sampled data, and A^{-1} is the inverse of A, and

$$C_{pi} = \overline{\theta_p \varphi_i} = F(p - p_i),$$

is the covariance between the estimated value θ_p and the *ith* observation. The variance of the error in θ_p is

$$(\hat{\theta}_p - \theta_p)^2 = C_{pp} - \sum_{i,j=1}^{N} C_{pi} C_{pj} A_{ij}^{-1},$$

which requires only the location of the data points, a noise level E, and some correlation function $F(R)$.

Carter and Robinson, (1981), present the idea of applying the objective analysis equations at each interpolation point. Four specific parameters are identified that determine the selection of observations that will affect an interpolation. These are:

- Maximum time increment between observations,
- Radius of influential points, $R = [(\Delta x - c_x \Delta t)^2 + \Delta y^2]^{1/2}$,
- A dominant phase speed, c_x,
- The maximum number of influential points.

With application to synoptic mapping, only the radius of influence and number of influential points are used. It is best to use observation points near the interpolation point. By specifying a maximum range at which observations can effect an interpolation, this will eliminate the influence from distant points. Additionally, the specified maximum number of points limits only those observations within the radius that are the most highly correlated (closest to) an the interpolation point. The time increment and phase speed are disregarded because the propagation distance of the quasi-geostrophic features (phase speeds of the order 2 to 5 km/day), is negligible over the duration of a survey flight ($\sim$8 hrs). The radius of influence is now only the distance between the interpolation point and the observation $R = (\Delta x^2 + \Delta y^2)^{1/2}$.

2. ADDAS Software Application

a. Input Parameters

Having acquired the observations, the following parameters must be specified before performing the objective analysis:

- Some form of the correlation function, $F(R)$,
- The percentage of the observed variance attributed to noise, σ^2_n,
- The maximum radius of influence, RI_{max},
- The limiting number of influential observations, N_{lim},
- The objective analysis interpolation points, $\psi_n \equiv \{ x_n, y_n \}$, $(n = 1,...,I)$,
- A maximum autocorrelation value, A_{max}.

These parameters may be incorporated into the program as constants based on previous experience or determined for each observation field. A flow diagram (Figure 4.2) summarizes the decision process. These parameters are presented below.

(1) *Correlation Function and Noise Variance Level.*

There are two distinct uses for the correlation function in the objective analysis technique: 1) to determine the correlation between an interpolation point and an observation, and 2) to compute the elements of the autocorrelation matrix between all pairs of observations selected to influence an interpolated value.

The correlation function can be defined in any number of ways depending on the user's requirements. For a space-time correlation of asynoptic data, as is used in the statistical model, the form of the correlation function is

$$F(R2) = \gamma (1 - \alpha R2) \exp(-\beta R2), \qquad (4.1)$$

where

$R2 = (\Delta x - c_x \Delta t)^2 + (\Delta y - c_y \Delta t)^2$, the influential radius, squared,

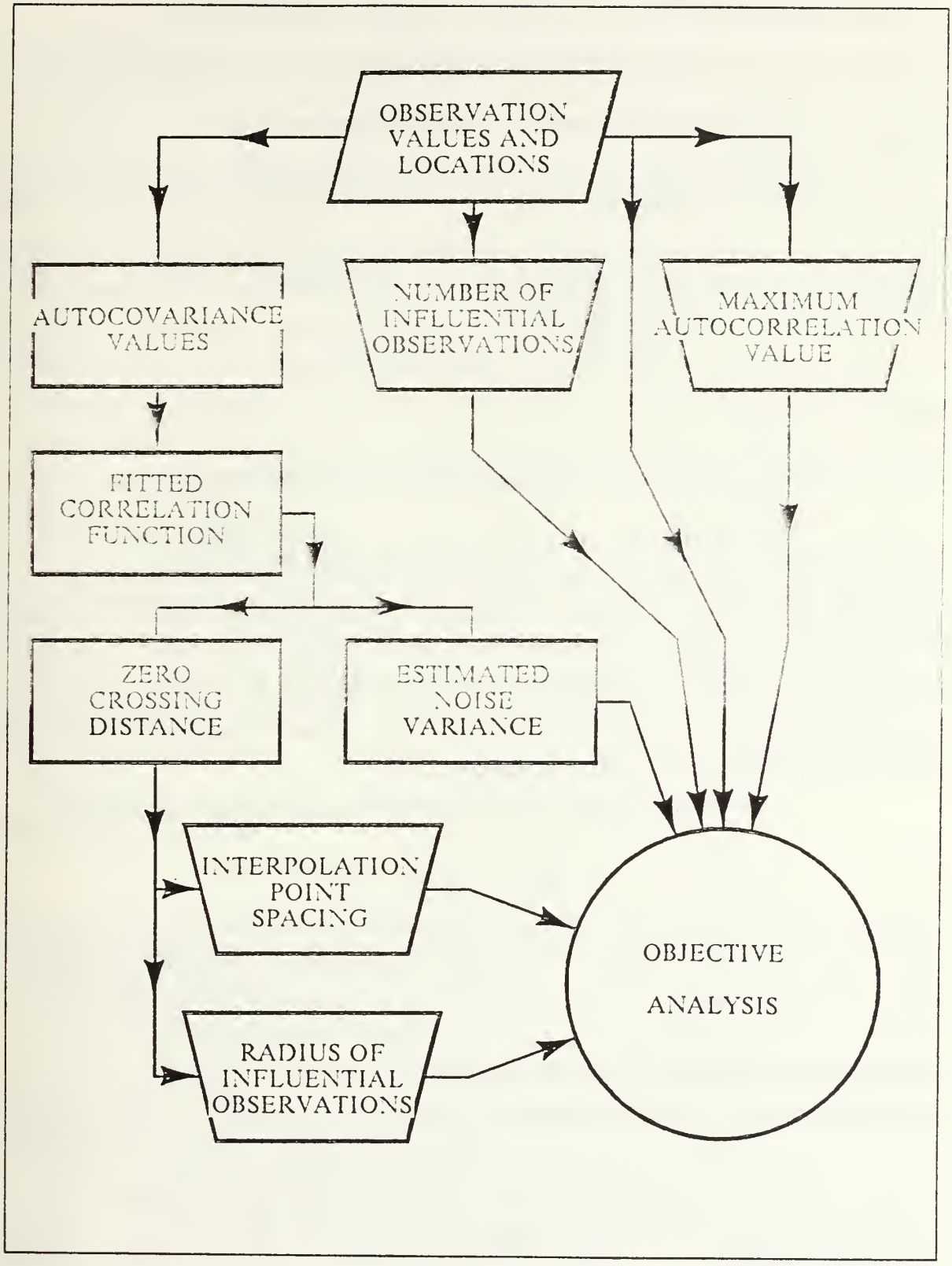

Figure 4.2 Flow Diagram of Objective Analysis Inputs.

c_x, c_y: x and y phase velocity components, respectively,

Δx, Δy: spatial difference between interpolation and observation points,

Δt: time difference between observation and analysis times,

α, β, γ: parameters computed by an iterative nonlinear least squares fit to the function.

A simple, yet effective form is employed in the ADDAS objective analysis software for synoptic mappings,

$$F(R2) = (1 - R2)\exp(-R2/2), \qquad (4.2)$$

where

$R2 = (\Delta x^2 + \Delta y^2) / (RI_{max})^2$, the influential radius squared.

An advantage in using Equation 4.1 in synoptic mapping (let c_x and c_y both equal zero) is that an estimate of the noise variance in the observations can be made if not already known. First, a bilinear trend is removed (if desired) from each observation. It is of the form $\varphi_i = Ax_i + By_i + C$, where A, B, and C are either specified or computed by a least squares method. The mean, μ, and the variance, σ^2, of the observations are computed next, and the mean is removed from each observation to satisfy the basic assumptions.

The distances between each observation and every other observation,

$$D_{ij} = [(x_i - x_j)^2 + (y_i - y_j)^2]^{1/2}, (i,j = 1,...,N),$$

are computed and binned as if isotropic. Bin size should be greater than the minimum inter-observation distance (D_{ij}, $i \neq j$) in order to accumulate a statistically significant number of values in each bin. The first bin should be from 0 to 1 km, to contain those D_{ij}, when i = j, and other closely-spaced observations ($D_{ij} \leq 1$ km). The number of bins, *nbin*, should cover all the inter-observation distance scales. As each D_{ij} is located in its respective bin, b, the total number of elements in that bin, NB_b, is incremented by 1. The autocovariance is computed and summed for that bin ($C0_b = \sum \varphi_i\varphi_j$). Once all the pairs of observations have been binned, the final autocovariance for each bin, C_b is computed by normalizing each $C0_b$ by the quantity $NB_b\sigma^2$ ($C_b = C0_b/(NB_b\sigma^2)$).

The midpoints of the bins, BM_b, for b = 2,...,*nbin*, are computed. These values, along with the total number of observations (NB_b), the normalized correlations (C_b), the variance (σ^2), and the limiting number of observations ($N/2$), are applied in an iterative nonlinear least squares fit to the correlation function (Equation 4.1). The values of α, β, γ, and the zero-crossing distance are computed. Some quality checks are made on the data. If the total number of values in either bin 2, 3, or 4 is less than $N/2$, there are not a statistically significant number of observations used in computing the correlation, and the least squares fit is not attempted. Additionally, the application of the least squares routine for this form of the correlation function requires at least three points to fit a curve, and these points must also occur before the second zero-crossing of the correlation values. The 95% confidence limits, based on a test for white noise and assuming a normal distribution, can be computed for each bin using the formula $C_b \pm 1.96/(NB_b^{1/2})$ (Jenkins and Watts, 1968; pp. 187-188).

If a successful fit is achieved, the signal and noise parts of the variance can be estimated by extrapolating the fitted correlation function to zero lag. Assuming perfect correlation at zero lag (C = 1.0) and that the variance contains some percentage of noise, if the extrapolated value, C_{ext}, is less than 1.0, the signal variance can be computed,

$$\sigma^2_s = C_{ext}\sigma^2,$$

and the noise variance is

$$\sigma^2_n = (1 - C_{ext})\sigma^2.$$

The noise variance must be specified as a fraction of the total variance for input into the objective analysis routine.

(2) *Maximum Radius of Influence.*

RI_{max} is selected to be less than or equal to the zero-crossing distance of the correlation function. This ensures that only observations that are positively correlated with the interpolation point are used.

(3) *Maximum Number of Influential Observations.*

In surveys with a large number of observations, N_{lim} limits the number of observations within the radius that will be used in an interpolation. These observations will be those that are the most highly correlated with (i.e. closest to) the interpolation point.

(4) *Grid Selection.*

For synoptic mappings in the OPTOMA Program, the survey domains are rectangular in shape, with observations distributed regularly over the domains. The objective analysis interpolation points, $\psi_n \equiv \{ x_n, y_n \}$, (n = 1,...,$I$), are organized in a rectangular pattern encompassing the domain, with equal spacing in both the local x and y directions. The grid spacing should be less than one-half of the zero-crossing distance of the correlation function to adequately resolve the scales of the sampled field. The interpolation points should lie within the dimensions of the domain in order to provide enough observations for interpolation at the boundaries.

(5) *Maximum Autocorrelation Value.*

A_{max} is used in computing the autocorrelation matrix, **A**, at each interpolation point. Once the observations are selected that will influence an interpolation, the autocorrelation of each point with every other point, A_{ij}, is computed using the autocorrelation function $F(R)$ previously determined. If for a given j, the absolute value of A_{ij}, is greater than A_{max} for any i, then the *jth* observation will be discarded. This removes observations that are too closely spaced to one another and helps maintain a diagonally-dominant matrix.

b. The Objective Analysis

Once the input parameters are specified, the following steps are performed for each interpolation point,

- Selection of the influential observations,
- Generation of the autocorrelation matrix,
- Computation of the interpolated value and error limit.

These are discussed below.

(1) *Selection of Influential Observations.*

The influential radius is computed between the interpolation point and each observation. If the radius is less than or equal to RI_{max}, then the correlation between the observation and the interpolation point $C_{ni} = F(R)$, is computed. Once the observations have been selected, they are sorted in order of decreasing correlation (increasing distance from an interpolation point). Only the first N_{lim} of the sorted observations and their respective correlations will be used. Next, the autocorrelations, A_{ij}, between each of the selected observations are computed. Only the best correlated and distributed observations with the interpolation point remain.

(2) *The Autocorrelation Matrix.*

The autocorrelations, A_{ij}, between the remaining selected observations are calculated using $F(R)$, and become the elements of the autocorrelation matrix. The percentage of the variance due to noise is then added to each element of the main diagonal of **A**. This biases the the matrix towards diagonal dominance. The matrix is then inverted. This provides the weights to compute the interpolated value. The observation correlation vector C_{ni} between each selected observation and the interpolation point is computed using $F(R)$.

(3) *The Interpolated Value and Interpolation Error.*

The values of the inverted autocorrelation matrix, A^{-1}, and the correlation vector, C_{ni}, are used to compute the interpolated value, B_n,

$$B_n = \sum_{i=1}^{N} C_{ni} \sum_{j=1}^{N} A_{ij}^{-1} \varphi_{ij}$$

and the RMS interpolation error is

$$E_n = F(0) - \sum_{i=1}^{N} \sum_{j=1}^{N} C_{ni} C_{nj} A_{ij}^{-1}.$$

The interpolated value must now be be brought back to its original scale. If a bi-linear trend was removed, it must be added back, as well as the mean. The final result, R_n, is

$$R_n = B_n + \mu + Ax_n + By_n + C,$$

which is stored, along with E_n, for later contour plotting. The process is again executed for the remaining interpolation points.

3. Possible Problem Areas

From the numerous runs of the objective analysis that have been made in gaining an understanding of the technique and processing data, two interrelated factors have been found that determine the caliber of the objectively analyzed fields: data density and quality, and the noise variance estimate.

Generally, the more robust the sample field, the better the quality of the resulting objective analysis. However, this may not always be the case. Too many selected observations too close to each other (high autocorrelation values) may result in an autocorrelation matrix that is not diagonally dominant, and an ill-conditioned

(singular or near-singular) matrix may result. If this happens to be the case, the interpolated value may be grossly non-representative of the data it was computed from, and the RMS interpolation error will be high. By specifying A_{max} to be less than a certain value (limiting the minimum distance between observations), this will limit the magnitude of the off-diagonal elements and result in a properly conditioned matrix, which should produce acceptable results.

The estimated noise variance is another factor that can affect an interpolation, although the effect will not be as great as improperly specifying the maximum autocorrelation value. If the noise variance is specified to be too small, especially in sparse data fields with a high noise variance, this may also cause the autocorrelation matrix to become ill-conditioned. As the noise is added to the main diagonal of the matrix, it also biases it toward diagonal dominance so a successful inversion can be accomplished. With a higher density of observations, smaller bin sizes can be used to compute the autocorrelation values and more points will be available for the least squares fit. This could result in a better estimate of that part of the variance attributable to noise.

Another name for the objective analysis technique is optimal interpolation. With a knowledge of the statistics of the data and a correlation function, the fraction of the variance due to noise can be calculated. These factors, along with a specified maximum autocorrelation value and the observations will result in an optimal interpolation of the observations to each interpolation point, and an acceptable representation of the sampled field. Failure to properly specify these parameters may result in erroneous mappings due to the problems of non-singular matrices and observations that are too closely spaced. The effectiveness of a system such as the ADDAS for synoptic mappings is directly related to quality of the acquired data and the proper processing of this data.

D. THE OPTOMA PROGRAM SAMPLING STRATEGY

Applying the considerations discussed in the previous sections, and with the knowledge gained from earlier OPTOMA Program AXBT survey flights, the following key factors were considered in the development of the airborne sampling strategy in the NOCAL and CENCAL domains of the OPTOMA Program:

- Size of region: The 250-km square covers the maximum area that can be surveyed by a Navy P-3 aircraft based at Moffett Field Naval Air Station, California, on a single mission.

- Number of AXBT's: 96 AXBT's is the maximum number that can be carried by the P-3 to remain within specified gross weight limitations and still have adequate fuel, including reserve, to complete a mission in this size region and at this distance from base, and to provide an adequate resolution of the mesoscale processes.

- AXBT spacing: This is a function of many variables. AXBT's are deployed at five minute time intervals (~28 km spacing). This increment has been determined from previous flights to provide an optimal coverage of the region, and it takes into account the spatial scale of oceanic features to be observed, ADDAS response, AXBT fall time from the aircraft, AXBT transmission time, and AXBT-aircraft line-of-sight transmission range, for aircraft on-station groundspeed of 180 to 200 kts and altitude of 500 to 1000 ft AGL.

V. SIMULATED APPLICATION OF THE SAMPLING STRATEGY

The sampling strategy was applied to "simulated" AXBT survey flights in "synthetic" oceanic domains. The oceanic variability in these domains was synthesized from the superposition of linear planetary Rossby waves (LPRW's). The simulated survey domains were 256-km by 256-km square, representing a nominal areal survey domain as in the OPTOMA Program. Synoptic mappings were generated from the simulated AXBT observations using the objective analysis technique. Some assumptions were made in applying the sampling strategy; these were:

- No limit to aircraft endurance, airspeed, or payload capability,
- Unlimited number of AXBT's,
- No AXBT failures,
- No limitations on the ADDAS,
- Temporal scales of the fields were not considered.

Although not fully realistic, these assumptions provide a basis to exercise the objective analysis technique on controlled data.

A. DEVELOPING THE SYNTHETIC FIELDS

A field of eddy-like features can be generated from the superposition of LPRW's. Starting with the non-linear, hydrostatic, Boussinesq equations, and using a non-dimensionalization and perturbation expansion in terms of the Rossby number, a quasi-geostrophic potential vorticity (QGPV) equation can be derived:

$$\frac{D}{Dt}\{\nabla^2_h p_0 + \beta y + \frac{\partial}{\partial z}[\frac{1}{N^2}\frac{\partial p_0}{\partial z}]\} = 0,$$

where

$$\frac{D}{Dt} = \frac{\partial}{\partial t} + u\frac{\partial}{\partial x} + v\frac{\partial}{\partial y}.$$

(The reader is directed to Gill, 1982, Ch.11, for the complete derivation.) The governing equation (GE) for LPRW's can be obtained by linearizing the QGPV equation,

$$\frac{\partial}{\partial t}[\nabla^2_h p_0 + \frac{\partial}{\partial z}(\frac{1}{N^2}\frac{\partial p_0}{\partial z})] + \beta\frac{\partial p_0}{\partial x} = 0,$$

where,

$$\nabla^2_h ( ) = \partial^2( )/\partial x^2 + \partial^2( )/\partial y^2.$$

The assumed plane-wave solution for the GE,

$$p_0 = P(z) \exp [i (\sigma t - \kappa (x \cos\theta + y \sin\theta))],$$

where the real part,

$$p_0 = P(z) \cos (\sigma t - kx - ly),$$

with

$$k = \kappa \cos\theta, \text{ and } l = \kappa \sin\theta,$$

is substituted into the GE and simplified, resulting in

$$\sin(\sigma t - kx - ly) \{ P(z) [(k^2 + l^2) + (\beta k/\sigma)] - \frac{\partial}{\partial z} (\frac{1}{N^2} \frac{\partial P(z)}{\partial z}) \} = 0,$$

which is the GE for the vertical structure. Letting

$$-\mu^2 \equiv (k^2 + l^2) + (\beta k/\sigma),$$

gives the resulting form of the equation,

$$\frac{\partial}{\partial z} (\frac{1}{N^2} \frac{\partial P}{\partial z}) + \mu^2 P = 0$$

which is a Sturm-Liouville problem. Applying the rigid (kinematic) boundary condition, $\partial p/\partial z = 0$, at $z = 0$, and at $z = -D$ (where D is the water depth), there will be an infinite number of eigenvalues and eigenfunctions, where μ_n are the eigenvalues. Solving for σ_n, the dispersion relation (DR) for the n*th* vertical mode is

$$\sigma_n = \frac{-\beta k_n}{\mu^2_n + (k^2_n + l^2_n)}, \quad (n = 0, 1, 2, \ldots).$$

The n*th* mode Rossby radius of deformation can be defined as $\lambda_n = \mu_n^{-1}$. In dimensional form, the barotropic Rossby radius is $\lambda_0 = c_0 / f_0$, where $c_0 = (gD)^{1/2}$ (wave speed) and $f_0 = 2\Omega \sin(\varphi)$ (coriolis parameter, and φ is the latitude). Assuming a constant Brunt-Väisälä (N^2) profile, the baroclinic Rossby radii can be defined as $\lambda_n = ND / n\pi f_0$. By convention, σ_n must be greater than or equal to zero;

therefore, $\cos\theta$ must be less than or equal to zero, ($\pi / 2 \leq \theta \leq 3\pi / 2$), giving a westward, with a northward or a southward component, direction of propagation.

B. THE SYNTHETIC FIELDS

The synthetic fields were calculated by the following general equation for *M* different waves, each with *N* normal modes. Each wave is a suite of progressive modes, all having the same (*k*,*l*), and instantaneously in phase at t = 0.

$$F(x, y, z, t) = \sum_{m=1}^{M} \sum_{n=1}^{N} A_{m,n} \Phi_n(z) \cos(\sigma_{m,n} t - \kappa_m (x \cos\theta_m + y \sin\theta_m)),$$

where

F: is the value of the synthetic field at some x, y, z, t,

$A_{m,n}$: is an arbitrary amplitude function,

$\Phi_n(z)$: is a depth function, $\cos(\pi z / D)$,

$\sigma_{m,n}$: is the frequency for the *nth* normal mode,

κ_m: is the total wave number, $2\pi / L$, and

θ_m: is the propagation direction.

The physical constants used in the calculations were $g = 9.8\ ms^{-1}$, $D = 4$ km, $\varphi = 38.5°$, and $N = 1.0 \times 10^{-2}\ s^{-1}$, giving $f_0 = 9.07 \times 10^{-5}\ s^{-1}$, $\beta = 1.79 \times 10^{-11}\ (ms)^{-1}$, which are representative of a mid-latitude oceanic region as in the OPTOMA domains. The limits of the synthetic fields are $-32 \leq x, y \leq 288$ km, to provide flexibility in sampling at the boundaries of the subdomain. The simulated sampling subdomain is within the region bounded by $0 \leq x, y \leq 256$.

C. PROCEDURE

1. Synthetic Field Generation

Two synthetic fields were generated through use of the general equation presented above. Each field was computed at t = 0 ($\sigma_{m,n} t = 0$) and z = 0 ($\Phi_n(z) = 1$), with $A_{m,n} = 1$ for all waves and all modes. A summary of the specific parameters for each field is presented in Table 3. The origin of each wave contributing to the field is referenced to the origin of the subdomain, (0, 0). "SYNFLD1" (Figure 5.1) produced a standing pattern of eddy-like features with a wavelength of ~216 km (eddy diameter ~108 km). This field was scaled from 10 to 18 °C, representing a nominal SST range as observed in the OPTOMA domains. "SYNFLD2" (Figure 5.2)

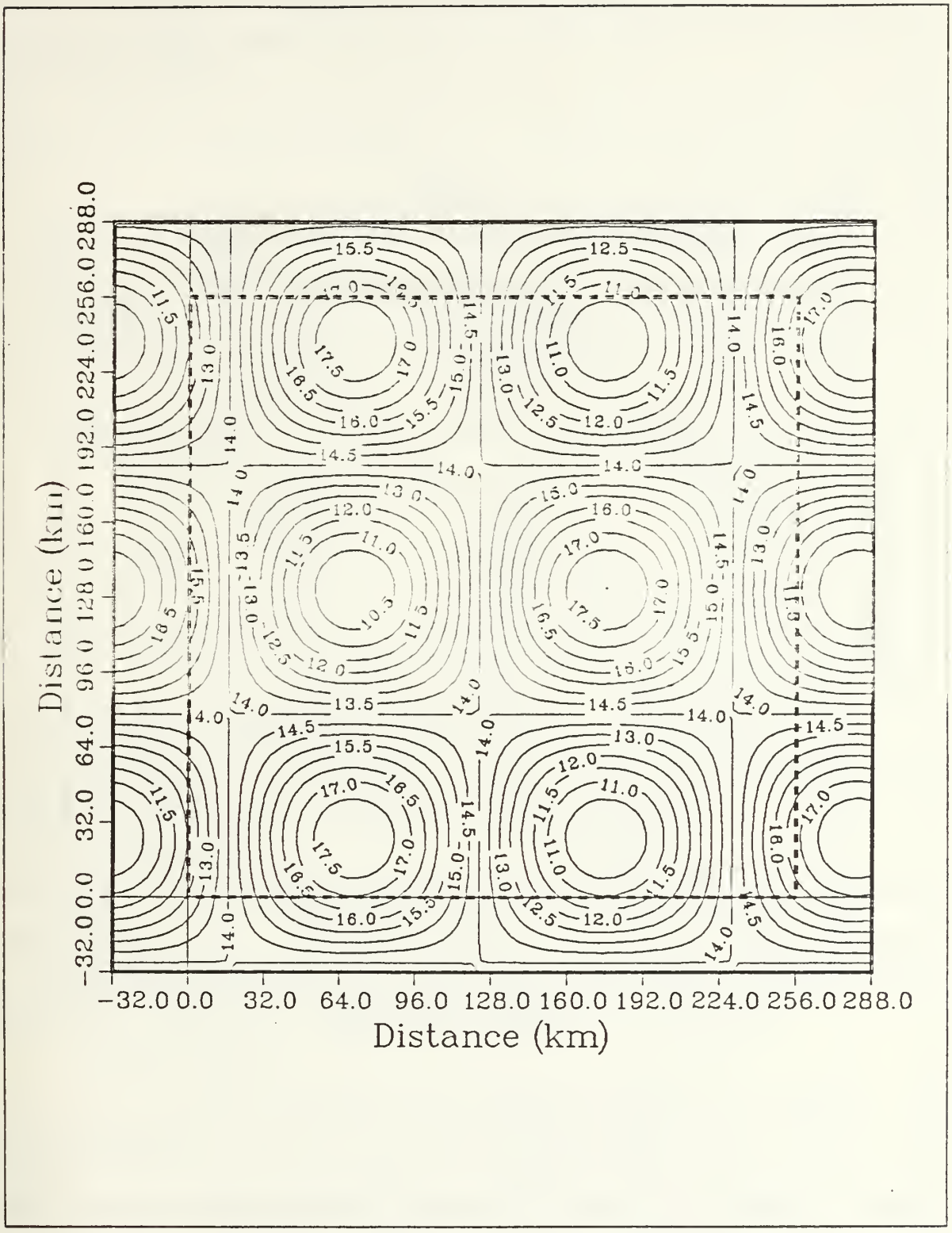

Figure 5.1 Synthetic field, SYNFLD1 and sample subdomain (dashed line), representing SST in °C. Contour interval 0.5°C.

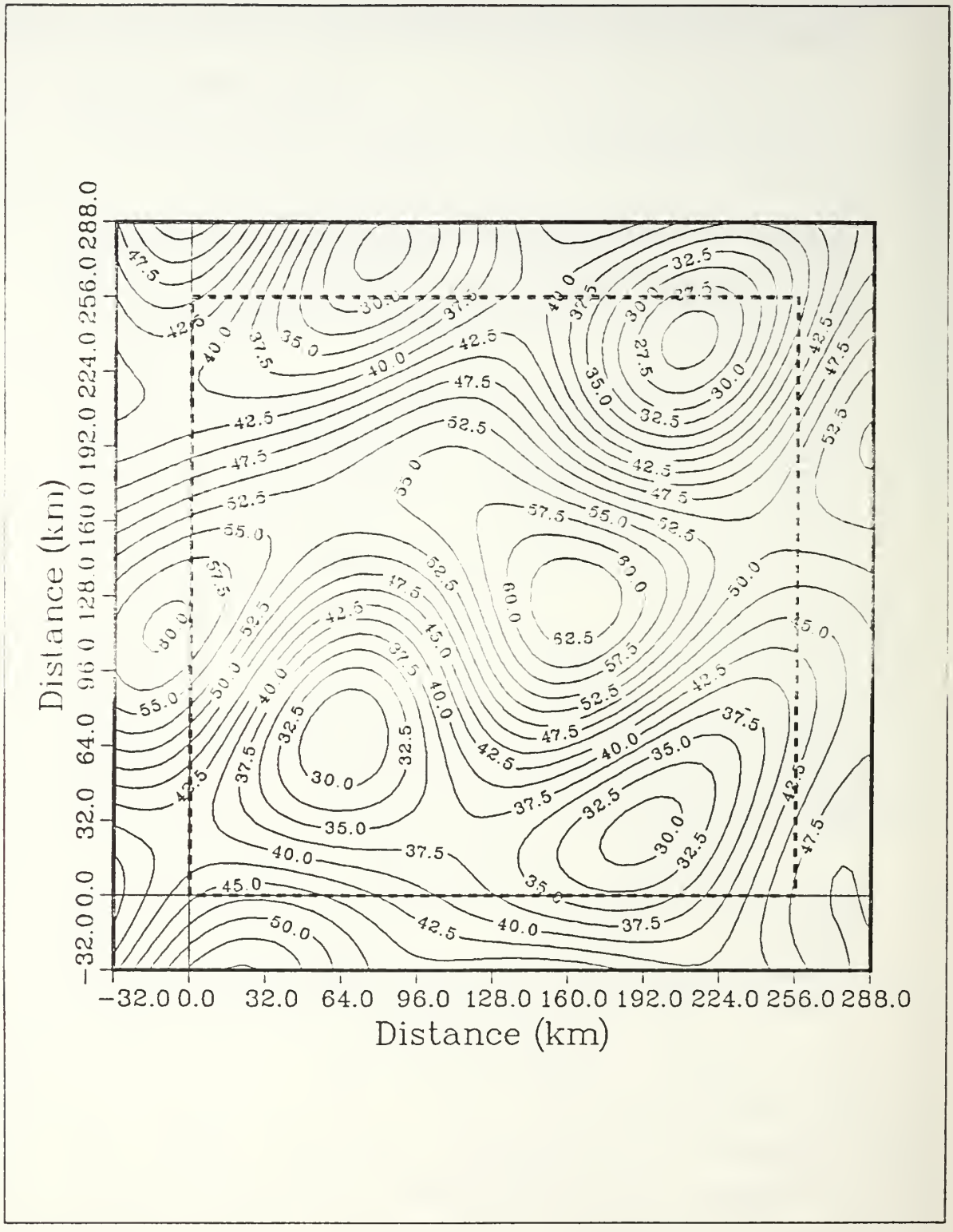

Figure 5.2 Synthetic field, SYNFLD2 and sample subdomain (dashed line), representing MLD in meters. Contour interval 2.5 m.

was scaled to represent a mapping of mixed layer depth, with representative values from 20 to 70 meters. Again this was based on a similar range of MLD's observed in the OPTOMA domains.

TABLE 3
SYNTHETIC FIELD SPECIFIC PARAMETERS

Field: SYNFLD1 Number of Waves: 2 Number of Modes: 2

$Wave_m$	Origin	Wavelength (km)	θ_m(°)
1	(-42, 3)	150.0	135
2	(11, 106)	150.0	225

Field: SYNFLD2 Number of Waves: 5 Number of Modes: 3

$Wave_m$	Origin	Wavelength (km)	θ_m(°)
1	(-23, 52)	200.0	090
2	(42,-70)	125.0	135
3	(6, 23)	150.0	180
3	(-65, 26)	175.0	225
5	(74, 110)	250.0	270

2. Simulated AXBT Surveys

The simulated survey flights are based on the flight plan employed on OPTOMA20P, with flight tracks oriented parallel to the local x axis.

a. SYNFLD1

Progressions of six AXBT survey flights, each with a different AXBT spacing were conducted in SYNFLD1. Each different spacing was based on the reference spacing of $\Delta x = \Delta y = 28$ km, as is used in OPTOMA Program survey flights. Four symmetric grids and two "checkerboard' patterns were completed in each progression.

(1) *Progression 1.*

In this progression, four surveys simulated a symmetric x, y observation pattern with $\Delta x = \Delta y = 14$, 21, 28, and 42 km. These surveys were designated S1-14, S1-21, S1-28, and S1-42, respectively. The two remaining surveys were variations on the 21 and 28 km observations. Every other observation was used so that in each row, the samples were offset from each other, as the black squares on a checkerboard. These were designated S1-42X and S1-56X.

(2) *Progression 2.*

In the second progression the same data were used, but a random position error, varying between ± 4 km (~2 NM) was introduced to represent aircraft navigational error in AXBT locations. These represent one particular realization of the random position errors (used in the computations), and were designated S1-14N,...,S1-56XN.

b. SYNFLD2

One survey was completed in this field with $\Delta x = \Delta y = 28$ km, and a ± 4 km position error. Again this represents a nominal OPTOMA survey flight. A progression of six objective analysis computations were completed on the survey data. The two versions of the correlation function as presented in Chapter IV were used. The input parameters, fraction noise variance and maximum autocorrelation value, were varied for each computation.

3. Application of Objective Analysis

For each simulated AXBT survey in a progression, the objective analysis technique was applied as Chapter IV. It is briefly summarized:

- The autocovariance function and the fitted correlation function are computed, and confidence limits at each point on the curve, based on the 95% confidence interval for a normal distribution are calculated.
- From the fitted function, the fraction of the variance due to noise is estimated and the zero-crossing distance is determined. The noise variance, radius of influential points, interpolation point spacing, number of influential observations, and maximum autocorrelation value are then input into the objective analysis program.
- The objective analysis technique is applied at each interpolation point, and quality checks on the value of the autocorrelation matrix determinant and maximum autocorrelation values are computed. The objectively analyzed fields and their RMS interpolation errors were computed and then mapped.

4. **Comparisons**

For each progression, the correlation (CORR), root mean square error (RMS), both the systematic (RMSS) and unsystematic (RMSU) root mean square error, and mean absolute error (MAE) were computed between interpolation points of each simulated survey and the true field (synthetic field observed at the interpolation points). Also each survey was compared with the reference survey ($\Delta x = \Delta y = 28$ km). The RMSS error is a measure of the linear bias in the objective analysis, while the RMSU error is a measure of the precision of the interpolated field. For a complete description of the formulas applied, the reader is directed to Willmott, *et al.*, (1985).

D. SUMMARY OF RESULTS

1. SYNFLD1

The autocorrelation computations (Table 4) show an increasing estimated noise variance with an increase in sample spacing. The worst case was the 42 km symmetric surveys, S1-42 and S1-42N, for both progressions 1 and 2. The zero-crossing is also much shorter. This could be the result of the larger bin size used to compute the autocovariance values as the sample density was more sparse when compared to the other surveys. The relative magnitudes of the autocorrelation values in each progression are approximately the same. The observation positions, covariance function, and fitted correlation function are presented for surveys S1-42, S1-42X, S1-56X (Figures 5.3, 5.4, 5.5) and S1-42N, S1-42XN, S1-56XN (Figures 5.6, 5.7, 5.8).

TABLE 4

AUTOCOVARIANCE AND CORRELATION FUNCTION CALCULATIONS, SYNFLD1

Progression 1

Survey	Bin Size (km)	Estimated Signal Variance $°C^2$	Estimated Noise Variance $°C^2$	Fraction Noise	Zero Crossing Distance (km)
S1-14	30	3.604	0.316	0.081	55.9
S1-21	30	3.455	0.483	0.123	52.9
S1-28	30	3.081	0.858	0.218	52.0
S1-42	45	1.836	2.132	0.537	39.4
S1-42X	30	3.055	0.878	0.223	59.3
S1-56X	40	2.086	1.855	0.471	56.0

Progression 2

Survey	Bin Size (km)	Estimated Signal Variance $°C^2$	Estimated Noise Variance $°C^2$	Fraction Noise	Zero Crossing Distance (km)
S1-14N	30	3.551	0.370	0.094	56.2
S1-21N	30	3.584	0.343	0.087	55.1
S1-28N	30	3.262	0.675	0.171	54.2
S1-42N	45	2.115	1.852	0.467	43.6
S1-42XN	30	3.589	0.343	0.087	56.4
S1-56XN	40	2.927	1.011	0.256	60.5

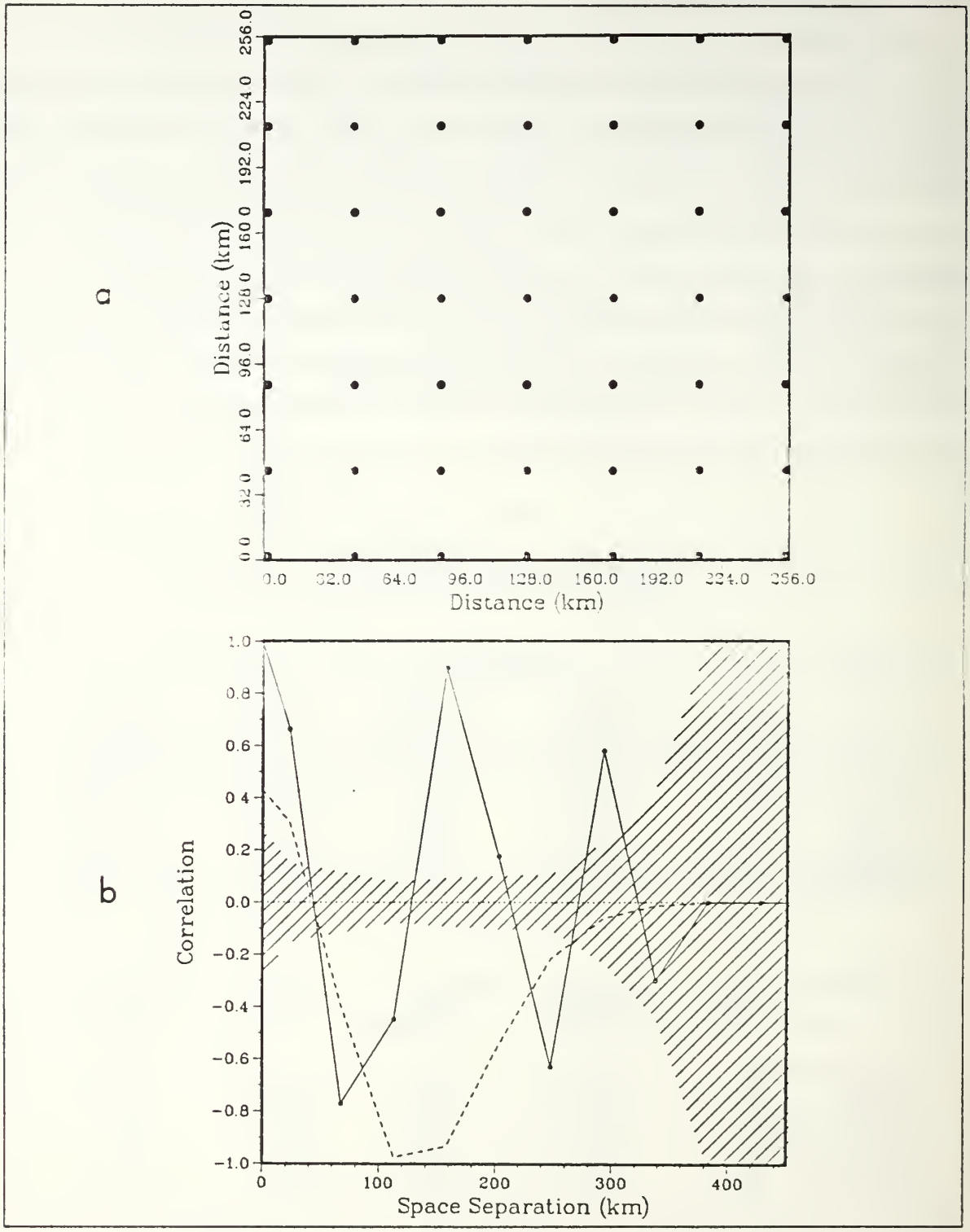

Figure 5.3 SYNFLD1, Progression 1, Sample S1-42. (a) Observation positions. (b) Autocorrelations (solid) and fitted function (dashed). 95 % confidence limits (shaded).

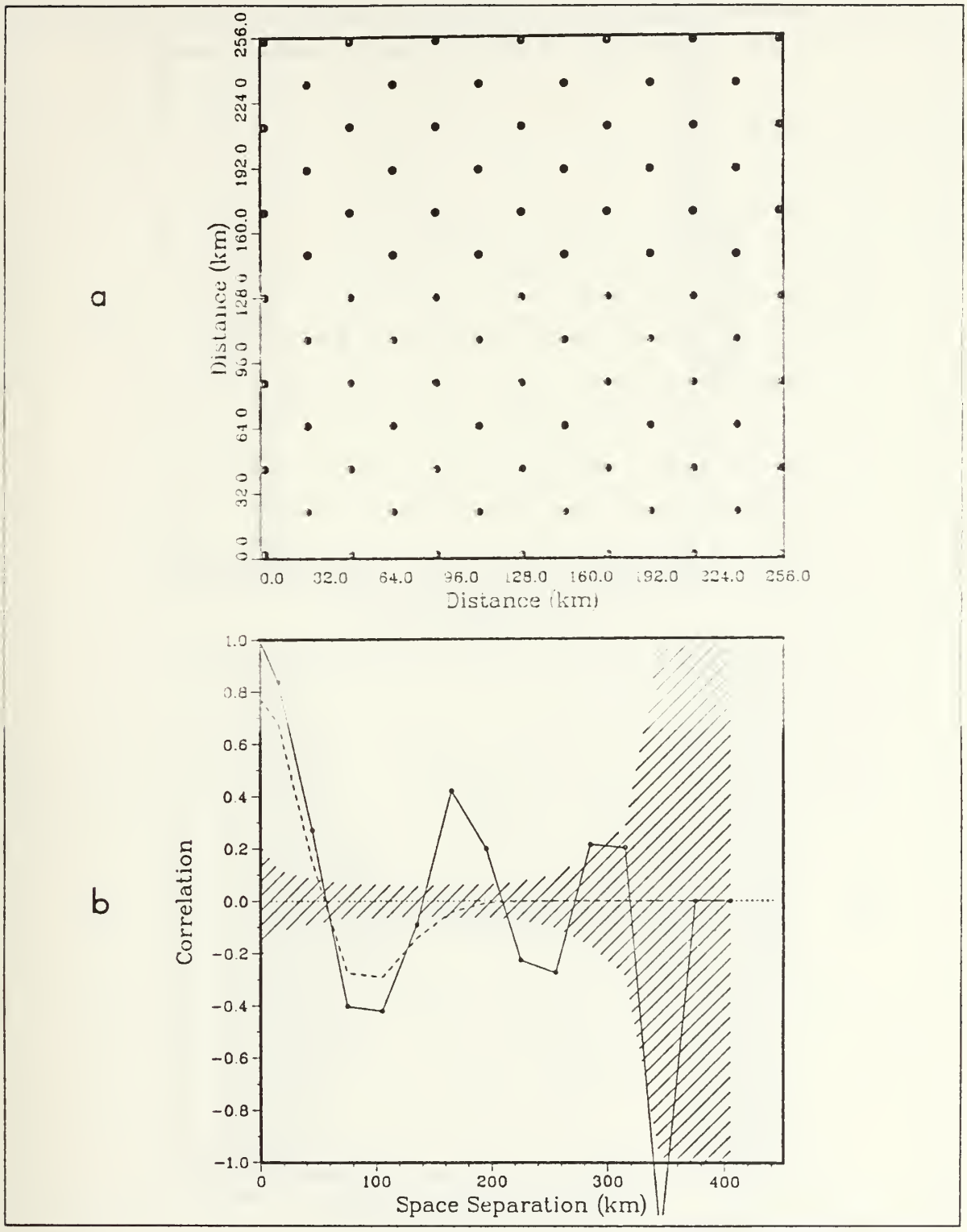

Figure 5.4 SYNFLD1, Progression 1, Sample S1-42X. (a) Observation positions. (b) Autocorrelations (solid) and fitted function (dashed). 95 % confidence limits (shaded).

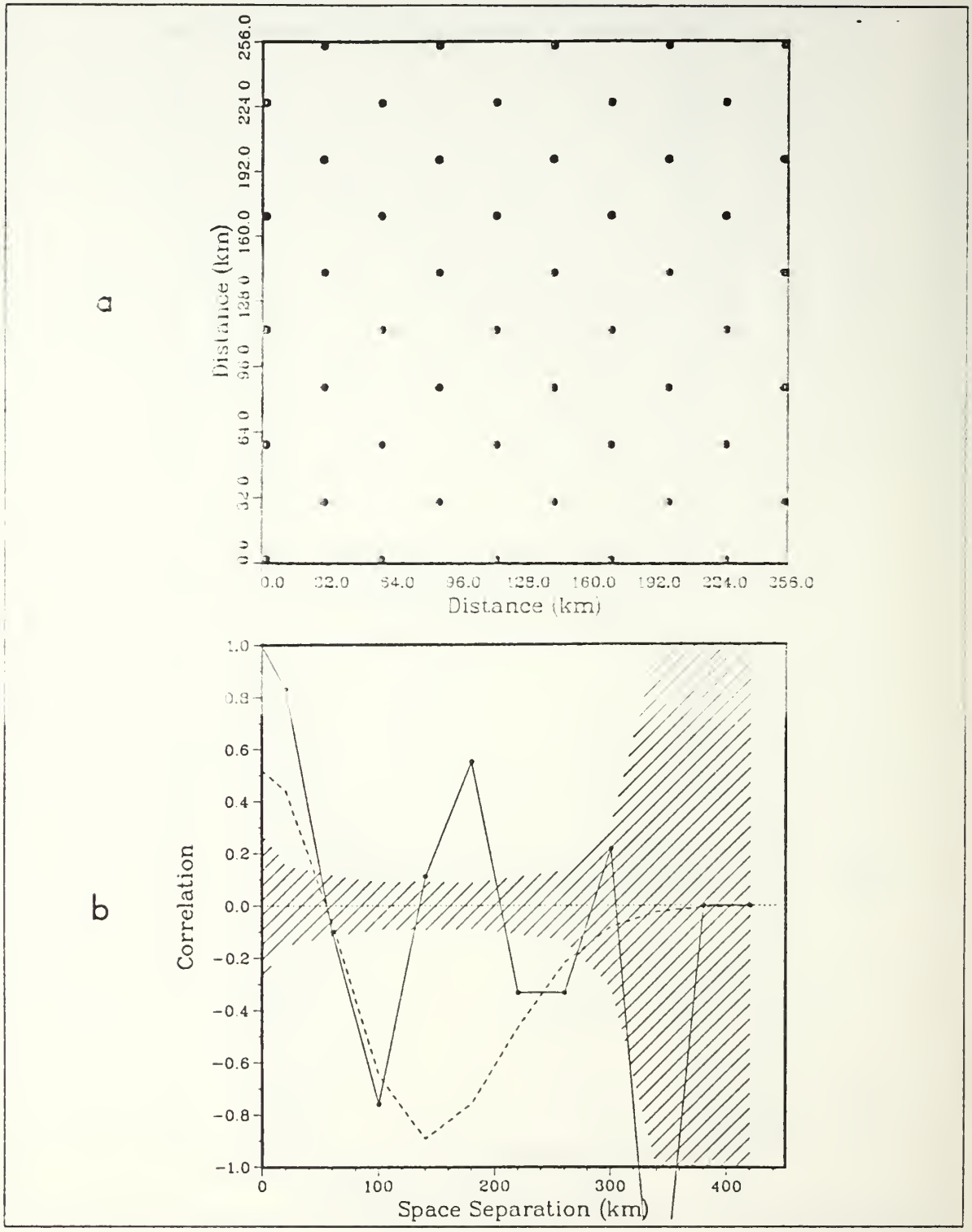

Figure 5.5 SYNFLD1, Progression 1, Sample S1-56X. (a) Observation positions. (b) Autocorrelations (solid) and fitted function (dashed). 95 % confidence limits (shaded).

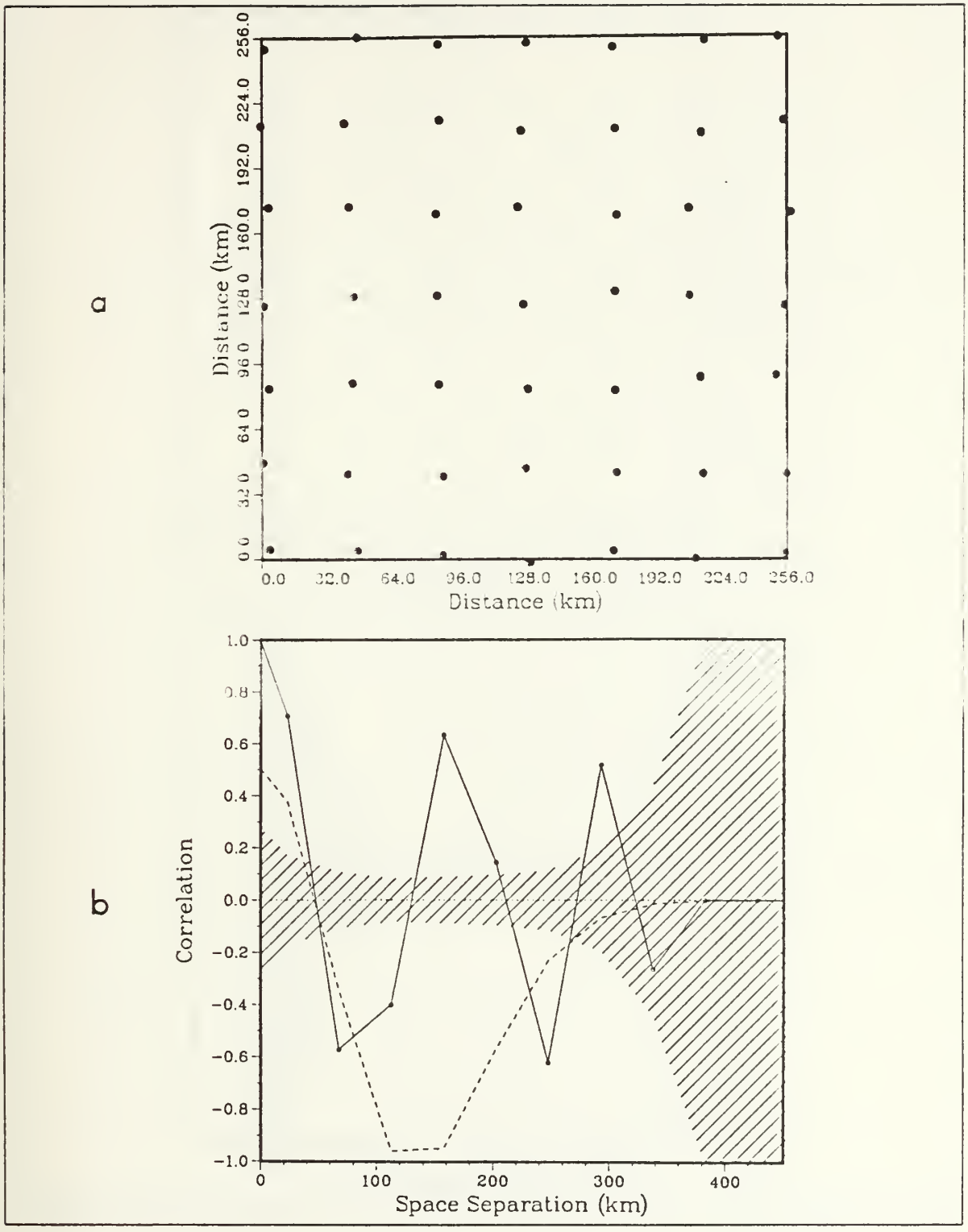

Figure 5.6 SYNFLD1, Progression 2, Sample S1-42N. (a) Observation positions. (b) Autocorrelations (solid) and fitted function (dashed). 95 % confidence limits (shaded).

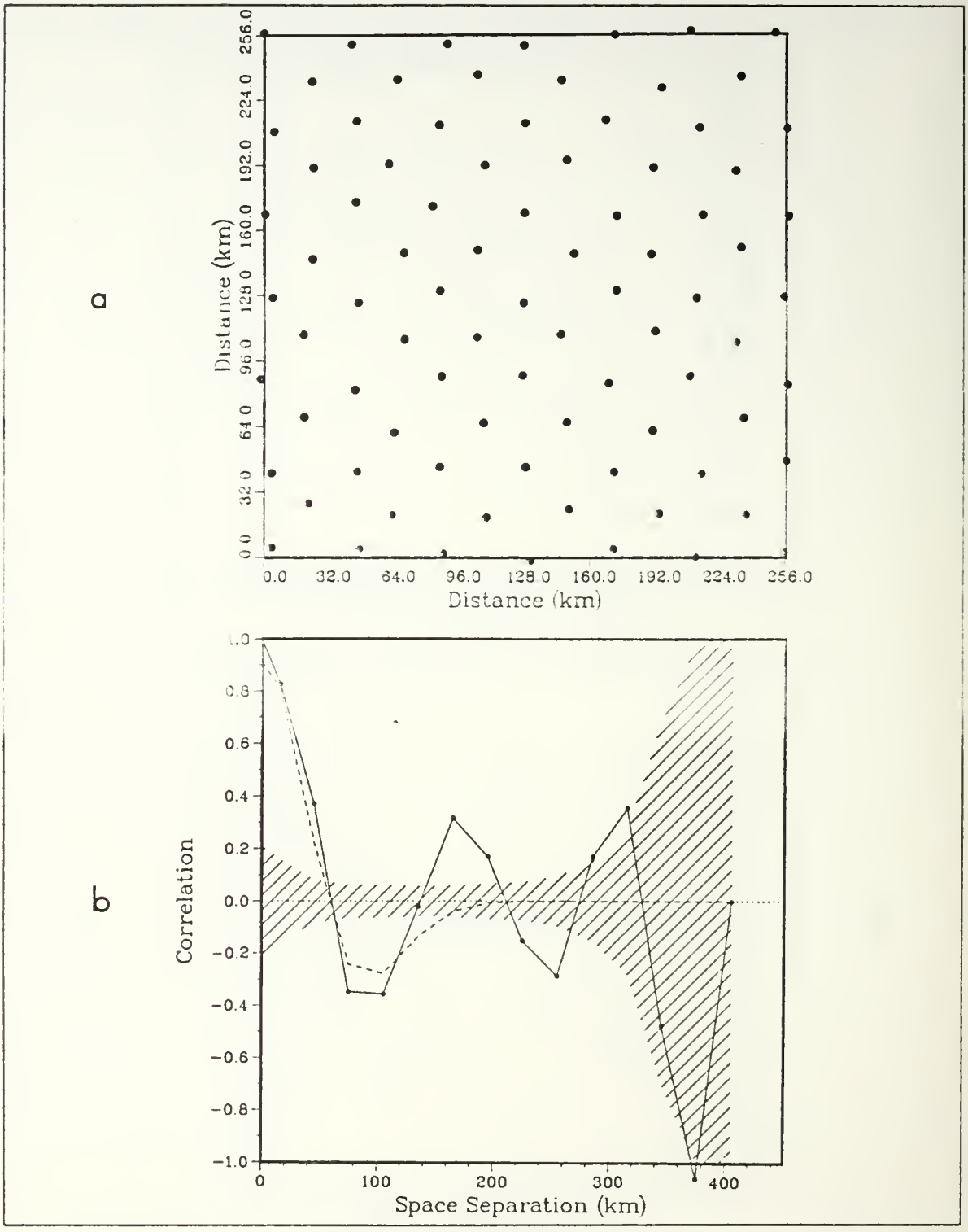

Figure 5.7 SYNFLD1, Progression 2, Sample S1-42XN. (a) Observation positions. (b) Autocorrelations (solid) and fitted function (dashed). 95 % confidence limits (shaded).

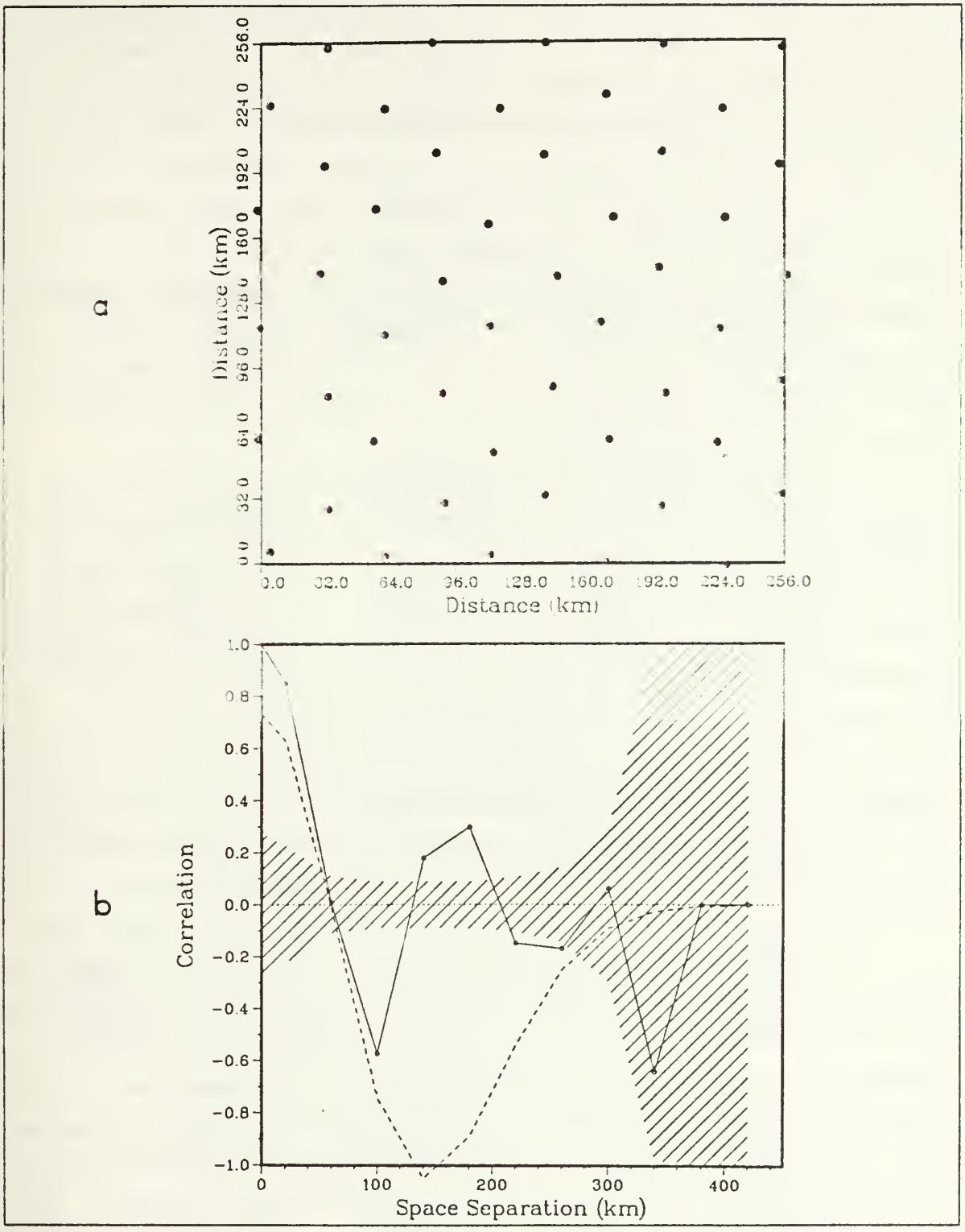

Figure 5.8 SYNFLD1, Progression 2, Sample S1-56XN. (a) Observation positions. (b) Autocorrelations (solid) and fitted function (dashed). 95 % confidence limits (shaded).

All objective analyses for SYNFLD1 were interpolated to a regular 13 by 13 grid with a spacing of 20 km. This spacing was chosen as it was less than half of the zero crossing distance of the reference survey, S1-28N. Input parameters were applied differently for each progression (Table 5). An estimated fraction noise variance of 0.05 and a maximum autocorrelation value of 1.0 were used in Progression 1 to illustrate the results of improper specification of the objective analysis input parameters. The radius of influence was fixed at 50 km and the zero-crossing distance was 55 km. For Progression 2, the radius of influence for each survey was the computed zero-crossing distance and the noise variance was as estimated. The maximum autocorrelation value was selected to be 0.7, which limits the distance between selected observations to greater than 25 km. Equation 4.2 was the correlation function selected to be employed, as in the ADDAS software.

The objective analysis RMS interpolation errors are slightly larger in Progression 2 than in Progression 1, but the range of values for the determinant is decreased by three orders of magnitude (Table 5). This is a direct result of the specification of a smaller maximum autocorrelation value for Progression 2. The appearance of the objectively analyzed fields remains consistent between the two progressions through surveys S1-28, Progression 1, and S1-28N, Progression 2. The fields become more erratic with the larger observation spacing, S1-42, S1-42X, and S1-56X in Progression 1 (Figures 5.9, 5.10, 5.11), while maintaining a consistent representation of the field in Progression 2 (Corresponding surveys S1-42N, S1-42XN, and S1-56Xn, Figures 5.12, 5.13, and 5.14, respectively). Again, the cause of the erratic nature observed in Progression 1 appears to be the improper specification of the maximum autocorrelation value. The fraction noise variance may have a minor effect.

The comparisons (Table 6) show that the correlation is very high for all samples in both progressions. However, samples S1-42N and S1-56XN in Progression 2 show better correlation than S1-42 and S1-56X in Progression 1 when "proper" input parameters are specified. The magnitudes of the error parameters are generally consistent between the two progressions with the exception of the RMS error between S1-56X and S1-56XN. The systematic parts are nearly equal whereas the unsystematic part is almost five times greater for S1-56X. Since the RMSS is a measure of the precision of the interpolated field, and although Progression 2 (S1-56XN) contained errors in the positions of the observations, the proper specification, by the user, of the input parameters for the objective analysis appears to increase the precision.

TABLE 5

OBJECTIVE ANALYSES SUMMARY, SYNFLD1

Progression 1

Input Parameters

Sample	Radius of Influence (km)	Maximum Number of Observations	Maximum Autocorrelation Value	Fraction Noise Variance
ALL	50	7	0.7	0.05

Computations

Survey	RMS Error (%)	Maximum Autocorrelation	Determinant Maximum	Determinant Minimum
S1-14	0.01	0.918	0.183E-4	0.152E-4
S1-21	0.01-0.03	0.819	0.590E-4	0.294E-4
S1-28	0.02-0.15	0.844	0.987E-1	0.103E-3
S1-42	0.01-0.20	0.917	0.850	0.906E-1
S1-42X	0.02-0.05	0.766	0.650E-1	0.874E-2
S1-56X	0.01-0.22	0.844	0.937	0.514E-2

Progression 2

Input Parameters

Sample	Radius of Influence (km)	Maximum Number of Observations	Maximum Autocorrelation Value	Fraction Noise Variance
S1-14N	56.15	7	0.7	0.094
S1-21N	55.09	7	0.7	0.087
S1-28N	54.18	7	0.7	0.171
S1-42N	43.56	7	0.7	0.467
S1-42NX	56.39	7	0.7	0.087
S1-56NX	60.45	7	0.7	0.256

Computations

Survey	RMS Error (%)	Maximum Autocorrelation	Determinant Maximum	Determinant Minimum
14N	0.04-0.07	0.700	0.107	0.109E-1
21N	0.04-0.04	0.696	0.418	0.115E-1
28N	0.07-0.12	0.699	0.405	0.674E-1
42N	0.31-0.49	0.446	4.121	2.126
42XN	0.04-0.12	0.697	0.174	0.130E-1
56XN	0.11-0.26	0.648	1.490	0.505

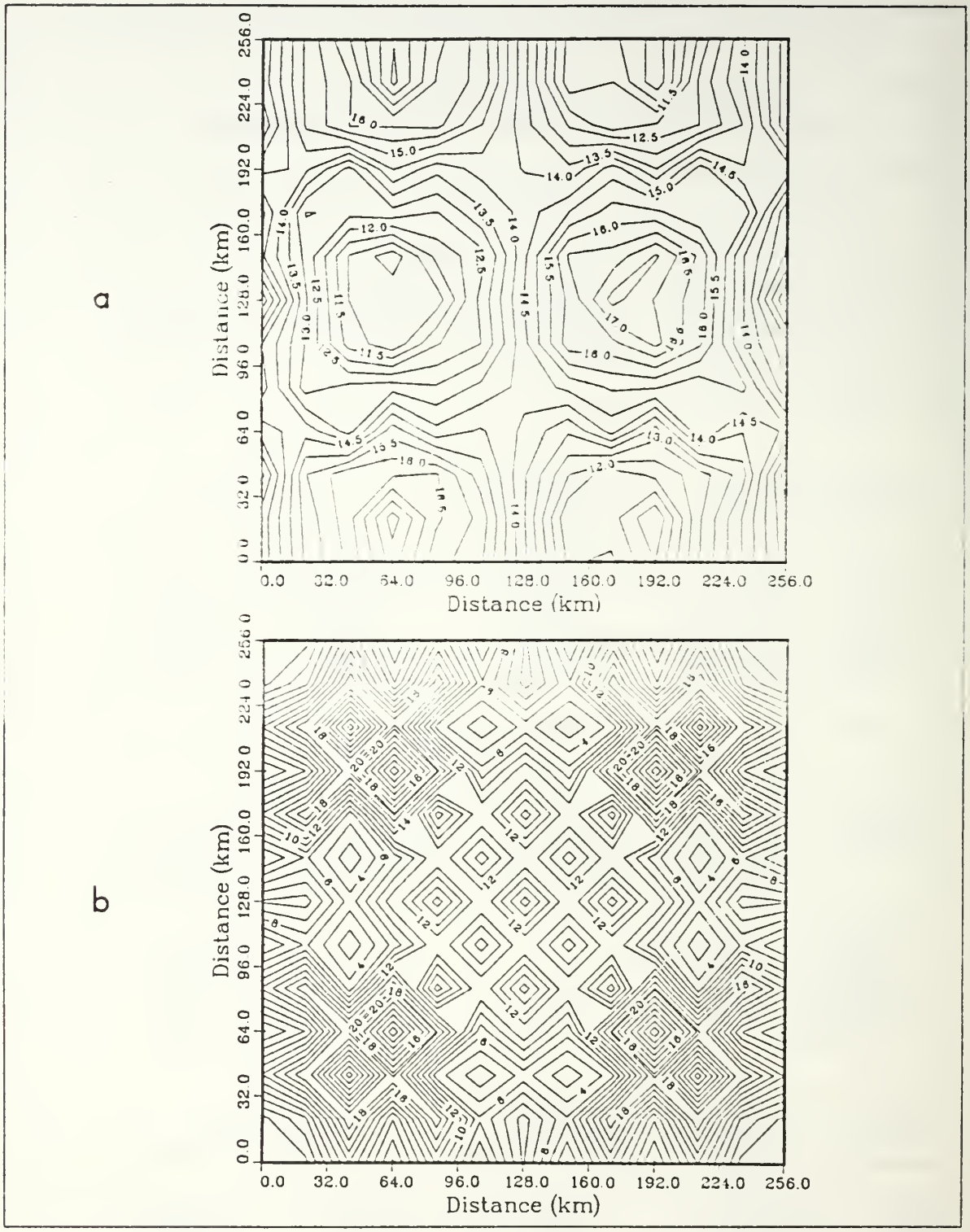

Figure 5.9. SYNFLD1, Progression 1, Sample S1-42.
(a) Objective analysis. Contour interval 0.5°C.
(b) RMS interpolation error (%).

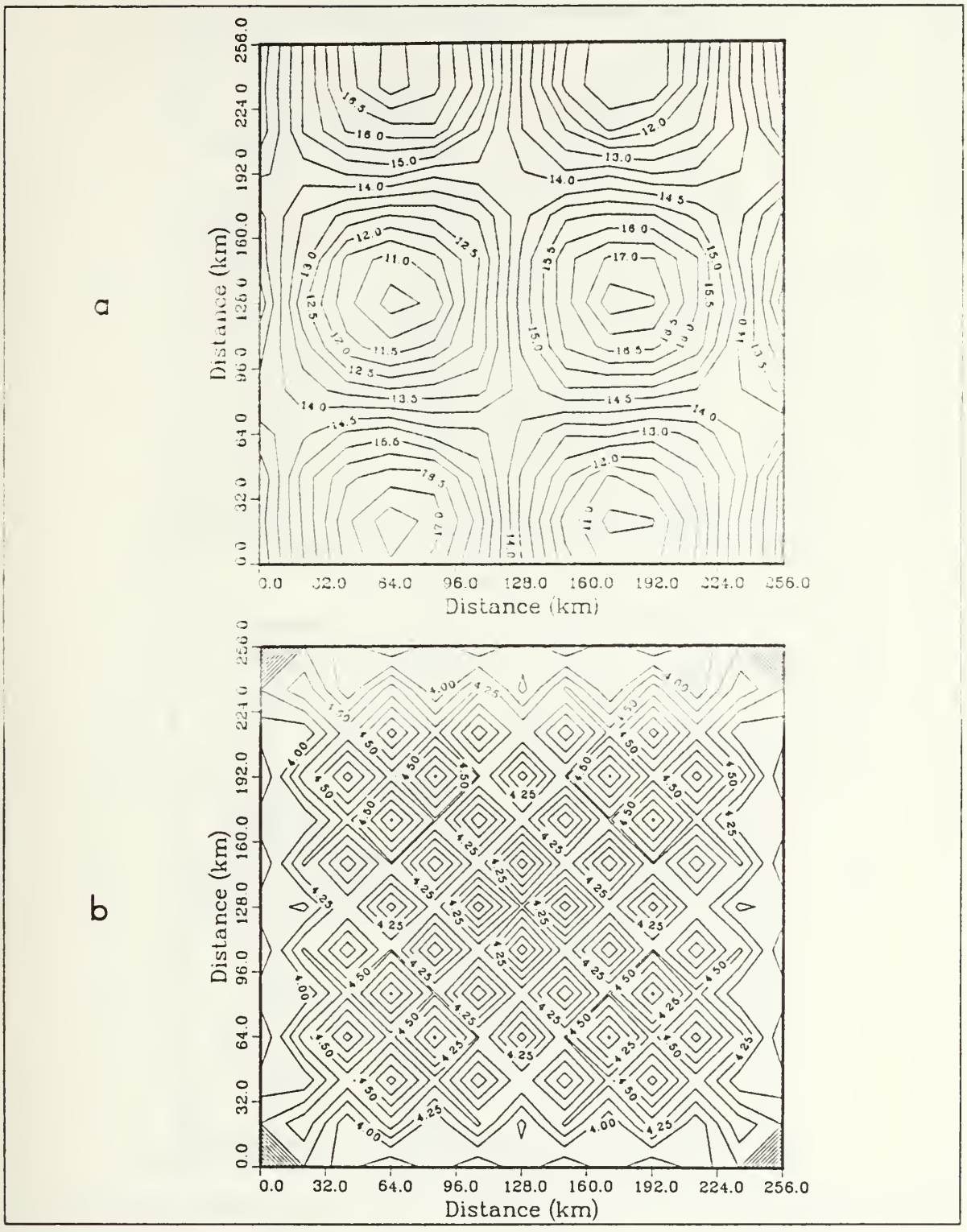

Figure 5.10 SYNFLD1, Progression 1, Sample S1-42X.
(a) Objective analysis. Contour interval 0.5°C.
(b) RMS interpolation error (%).

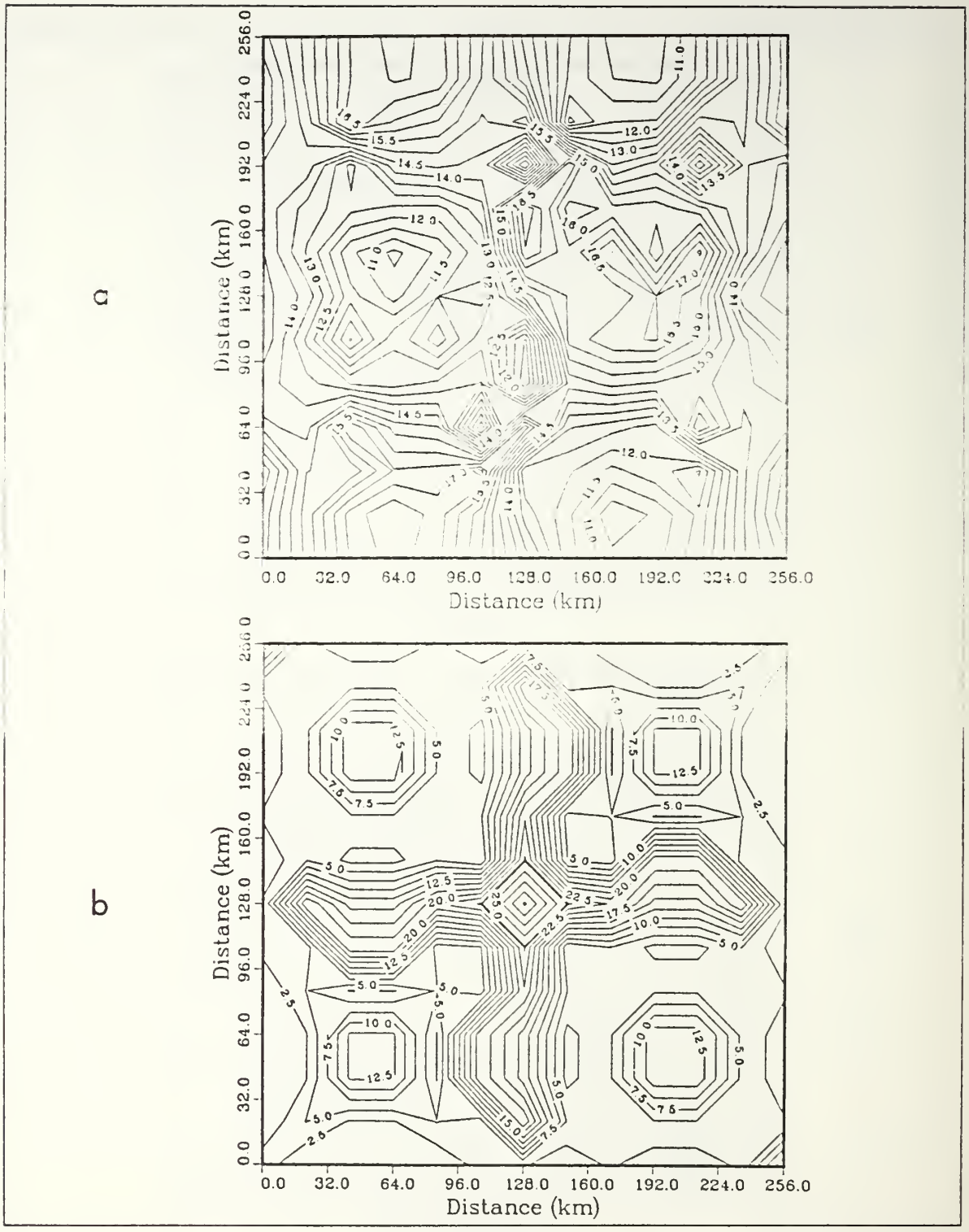

Figure 5.11. SYNFLD1, Progression 1, Sample S1-56X.
(a) Objective analysis. Contour interval 0.5°C.
(b) RMS interpolation error (%).

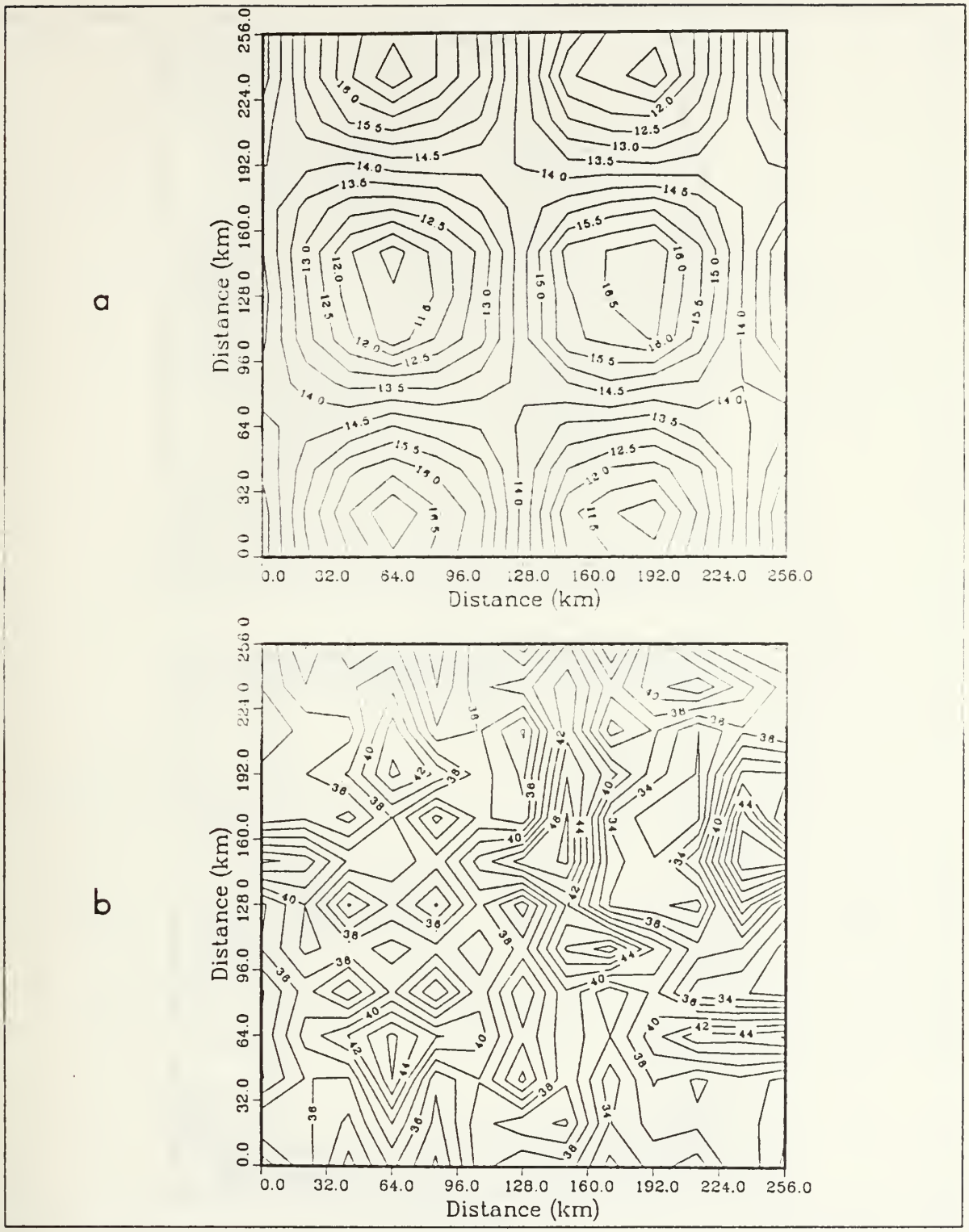

Figure 5.12 SYNFLD1, Progression 2, Sample S1-42N.
(a) Objective analysis. Contour interval 0.5°C.
(b) RMS interpolation error (%).

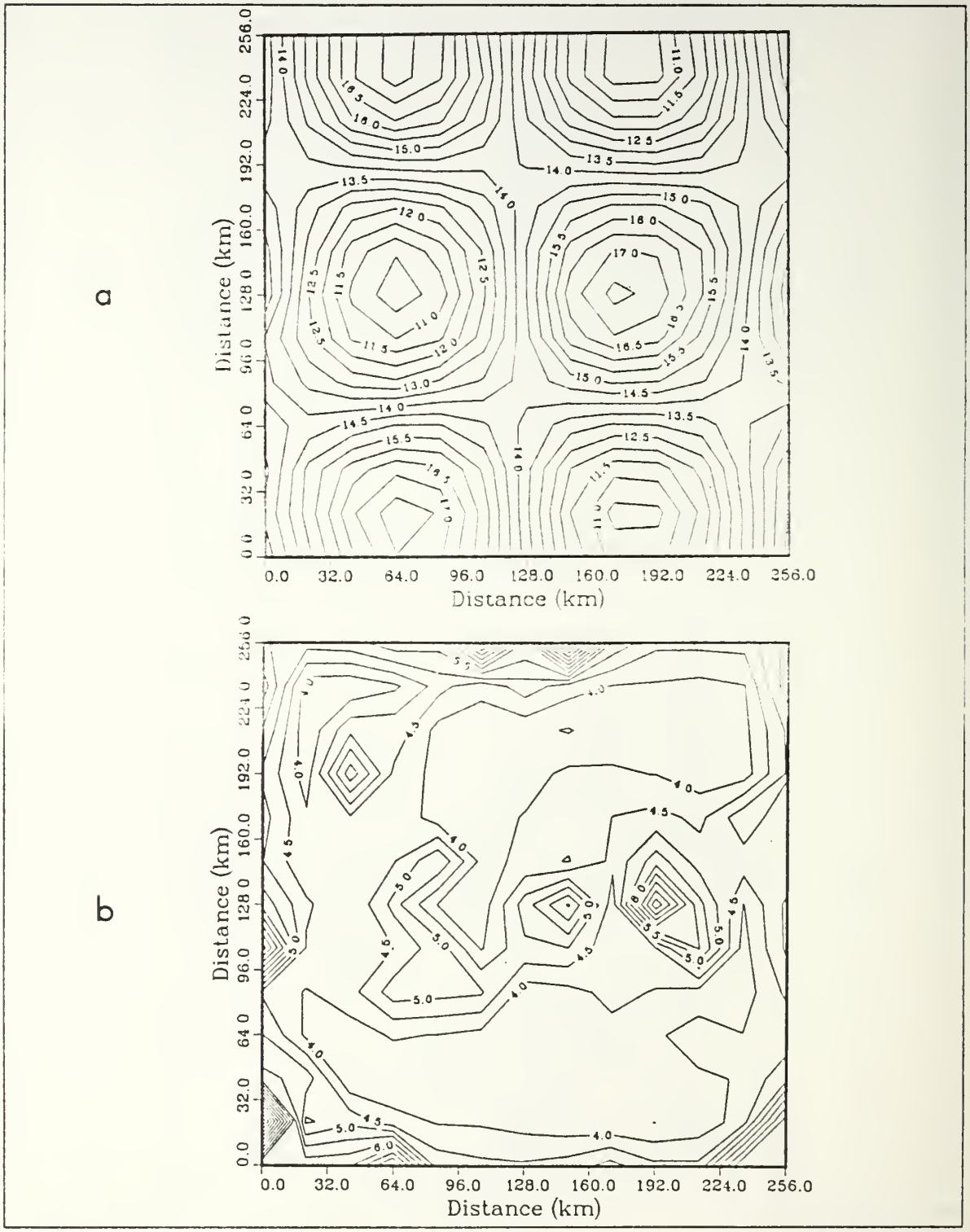

Figure 5.13 SYNFLD1, Progression 2, Sample S1-42XN.
(a) Objective analysis. Contour interval 0.5°C.
(b) RMS interpolation error (%).

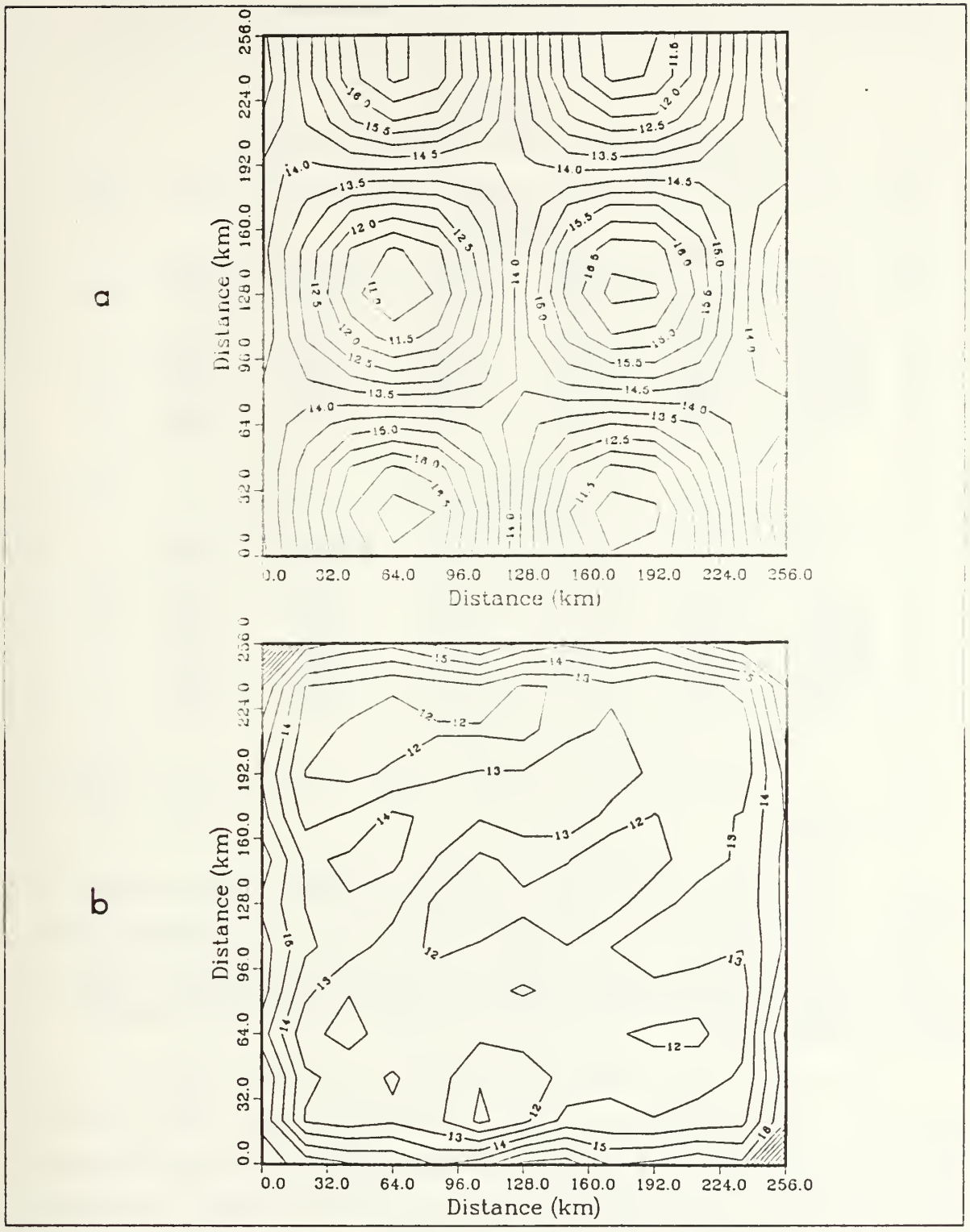

Figure 5.14 SYNFLD1, Progression 2, Sample S1-56XN.
(a) Objective analysis. Contour interval 0.5°C.
(b) RMS interpolation error (%).

TABLE 6

COMPARISON COMPUTATIONS, SYNFLD1

Progression 1

Survey	CORR	MAE (°C)	RMS (°C)	RMSS (°C)	RMSU (°C)
S1-14	0.999	0.028	0.035	0.022	0.027
S1-21	0.998	0.104	0.130	0.040	0.124
S1-28	0.991	0.197	0.281	0.090	0.267
S1-42	0.965	0.360	0.518	0.038	0.517
S1-42X	0.997	0.165	0.188	0.095	0.162
S1-56X	0.379	0.528	1.019	0.379	0.946

Progression 2

Survey	CORR	MAE (°C)	RMS (°C)	RMSS (°C)	RMSU (°C)
S1-14N	0.996	0.141	0.180	0.060	0.169
S1-21N	0.998	0.113	0.139	0.030	0.136
S1-28N	0.995	0.166	0.201	0.067	0.189
S1-42N	0.994	0.369	0.464	0.041	0.220
S1-42XN	0.996	0.143	0.190	0.086	0.169
S1-56XN	0.995	0.321	0.383	0.330	0.194

2. **SYNFLD2**

A single survey, representative of past OPTOMA survey flights, was completed. The autocovariance values and the fitted function were computed, resulting in a zero crossing distance of 74.9 km and a fraction noise variance of 0.162. The objective analysis interpolation points were selected to be at a 32 km spacing in a regular grid (Figure 5.15).

Both versions of the correlation function, as presented in Chapter IV, were used with the objective analysis technique for comparison (Figure 5.16). The fitted correlation function (Equation 4.1) had a correlation of 0.838 at zero lag as computed by the least squares fit (corresponding fraction noise variance of 0.162). In computing the fitted function, it was assumed that there was perfect correlation (1.0) at zero lag in order to compute an estimate of the fractional noise variance. This value was then added to the main diagonal of the autocorrelation matrix. The ADDAS correlation function (Equation 4.2) had a correlation of 1.0 at zero lag.

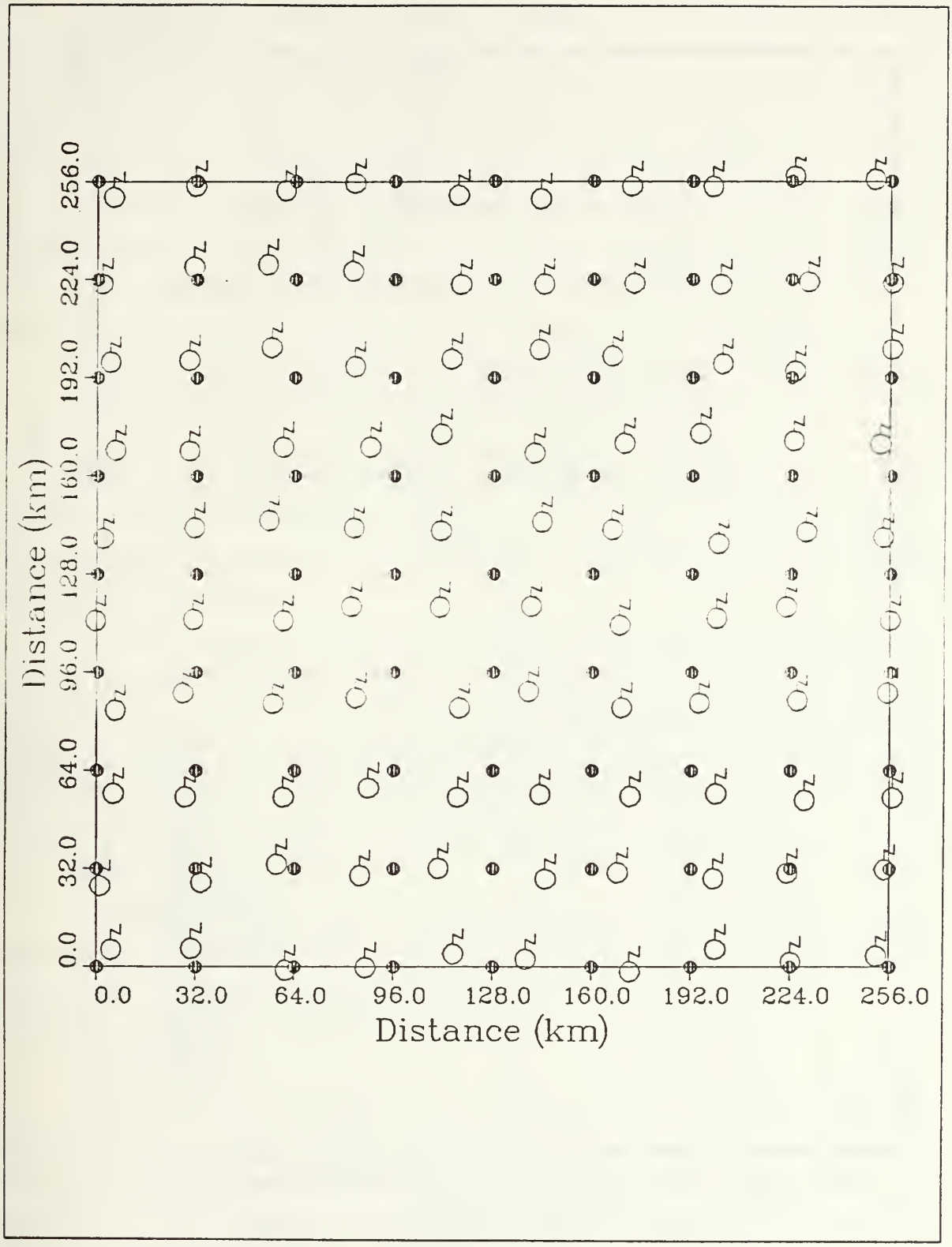

Figure 5.15 SYNFLD2. Sample observations (open symbols) and objective analysis interpolation points (dots).

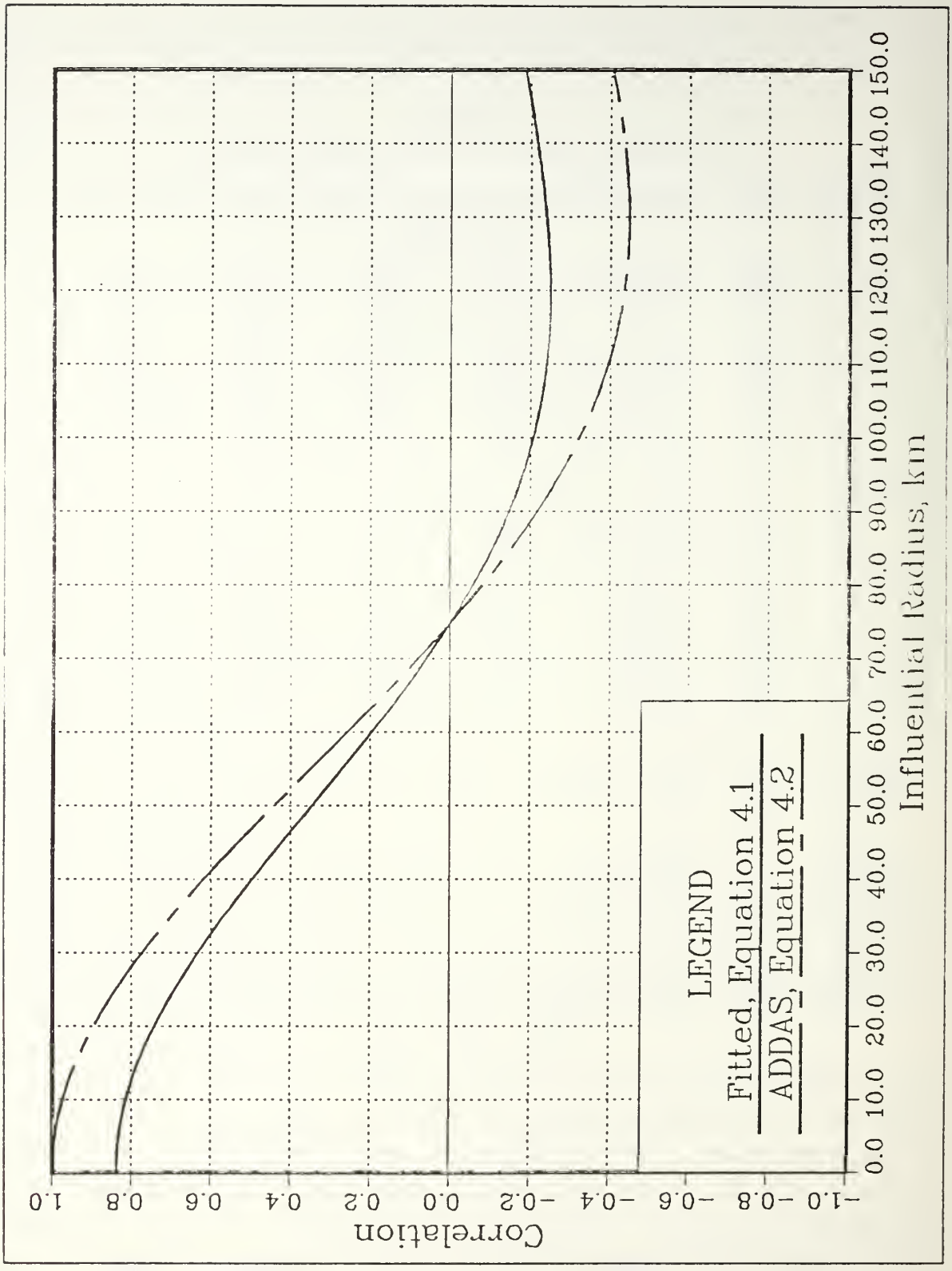

Figure 5.16 Correlation functions as used with SYNFLD2.

In addition to different correlation functions, the specific input parameters that were varied in the objective analysis were the fraction noise variance and the maximum autocorrelation value (minimum distance between selected observations). These two parameters have been identified as problem areas in the objective analysis technique and required further investigation after the surveys on SYNFLD1. Two runs of three objective analysis computations were completed. The maximum autocorrelation value was changed for the two runs. It was selected from the graphs of the respective correlation functions (Figure 5.16), corresponding to distances of 25 km and 35 km. The two correlation functions were applied in the following manner.

- The fitted function (Equation 4.1) was used with the least squares calculated values of the parameters α, β, γ. An estimated noise variance, as computed by the the least squares fit, of 0.162 (Runs A1 and B1) was used.
- The ADDAS function (Equation 4.2) was used in two different ways: 1) with the fraction noise variance selected to be 0.0 (Runs A2 and B2), and 2) with the fraction noise variance as computed, 0.162 (Runs A3 and B3).

The zero crossing distance remained constant at 74.9 km and the maximum number of influential points was chosen to be seven. Table 7 summarizes the input parameters and results of the comparisons.

All the objectively analyzed fields show a small range of RMS interpolation errors and represent the true field well, with only slight differences in the patterns and widely varying error fields. The smallest interpolation errors were observed on runs A2 and B2 (Figures 5.17 and 5.18, respectively), using the ADDAS function and zero noise variance for both the 25 km and 35 km minimum distances. The range of determinants for runs A2 and B2 was approximately one order of magnitude smaller than the other runs, however.

In the comparisons, all the runs had a very high correlation with the true field, with runs A2 and B2 being the best correlated. The MAE, RMS and RMSU errors for runs A2 and B2 were one-half the value of the other runs, also indicating a better representation of the true field. Runs A1 and B1 show the highest errors.

3. **Overall**

From the series of calculations presented, it appears that the higher the density of the observations, more observations will be available to influence an interpolation, and a better objectively analyzed field will result. However, the proper specification of the maximum autocorrelation value (minimum distance between selected observations) appears to be the key factor in the accuracy of the interpolations. Maximum autocorrelation values corresponding to one-third or one-half of the zero crossing distance appear sufficient for these data sets and should

TABLE 7

CALCULATIONS, SYNFLD2

Objective Analysis Input Parameters

Run	Correlation Function	Fraction Noise Variance	Maximum Autocorrelation Value	Corresponding Minimum Distance
A1	4.1	0.162	0.69	25 km
A2	4.2	0.0	0.83	25 km
A3	4.2	0.162	0.83	25 km
B1	4.1	0.162	0.56	35 km
B2	4.2	0.0	0.70	35 km
B3	4.2	0.162	0.70	35 km

Objective Analysis Computations

Run	RMS Error (%)	Determinant Maximum	Determinant Minimum
A1	5.0-13.0	0.143	0.966E-2
A2	0.0- 0.4	0.191E-1	0.415E-1
A3	5.0-14.0	0.2569	0.170E-1
B1	7.0-16.0	0.837	0.502E-1
B2	0.0-1.0	0.220	0.112E-2
B3	7.0-16.0	0.755	0.917E-1

Comparison Computations

Run	CORR	MAE (km)	RMS (km)	RMSS (km)	RMSU (km)
A1	0.989	1.168	1.430	0.540	1.324
A2	0.997	0.598	0.761	0.111	0.752
A3	0.990	1.099	1.358	0.478	1.271
B1	0.988	1.299	1.593	0.770	1.394
B2	0.996	0.650	0.824	0.179	0.804
B3	0.989	1.267	1.526	0.686	1.368

work well in regions of similar variability, using a similar correlation function. The noise variance does not appear to be a factor according to the SYNFLD2 results, and could also be applied to the SYNFLD1 results as well. More work still needs to be done with the objective analysis technique and its application to synoptic mapping.

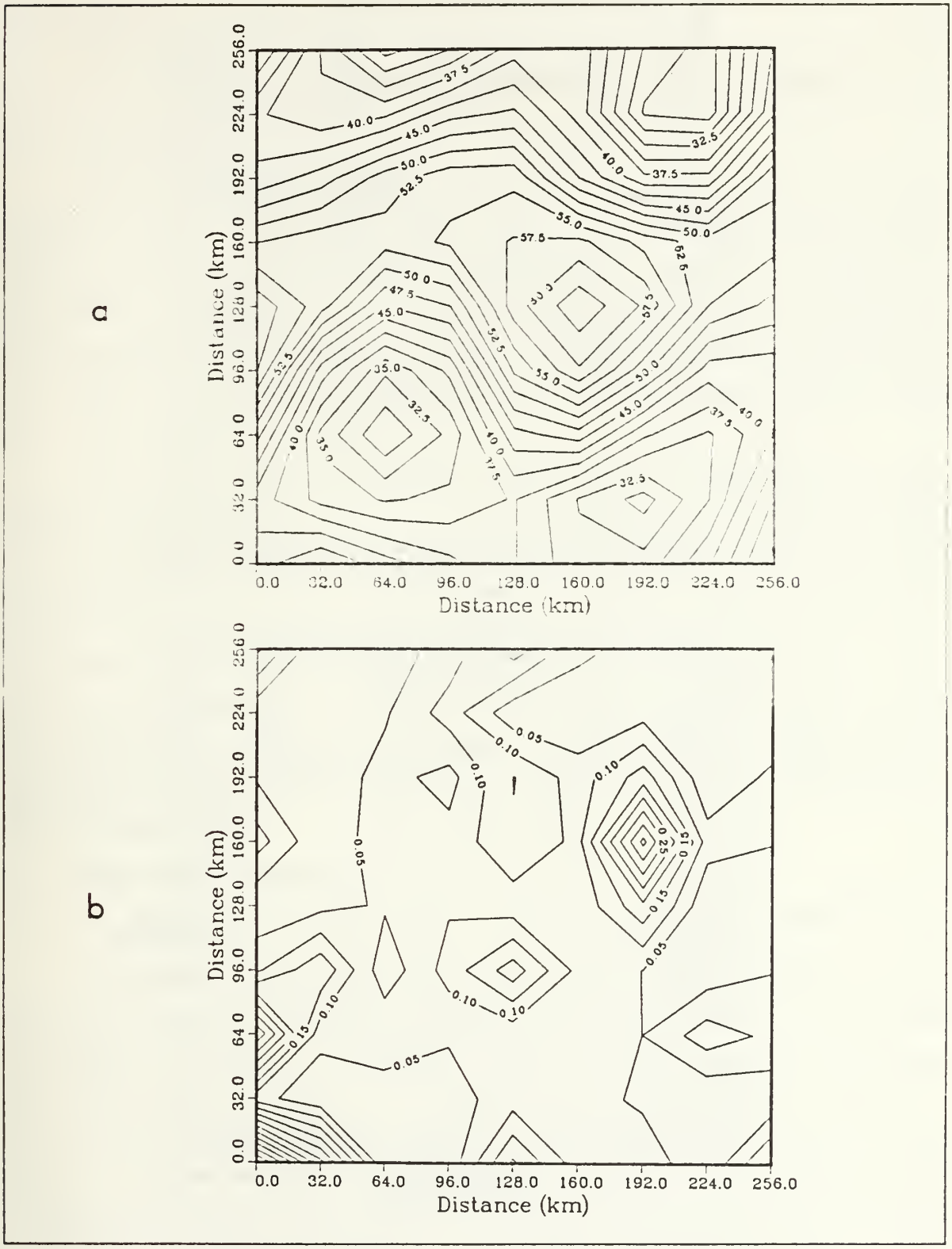

Figure 5.17 SYNFLD2, Run A2 (a) Objective analysis (m). (b) RMS interpolation error (%).

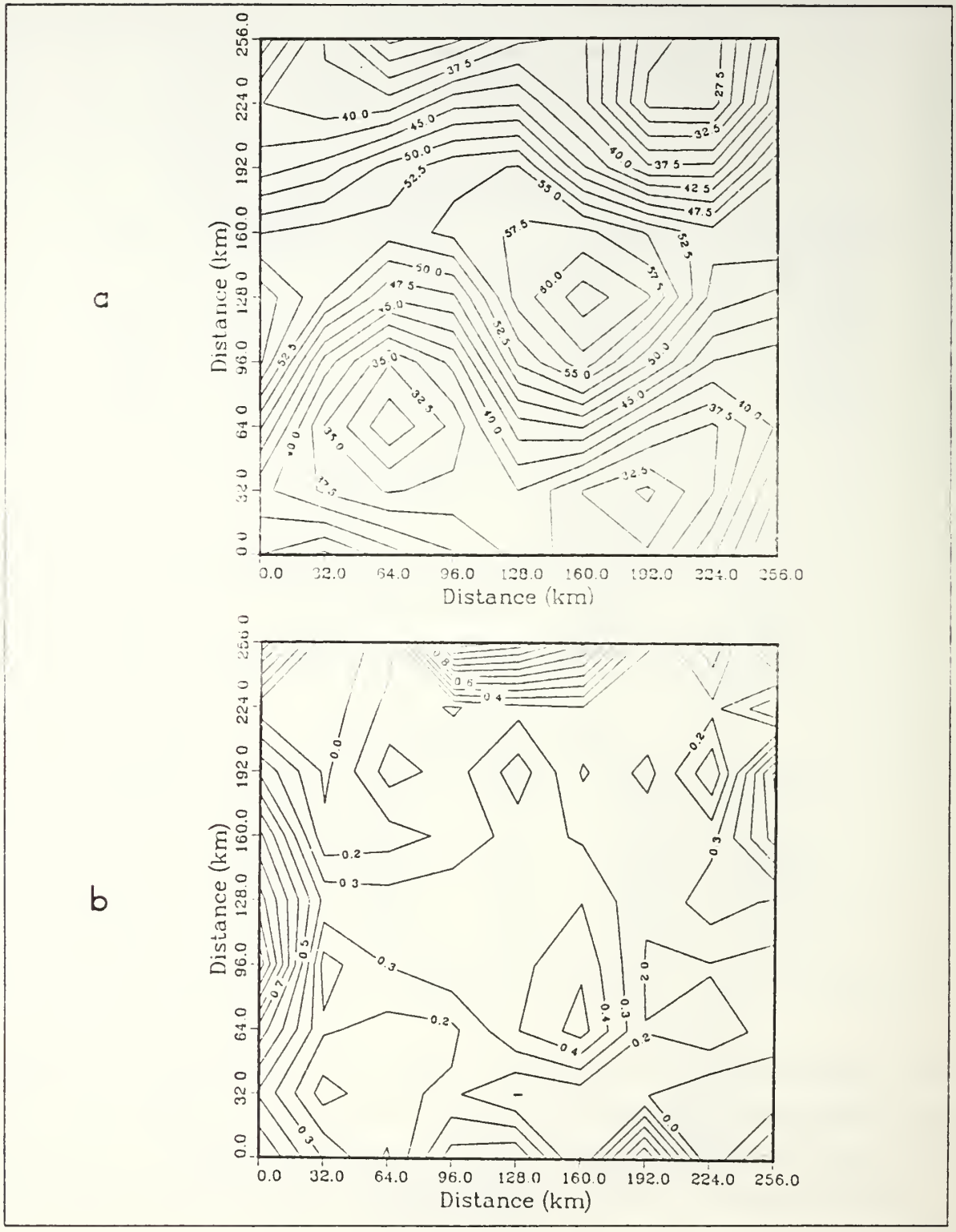

Figure 5.18 SYNFLD2, Run B2 (a) Objective analysis (m). (b) RMS interpolation error (%).

VI. SUMMARY, RECOMMENDATIONS, CONCLUSIONS

A. SUMMARY

With the increasing array of aircraft deployable sensors, systems such as the ADDAS, ADAPS, and the Scripps System have proven invaluable in airborne ocean sampling and the real-time acquisition and analysis of oceanic data in the research community. In a matter of hours, aircraft surveys can cover an area that would require weeks with a research vessel. Synoptic mappings of the oceanic fields obtained from AXBT data can provide valuable information for the oceanographer and also have a direct application in ASW.

Proper use of such data acquisition systems requires a sampling strategy which acquires a representative sample of the field that will optimize the information returned with the minimum amount of effort and time expended. A solid knowledge of the dynamics of the oceanic variables in the region must be considered, including both the temporal and spatial scales in order to sample the field at a proper interval to adequately represent the significant features. Additionally, knowledge of the aircraft platform and its capabilities, as well as the limitations of the airborne sensors, must also be considered. With the data acquired, correct application of the objective analysis technique is essential for the accurate representation of the synoptic mappings that will be generated.

B. RECOMMENDATIONS

1. A Proposed Ship-Aircraft Data Acquisition, Display, and Analysis System (SADADAS)

The addition of real-time oceanic data acquisition and processing to a battle group can provide a stand-alone capability for the understanding of the oceanic environment and the tactical exploitation in ASW. Synoptic mappings in operation areas and at strategic transit points would give the warfare commander a "nowcast" of the oceanic temperature/sound-speed structure from which appropriate tactics can be employed. Furthermore, additional mappings at a later time in the same region can provide an assessment of the temporal variability in the region and also of the effectiveness of the tactics employed.

A system based on the ADDAS, ADAPS, and Scripps System is currently possible as these systems are research-proven, both in their hardware and software, and would not require a substantial lead time for development for fleet applications. The ADDAS is especially feasible as it uses totally off-the-shelf hardware. The ADDAS software is based on shipboard data acquisition software developed in the OPTOMA Program so a ship/aircraft software package is already available. The software suites of both the ADDAS and ADAPS are written in Hewlitt-Packard (HP) BASIC and could easily be transferred to other HP-BASIC systems. A software suite could be incorporated into the Geophysics Fleet Mission Program Library (GFMPL), and with the addition of a digitizing unit, could provide an interim real-time data acquisition and analysis capability until a comprehensive system is available.

a. System Description

The main hardware components of the SADADAS would be a multi-channel digitizing unit and a multi-tasking computer. The digitizing unit should be easily selectable between the array of air-deployable sensors (AXBTs, AXSVs, AXSVs, AXCTDs), as well as expendable sensors such as the XBT and XCTD. With a multichannel system, the simultaneous processing of two sensors would require a computer with multi-tasking capability. Both of these components are well within the available technology on the market today. Additionally, a printer and hard-copy graphics capability should be included. The HP-9020 and related hardware, currently being deployed with the Tactical Environmental Support System (TESS) in the Naval Oceanography Community, could provide the hardware capability with only the addition of a suitable digitizing unit. However, TESS uses FORTRAN-based software so the programs would have to be translated from HP-BASIC.

The software suite would contain a menu-driven acquisition and storage program for each expendable sensor, both air and ship deployable. A program to generate the standard Navy and WMO AXBT- and XBTJJXX messages as the profiles are digitized should be included. This would result in less man-hours being used in manually selecting the inflection points from a hard-copy profile and provide more accurate profiles for archiving at Fleet Numerical Oceanography Center (FNOC). Another menu-driven software package would select which field is to be displayed. The data would be read from storage and objectively analyzed to produce the synoptic mappings. Hard-copy output would then be available to the warfare commander and oceanographer for tactical briefing and planning.

b. System Employment

As the name SADADAS implies, the proposed system will be able to be deployed in land-based ASW aircraft as well as in ships with deployed air assets. These systems are presented below.

(1) *Land-Based Aircraft.*

The aircraft variant of the system would be employed in much the same manner as in the OPTOMA Program aerial surveys as presented in Chapter III. The hardware and operator would be physically located onboard the aircraft so the system must be portable and compact. A system such as this could prove particularly attractive in regions of repeated coverage or continuous on-station operations. Although there will be some time lag between the initial survey flight and the availability of data to subsequent flight crews, synoptic mappings of the oceanic variability would be available for tactical planning and could be updated regularly on following flights. A data base could be built up and archived at the local ASW Operations Center (ASWOC) for future missions. A system such as this would interface with the TESS rather well.

(2) *Deployed Aircraft Assets.*

A shipboard variant of the ADDAS could be developed with little effort and would provide another facet to real-time data acquisition. The hardware and operator would be stationed either in the carrier ASW module or in the Combat Information Center (CIC) in destroyers and battleships. AXBTs could be deployed by S-3 Viking carrier-based ASW aircraft and the SH-2 Sea Sprite, SH-3 Sea King, and SH-60 Seahawk ASW helicopters deployed in frigates and destroyers in the battle group. The AXBT audio signal would be transmitted to the ship by the aircraft-ship data link. AXBT locations would be provided by either the shipboard air controller or by the aircraft onboard navigation and transmitted to the ship. The AXBT audio signal would be received from the shipboard sonobuoy lofargram recorder and fed into the digitizing unit. Two or more aircraft could be utilized to perform the survey and provide larger areal coverage of the region. With the survey complete, near real-time synoptic mappings would be available for operational use and tactical decisions. Again, this capability could be accomplished with the TESS now being deployed.

Factors such as the AXBT loadout, data link transmission range, navigational accuracy of AXBT positions, and speed and endurance of the helicopters need to be investigated more fully to determine the feasiblity of a shipboard data acquisition capability and its employment.

c. Operationally Applicable Synoptic Fields

The following fields are presented as tactical decision aids for the warfare commander:

- Sea Surface Temperature. This will indicate the surface manifestations of fronts and eddies that may have tactical significance in ASW.
- Temperature/Sound speed at selected depths. This will determine the depth extent of the surface features and provide mappings of tactically significant oceanic structure, especially with respect to acoustic propagation.
- Mixed layer depth. This will provide the warfare commander with the depth of the surface duct (if one exists). This has particular application in surface ship bow-mounted sonar, towed-array sonar, and sonobuoy employment. The acoustic properties of the mixed layer will ultimately determine the transmission ranges in the surface duct for bow sonars. A knowledge of the mixed layer depth can provide the towed-array operator with an optimum depth to employ the array. Sonobuoys are limited by the depth of their hydrophones. The shallow sonobuoys have a hydrophone depth of 90 feet (~27 meters). With variability in the mixed layer, the hydrophone may be in the layer at one location while below the layer at another. This will affect the transmission and receiving capabilities of the sonobuoy.
- Subsurface ducts and sound channels. This will have a similar application as in the depth of the surface duct (mixed layer). Subsurface sound channels may affect the the acoustic propagation in the survey region.
- Vertical sections of temperature/sound speed. Vertical sections through a survey region can indicate temperature/sound speed gradients along a specific track from the surface to the depth of the survey (normally 300 m). Sound speed profiles could also be generated for input to acoustic prediction models to get the transmission loss and acoustic paths along the track.

C. CONCLUSIONS

With the capability of research-proven systems and the availablity of off-the-shelf hardware and expendable sensors, the development of a SADADAS for the operational Navy is currently feasible. The addition of a multichannel digitizing unit and data acquisition software to the TESS could provide the Naval Oceanographer and the warfare commander with a near-real-time, stand-alone ocean sampling and analysis system that can enhance tactical readiness.

There is an emerging need for ocean sampling and synoptic mapping of the mesoscale variability in naval operations, especially in antisubmarine warfare. As submarine-radiated noise has been decreasing as advances in quieting technology are implemented, the warfare commander will have an ever increasingly difficult task of localizing and tracking submarines. Real-time synoptic mappings from AXBT surveys can provide the Naval Oceanographer and the warfare commander with a three-dimensional representation of the thermal (and hence acoustic) structure of the submarine's environment. Standard ASW tactics can be modified and new ones developed as the fleet is educated in the variability of the oceans.

A most valuable, though unanticipated result of the ADDAS deployment in the OPTOMA Program, was that Navy aircrews became aware of the variability of the ocean. Usually only one or two AXBTs are deployed in an exercise or mission. These AXBTs may not be representative of the ocean structure in the region yet are used to compute acoustic parameters which are applied to the sensors. A system such as the SADADAS could provide aircrews and shipboard tacticians with a new perspective of the ocean, mesoscale variability and its effects on operations. It is time for such a system to be developed further and evaluated in actual fleet operations.

APPENDIX A

ADDAS HARDWARE COMPONENTS

The following components are used in the current version of the ADDAS. Prices listed are the approximate retail cost as of July 1986. System build-up requires approximately 40 hours at the GS-7 level. Software testing/maintenance requires about 10 hours at the GS-9 level.

HP9816 MC68000 16-bit Microprocessor w/HP9121 3.5 inch microfloppy dual disk drive	$5,000.00
Sippican Mark 9 Front-end Digitizing Unit AXBT Circuit Board	5,000.00 700.00
HP7470A Two-pen Plotter	1,200.00
Avionic Instruments Model 2A125-1A Inverter	3,000.00
VHS Stereo HI-FI Videocassette Recorder	800.00
Tektronix 211 Oscilloscope	750.00
Portable Rack-Mount Storage/Transit Case	500.00
ARNAV R40 LORAN-C Unit (optional) w/Antenna and cable	400.00
Assorted electronic supplies Computer interface cables System wiring Assorted knobs and switches	200.00
Total Cost	$17,550.00

LIST OF REFERENCES

Bane, J.M., and M.H. Sessions, 1984: A field performance test of the Sippican deep aircraft-deployed expendable bathythermograph. *J. Geophys. Res.*, 89, 3615-3621.

Bretherton, F.P., R.E. Davis and C.B. Fandry, 1976: A technique for objective analysis and design of oceanographic experiments applied to MODE-73. *Deep-Sea Res.*, 3, 559-582.

Carter, E.F., and A.R. Robinson, 1981: Time series of synoptic maps of the western North Atlantic: A space-time objective analysis of PLOYMODE XBT's. *Reports in Meteorology and Oceanography, Number 15*, Division of Applied Sciences, Harvard Univ., 14 pp.

Ciandro, M.L., P.A. Wittmann, A.A. Bird and C.N.K. Mooers, 1986: Hydrographic data from the OPTOMA Program, OPTOMA20: OPTOMA20P, 16 March 1986; OPTOMA20 Leg MI, 24 March to 03 April 1986: OPTOMA20 Leg MII, 07 to 15 April 1986; OPTOMA20 Leg D, 25 April to 06 May 1986. *Tech. Rep. NPS-68-86-008*, Department of Oceanography, Naval Postgraduate School, 60 pp.

Colton, M.C., and C.N.K. Mooers, 1985: OPTOMA Program Interim Report: The Airborne Ocean Thermal Structure Mapping Project, February 1983 through February 1985. *Tech. Rep. NPS-68-85-008*, Department of Oceanography, Naval Postgraduate School. 98 pp.

Emery, W.J., Lee, W.G. and Maagard, L. 1984: Geographic distributions of Brunt-Vaisala frequency and Rossby radii in the North Pacific and North Atlantic. *J. Phys. Oceanog.*, 14, 294-317.

Gandin, L.S., 1965: *Objective analysis of meteorological fields.* Israel Program for Scientific Translations.

Gent, A.E., 1982: An evaluation of the airborne expendable bathythermograph (AXBT SSQ-36BT's), *Tech. Rep. 277*, Naval Oceanographic Office, 80 pp.

Gill, A.E., 1982: *Atmosphere-Ocean Dynamics.* Academic Press, Inc., 662 pp.

Jenkins, G.M., and D.G. Watts, 1968: *Spectral Analysis and its Applications.* Holden-Day, Inc., 525 pp.

Kelley, J.C., 1976: Sampling the Sea. *The Ecology of the Seas.* D.H. Cushing and J.J. Walsh, Eds., W.B. Saunders and Co., 361-387.

Miles, R.T., 1984: ADAPS operation and maintenance manual. *Tech. Note 265*, Naval Ocean Research and Development Activity, 41 pp.

Mooers, C.N.K., 1986: Keynote address: Experience with real-time mesoscale ocean prediction (analysis and forecast) in the EEZ off California. In *Applications of real-time oceanographic circulation modeling*, (Ed. B.B. Parker), Marine Technical Society.

Pedlosky, J., 1979: *Geophysical Fluid Dynamics.* Springer-Verlag, 624 pp.

Sessions, M.H., T.P. Barnett and W.S. Wilson, 1976: The airborne expendable bathythermograph. *Deep-Sea Res.*, **23**, 779-782.

———, and T.P. Barnett, 1980: The AXBT for oceanographic measurements. Near Surface Ocean Experimental Technology Workshop Proceedings, Naval Ocean Research and Development Activity, 125-138.

Willmott, C.J., S.G. Ackleson, R.E. Davis, J.J. Feddema, K.M. Klink, D.R. Legates, J.J. O'Donnell and C.M. Rowe, 1985: Statistics for the evaluation and comparison of models. *J. Geophys. Res.*, **90**, 8995-9005.

Wittmann, P.A., M.C. Colton, J.J. Rendine and C.N.K. Mooers, 1986: Hydrographic Data from the OPTOMA Program, OPTOMA18P, 31 October and 2 November 1985. *Tech. Rep. NPS-68-86-001*, Department of Oceanography, Naval Postgraduate School, 48 pp.

INITIAL DISTRIBUTION LIST

		No. Copies
1.	Chairman (Code 68) Department of Oceanography Naval Postgraduate School Monterey, CA 93943	1
2.	Chairman (Code 63) Department of Meteorology Naval Postgraduate School Monterey, CA 93943	1
3.	Department of Oceanography Naval Postgraduate School Monterey, CA 93943	
	Prof. C.N.K. Mooers (Code 68Mr) Dr. Michele M. Rienecker Dr. Mary L. Batteen LCDR J. E. Johnson, USN	25 1 1 1
4.	Dr. Gordon W. Groves 6708 Radio Drive San Diego, CA 92114	1
5.	LT John J. Rendine, USN Naval Oceanography Command Center Box 31 FPO New York 09540-3200	1
6.	Commander, Naval Oceanography Command NSTL Station Bay St. Louis, MS 39522	1
7.	Director Naval Oceanography Division Naval Observatory 34th and Massachusetts Avenue NW Washington, DC 20390	1
8.	Commanding Officer Naval Oceanographic Office NSTL Station Bay St. Louis, MS 39522	1
9.	Commanding Officer Fleet Numerical Oceanography Center Monterey, CA 93943	1
10.	Commanding Officer Naval Ocean Research and Development Activity NSTL Station Bay St. Louis, MS 39522	1
11.	Commanding Officer Naval Environmental Prediction Research Facility Monterey, CA 93943	1
12.	Commander Oceanographic Systems Pacific Box 1390 Pearl Harbor, HI 96860	1

13.	Commanding Officer Naval Eastern Oceanography Center Naval Air Station Norfolk, VA 23511	1
14.	Commanding Officer Naval Western Oceanography Center Box 113 Pearl Harbor, HI 96860	1
15.	Commanding Officer Naval Oceanography Command Center Box 31 FPO New York 09540-3200	1
16.	Commanding Officer Naval Oceanography Command Center, Guam Box 12 FPO San Francisco, CA 96630	1
17.	Chairman, Oceanography Department U.S. Naval Academy Annapolis, MD 21402	1
18.	Chief of Naval Research Naval Ocean Research and Development Activity 800 N. Quincy Street Arlington, VA 22217	1
19.	Office of Naval Research (Code 1122) Naval Ocean Research and Development Activity 800 N. Quincy Street Arlington, VA 22217	
	Dr. Thomas W. Spence Dr. Thomas B. Curtain Dr. Dennis Conlon	1 1 1
20.	Scientific Liaison Office Office of Naval Research Scripps Institution of Oceanography University of California, San Diego La Jolla, CA 92037	1
21.	Harvard University Division of Applied Sciences Pierce Hall, Room 100D Cambridge, MA 02138	
	Prof. Allan R. Robinson Mr. Leonard J. Walstad Mr. Wayne G. Leslie	1 1 1
22.	Dr. Laurence C. Breaker Moss Landing Marine Labs P.O. Box 450 Moss Landing, CA 95039	1
23.	College of Oceanography Oregon State University Corvallis, OR 97331	
	Prof. Robert L. Smith Dr. Adriana Huyer	1 1
24.	Dr. Stuart L. Kupferman Sandia National Laboratories Division 6334 Albuquerque, NM 97185	1

25. Scripps Institution of Oceanography
University of California, San Diego
La Jolla, CA 92093

Prof. Russ E. Davis	1
Dr. Jerome A. Smith	1
Mr. Phillip Bogden	1
Dr. Meredith Sessions	1

26. Dr. William J. Schmitz — 1
Woods Hole Oceanographic Institution
Department of Physical Oceanography
Woods Hole, MA 02543

27. Naval Ocean Research and Development Activity
NSTL Station
Bay St. Louis, MS 39522

Dr. Janice Boyd	1
Dr. Alexander Warn-Varnas	1

28. Dr. Otis Brown — 1
Division of Oceanography
RSMAS, University of Miami
4600 Rickenbacker Causeway
Miami, FL 33149

29. Dr. Thomas B. Stanford — 1
Applied Physics Laboratory
University of Washington
1013 NE 40th St.
Seattle, WA 98105

30. Dr. Steven C. Riser — 1
School of Oceanography
University of Washington
Seattle, WA 98195

31. Dr Robert L. Bernstein — 1
California Space Institute, MS-A021
Scripps Institution of Oceanography
University of California, San Diego
La Jolla, CA 92093

32. Dr. Jack Calman — 1
Applied Physics Laboratory
Johns Hopkins University
Laurel, MD 20707

33. Ms. Marie Colton — 1
Naval Environmental Prediction Research Facility
Monterey, CA 93943

34. Dr. Everett F. Carter — 1
Graduate School of Oceanography
University of Rhode Island
Kingston, RI 02881

35. Defense Technical Information Center — 2
Cameron Station
Alexandria, VA 22304-6145

36. Library, Code 0142 — 2
Naval Postgraduate School
Monterey, CA 93943-5002

37. Research Administration — 1
Naval Postgraduate School
Monterey, CA 93943

Thesis
R3373 Rendine
c.1 Real-time airborne ocean sampling and application to naval operations.